Republic of Iraq

Ministry of Higher Education and Scientific Research

University of Babylon

College of Science / Department of Physics

Quantum Transport Properties of Organometallic Molecular Junctions and Their Applications as Laser Active Media

A Thesis

Submitted to the Council of College of Science, University of Babylon in Partial Fulfillment of the Requirements of the Degree of Doctor of Philosophy in Sciences/ Physics

By

Abbas Ibrahim Obayes Mhesin Al-Zuhiry

B.Sc. in Physics 2002

M.Sc. in Physics 2010

Supervised by

Prof. Dr.

Enas Mohammed Selman Al-Robayi

2022 A.D. **1443 A.H.**

Summary

This thesis involves three novel scientific works, could be abstracted as follows: The first work confirms and proves that the single-molecule BiCyclobentedine with anchor group applications gain attention by using molecules as elementary blocks of electronic components involving metallic atoms. Theoretically, one type of molecular-scale BiCyclobentedine-metal-anchor groups device is used in this thesis, consisting of organometallic single molecules with different metals (Fe, Co, Ru and Pt), sandwiched between gold electrodes bound by Pyridil, thiol, thiomethyl anchor groups.

The electronic and thermoelectric properties of molecular junctions made up of single organometallic molecules are studied in this thesis. Exploration and understanding of the electronic properties of molecules coupled to metallic leads is critical for the future of molecular electronics. The Gaussian program and SIESTA code were used to investigate a variety of organometallic compounds using a combination of density functional theory (DFT) and the transport theory Green's function formalism (Gollum code). The following are the main findings of the thesis:

The first work demonstrates that the BiCyclobentedine-metal-anchor molecular junctions are of particular interest because of its electronic and structural features, which introduce it as a suitable candidate for optical and thermoelectric applications. Utilizing the DFT methods, and the Green’s function formulism, this work involves a theoretical investigation of optical, structural, electronic and thermoelectric properties of BiCyclobentedine-metal with different anchor group. This work predicates an important result, which

is an increase of the organometallic with deferent metal and anchor group, leads to a significant increase of the emission oscillator strength (*fem*) (0.0008 – 0.5014 $mol.cm^2.L^{-1}$). In contrast, the lowest electrical conductance (0.113×10^{-3} Siemens), is presented via in the group3 with Fe-metal, while it exhibits the highest thermopower (-0.113×10^{-3} μVK^{-1}). This may aids in innovate promising new candidates for the design of optical and thermoelectric devices, as well as the active mediums for lasers.

The second part the transmission and Seebeck coefficients for Au|molecule|Au configurations were computed by using DFT. The findings show that there is a robust anti-resonance in the transport behavior around the Fermi energy, only for the BiCyclobentedine-based device with all metal. This result is attributed to the destructive quantum interference between continuous and discrete states. This work not only indicates that there is a relationship between the electrical conductance and thermopower, but also it introduces a promising strategy to affect and control these characteristics via creation of anti-resonance phenomenon.

The third work defines the state-of-the-art in single molecule quantum interference devices by bringing together, pioneering work on molecular wires. In addition, it exhibits a novel strategy to control the quantum mechanical interference and enhance the electronic and thermoelectric properties of the molecular based devices, and its applications. The results of this work show that the transmission coefficient value of closed organometallic for this molecule (BCP-Pt) is more than that of the rest molecules. Rather, it represents a mechanism to control the quantum mechanical interference and enhance its characteristics.

Dedication

To My Family

Abbas

بسم الله الرحمن الرحيم

﴿ وَلِيَعْلَمَ الَّذِينَ أُوتُوا الْعِلْمَ أَنَّهُ الْحَقُّ مِن رَّبِّكَ فَيُؤْمِنُوا بِهِ فَتُخْبِتَ لَهُ قُلُوبُهُمْ وَإِنَّ اللَّهَ لَهَادِ الَّذِينَ آمَنُوا إِلَى صِرَاطٍ مُّسْتَقِيمٍ ﴾

صدق الله العلي العظيم

سورة الحج اية (٥٤)

Acknowledgments

First, I should thank my Almighty ALLAH, JALA JALALAH, for helping me in completing my Thesis.

I would like to express my thanks and gratitude to Prof. Dr. Enas Muhammad Salman Al-Robayi, who suggested and supervised this issue until we reached safety in the end.

Many thanks to the College of Sciences in University of Babylon and the Department of Physics for offering me the opportunity to complete my Thesis.

I would like to thank my dear brother and supporter, Assistant Professor Dr. Oday Arkan Abbas Al-Owaedi in College of Science for Women. Thank you very much my brothers and sisters in the theoretical studies lab for advanced physics at the College of Science for Women.

Abbas

List of Figures

Contents

List of Symbols

Symbol	Physical meaning
α	Alpha
(=CH−)	Thiol bridges
π-electrons	Two electronic bonds
f_{em}	Emission oscillator strength
Ψ	Wave function
n(r)	Ground-state density
H	Hamiltonian operator
M	Nuclei number
N	Electrons number
r_i	Position of the *i-th* electron
r_j	Position of the j-th nucleus
E_i	Numerical value of the energy of the i^{th} state
T_e	Kinetic energy for the electron
T_n	Kinetic energy for the nuclei
U_{ee}	Interaction energy between all electrons
U_{nn}	Interaction energy terms between the nuclei
U_{en}	Interaction between electrons and nuclei
m_e	Mass of the electron

Symbol	Physical meaning
m_n	Mass of the nucleus
e	Electron charge
Z_n	Nuclear charge
ε_o	Dielectric constant of the vacuum
∇_i^2	Laplacian operator
H_{ele}	Electronic Hamiltonian
E_{ele}	Electron energy
E_{total}	Total energy
Ψ_{Tri}	Trial wavefunctions
Ψ_{GS}	Ground-state wavefunctions
E_{Tri}	Trial energy
E_{GS}	Ground state energy
Z	Atomic number
$V_{ext}(\vec{r})$	External potential
n_{GS}	Ground state density
$F_{H-K}[n(\vec{r})]$	Energy functional of the Hohenberg-Kohn
T_{int}	Kinetic energy of the interacting system
H_{eff}	Effective Hamiltonian
V_{eff}	Effective external potential
$F_{K-S}[n(\vec{r})]$	Energy functional of the Kohn-Sham

Symbol	Physical meaning
T_{non}	Kinetic energy of the non-interacting system
E_{xc}	Exchange-correlation energy
E_X	Exchange energy of an electron
E_C	Correlation energy of an electron
V_{nl}^{ps}	Pseudopotential
$\Psi_{nlm}^{I}(r)$	Single basis function
R_{nl}^{I}	Radial wavefunction
Y_{lm}^{I}	Spherical harmonic
φ_i	Molecular orbitals (basis functions)
Ψ_v	Atomic orbitals
E^A	Energy of the isolated subsystem A
E^B	Energy of the isolated subsystem B
μ_L	Chemical potential in the left
μ_R	Chemical potential in the right
T	Probability the transition
R	Probability the reflection
δI^{in}	Incident electric current
v_g	Group velocity
$\partial n/\partial E$	Density of states (DOS) per unit energy in the lead

Symbol	Physical meaning
δV	Voltage associated with the chemical potential mismatch
G	Conductance
$\vec{t}_{ij}$	Transmission amplitude
$\overleftarrow{r}_{ij}$	Reflection amplitudes
S	Matrix, it connects states coming from the left lead to the right lead and vice versa:
$\Delta \mathcal{T}$	Temperature
ΔV	Potential drop
I	Charge current
$\mathcal{T}_L$	Temperature left
$\mathcal{T}_R$	Temperature right
f_i	Fermi distribution function
f_L	Fermi distribution from the left
f_R	Fermi distribution from the right
k	Wave number
$g(z, z')$	Retarded Green's function
G_+	Advanced Green's function
G_-	Retarded Green's function
ε_1	Single site energy
ε_2	Two site energy

Symbol	Physical meaning
ZT_e	Electronic figure of merit
$T(E)$	Transmission parameter
E_F	Fermi energy
$f(E)$	Fermi-Dirac function
Ry	Rydberg's
$S(T)$	Thermopower
G/G_0	Electrical conductance
G_o	Quantum of conductance
H	Planck's constant
K_B	Boltzmann constant
ε	Absorption intensity
σ_{em}	Emission cross section

List of Tables

List of Abbreviations

Abbreviation	Physical meaning
TD-DFT	Time dependent Density functional theory
DFT	Density functional theory
UV	Ultra-Violet
Vis	Visible rays
HOMOs	High Occupied Molecular Orbitals
LUMOs	Lowest Unoccupied Molecular Orbitals
1D	One-dimensional
2D	Tow-dimensional
3D	Three-dimensional
SIESTA	Spanish Initiative for Electronic Simulations with Thousands of Atoms
KS	Kohn and Sham
LDA	Local Density Approximation
GGA	Generalized Gradient Approximation
PZ	Perdew and Zunger
PBE	Perdew, Burke and Ernzherhof
LCAOBs	Linear Combination of Atomic Orbital Basis set
BSSE	Basis set superposition error correction
DOS	Density of states

Abbreviation	Physical meaning
QI	Quantum Interference
DQI	Destructive Quantum Interference
HF	Hartree-Fock
HK	Hohenberg-Kohn-Sham
GF	Green's Function
NEGF	Non-Equilibrium Green's function
LED	Light Emitted Diode
MO	Molecular Orbitals
B3LYP	Becke 3 (Lee-Yang-Parr**)**

Scientific activities

1. Two papers have been published in a Scopus container.

a- Abbas I. O., Enas M. Al-Robayi, Oday A. Al-Owaedi, "Investigation Quantum Electronic Transition of Organometallic Molecules", Journal of Physics: Conference Series, *J. Phys.: Conf. Ser.* **1973** 012147, (2021).

b- Abbas I. O., Oday A. Al-Owaedi, Enas M. Al-Robayi**, " EFFECT QUANTUM INTERFERENCE OF META-LINKED BRIDGED PYRIDYL RINGS FOR SINGLE MOLECULAR JUNCTIONS",** Turkish Journal of Physiotherapy and Rehabilitation**; 32(3), P.p(16562-16568), (2021).**

2. Certificate of attendance at international conferences.

3. Participation in two scientific symposiums for postgraduate students at the Faculty of Science, Department of Physics.

1.1 Introduction

Quantum theory physics has made tremendous strides in the previous two decades in terms of theoretical approaches. These advancements have enabled scientists to produce novel materials [1, 2], reduce the structural complexity of electronic circuits [3, 4], and construct sophisticated simulation tools [5-7]. Molecular electronics has emerged as a novel topic with ever-expanding possibilities since 1974, when Aviram and Ratner offered the first prediction [8]. However, shrinking the size of an organometallic devices to near or below 10 nm[9] necessitates the creation of new theories to describe and study the behavior of molecules in such domains, as well as the prediction of their features and phenomena [10]. For instance, DFT calculations characterize the ground state properties, whereas the GF (Green's Function) relies heavily on DFT for transmission calculations, as it requires the system's DFT Hamiltonian [11].

Nanoscale research and engineering enable revolutionary discoveries in both fundamental science and technology, which may have a direct impact on our daily lives. It is on a level with transistor-based electronics in terms of size and scope. At its most fundamental level, nanoscale science is the study of unique phenomena and properties of materials at extremely small length scales, namely at the nanoscale, which corresponds to the size of atoms and molecules [1].

The nanoscience revolution has emphasized the critical need for a more solid quantitative understanding of matter at the nanoscale through modeling and simulation, since the dearth of quantitative models that accurately characterize newly reported phenomena has stifled development in the area. Recently, fundamental modeling tools such as (DFT) and molecular dynamics

have been used to gain new insights in the field of nanoscience [2]. Increased computing capabilities enabled the modeling and simulation of complex systems with millions of degrees of freedom as a result of advancements in computer technology. The entire promise of modern theoretical and modeling techniques, on the other hand, has not yet been realized [6].

Single-molecule junction devices, which consist of a single molecule electrically linked to two electrodes, enabling the study of a wide variety of quantum-transport processes at ambient temperature. These quantum properties are related to the orbital and spin degrees of freedom of molecules and are quantified by a variety of energy scales that can be modified chemically and physically: level spacing, charging energies, tunnel couplings, exchange energies, and vibrational energies. The struggle between these several energy scales results in a rich range of processes that researchers are now beginning to theoretically regulate and adjust. The state of the field of molecular electronics from a quantum transport perspective is addressed in this technical review, with a particular focus on recent theoretical results obtained using single-molecule junction devices and electrically conductive gold junctions [12].

To get a better knowledge of electronic transport events at the atomic and molecular scales, as well as the practical use of a single-molecule junction for molecular electronics, a reliable electronic and structural characterization approach for single-molecule junctions is required. Recent improvements in characterization techniques enable the elucidation of the unique electrical properties of a quasi-one-dimensional conductor used in a single-molecule junction. This thesis discusses some of the most recent techniques for deciphering the electrical and structural features of a single-molecule junction.

The potential uses of single-molecule junctions in electronic devices such as molecular switches, diodes and transistors have been explored [1,13-15].

Organometallic compounds are chemical compounds that contain at least one bond between a metallic element and an organic molecule's carbon atom. Even metallic metals such as iron, cobalt, ruthenium, and platinum can create organometallic compounds that are employed in a variety of industrial chemical processes and as single molecules as active media in laser devices [16].

In general, the link between a metal atom and the carbon in an organic complex is covalent. When metals with a very high electronegativity (such as Sodium and Lithium) produce these compounds, the carbon bonded to the central metal atom demonstrates their carbonaceous character. Organometallic Compounds Qualities, a few of the properties of organometallic compounds are summarized below.

1- In nature, the link between the metal and the carbon atom is frequently extremely covalent.

2- Organometallic compounds are frequently discovered to be hazardous to people (especially the compounds that are volatile in nature).

3- The majority of organometallic compounds occur in solid forms, particularly those with aromatic or ring-structured hydrocarbon groups.

4- These compounds, particularly those produced by highly electropositive metals, can behave as reductants [16,17].

As the preceding paragraphs demonstrate, the properties of organometallic compounds vary according to the properties of the metals that comprise them. The fabrication, characterization, and application of metallic

nanoparticles (MNPs) have advanced dramatically during the last decade [17]. Despite its early engagement, organometallic chemistry is only a minor player in the field today. However, it appears that concepts and techniques from organometallic chemistry are ideally suited to the synthesis of nanoparticles with unique physical properties [18].

1.2 Quantum Interference

Quantum interference comprises a section showing another entirely quantum mechanical element of charge transport across single molecule connections — quantum interference — that occurs when the molecular length scale approaches the electronic phase coherence length as demonstrated three decades earlier by theoretical demonstration of the Aharonov–Bohm phenomenon in metal rings [19]. Theoretical calculations at the molecular level, on the other hand, do not only extend such calculations down to the atomic size; rather, they provide novel insights and ways for managing charge transport at the wave function level through chemical design and, potentially, electrical control. For instance, quantum interference effects can significantly reduce the conductance of a cross-conjugated (or meta-terminated) molecule in comparison to its linearly conjugated (or para-terminated) equivalent. The effect of quantitative interference is summarized in this work as follows: Quantum interference (QI) has garnered considerable attention both theoretically and experimentally. Numerous systems contain both constructive and detrimental QI. For example, a molecule with two parallel electron transfer pathways without a phase shift can exhibit constructive interference and thus have a higher conductivity, whereas a molecular junction with a meta-substituted pyridyl ring has a conductivity several orders of magnitude lower than a para-substituted pyridyl ring due to destructive QI [20,21]. This

may be intuitively understood from a chemical standpoint in terms of the electronic influence of substituents at meta- and salient positions on chemical reaction rate constants [22]. The low conductivity of conjugated molecular junctions is related to the junction transfer function's resonance impedance [23].

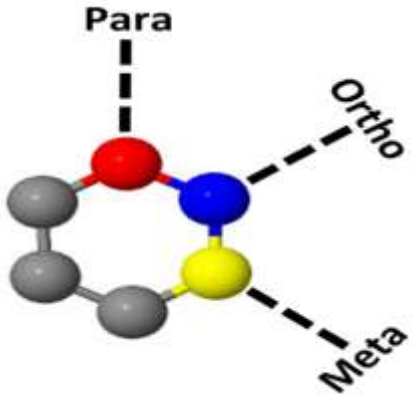

Figure (1.1): Shows the attachment points of the molecules with the electrodes.

Controlling the position of this anti-resonance in relation to the Fermi level of the electrode may pave the way for the development of a quantum interference-controlled molecular switch with a potentially huge on/off ratio [23-24]. Technologically, the discrete energy levels at a molecular junction allow for the preservation of interference effects at elevated temperatures. Thus, the capacity to manipulate the interference effects stored in a molecule's chemical structure enables innovative functionality to operate at room temperature. Chemical structure, at its most fundamental level, regulates interference effects in molecular junctions [24].

One difficulty in exploring transport across single-molecule junctions that exhibit destructive interference is the very tiny bias conductance of these junctions. Simply demonstrating that molecular junctions exist by measuring

current through them is insufficient, as the current through-space component can be greater than the current through-bond component [25].

While it was known that the para-terminated molecule functioned normally, destructive quantum interference effects were expected to result in a low- or non-conductive junction in the meta-terminated state. We were able to find evidence for junction creation in the force signature despite the meta-terminated molecule's lack of conductivity by doing simultaneous force and conductivity computations. These computations demonstrated that destructive quantum interference does not abate in these molecules' single-molecule circuits, even at room temperature and ambient circumstances. The resonance impedance in the transmission potential across a molecular junction is a characteristic of destructive interference; were able to demonstrate anti-resonant transmission in a single-molecule junction [20,23].

Understanding charge transport through molecular building blocks is critical for designing molecularly functional electric materials and devices. At the nanoscale, charge transport is governed by quantum processes that may be manipulated through the electron wave function. Among these phenomena, destructive quantum interference (DQI) in single-molecule junctions refers to a quantum process in which electron waves move via distinct molecular orbitals and combine destructively. This impact results in a decrease in the probability of electron transmission and hence a suppression of molecular conductance by orders of magnitude when compared to molecular junctions lacking DQI [25,27]. As a result, controlling DQI in single-molecule junctions represents an exciting opportunity for constructing high-performance molecular devices such as molecular switches [21], transistors [28] and thermoelectric devices [29]. Chemical design has been used to manipulate

molecular architectures in earlier works to manage DQI, including electronic structure modification [28], molecular topologies modification [30], heteroatom substitution modification [31], and even chemical interactions to change molecular structures. However, these indirect approaches do not provide for flexible and in-situ control, and fine tuning interference remains a significant barrier to the manufacturing of interference-based molecular electronics, such as single-molecule transistors [28,32].

1.3 Molecular Electronics

Molecular electronics is defined as the branch of science that studies the electronic transport properties of systems composed of individual molecules. Because certain molecular systems have dimensions of a few nanometers, molecular electronics should be considered a subsection of nanotechnology [33,34]. Molecular electronics as a prospective technology is based on a bottom-up approach, with the goal of assembling specialized and designed molecules to form increasingly complicated structures, active components, and connecting wires.

Gordon Moore's astounding prediction in 1965 that the number of transistors per square centimeter on a silicon chip will quadruple every 18 months [35] sparked an ongoing search for complementary technologies to silicon-based electronics, and molecular electronics is one such technology. Since the advent of accessible laboratory procedures for the fabrication of electrode |molecule| electrode molecular junctions and their application to the measurement of through-molecule conductance [36-41], the area of molecular electronics has grown fast. These studies enabled the investigation of the electrical properties of a wide variety of molecular structures, establishing a number of useful structure property relationships and resulting in improved

concepts for the design of molecular components with high electrical conductivity, exceptional rectification ratios, and transistor-like gated conductance [42-47].

Many decades ago, some fundamental problems remained unanswered, such as how an electrical current flows via a single molecule [48,49]. Electrons traveling through a single molecule is conceptualized in two distinct ways [50]. The first is electron transfer, which is the process by which charge is transferred from one end of the molecule to the other. The second is charge transfer, which entails current flowing via a single molecule coupled between two electrodes[51]. Both are connected, as they both attempt to answer the preceding question. From a fundamental scientific perspective, molecule electronics may provide answers to earlier inquiries and may be an ideal tool to investigate electrical and thermal conductivity at the atomic level, where quantum mechanical phenomena entirely dominate [25,52-54].

Additionally, novel molecular phenomena such as quantum interference have been identified, opening up new avenues for molecular design and resulting in proposals for the design of molecular materials[55] with useful properties such as an enhanced thermoelectric figure of merit ZT and promisingly high power factors GS^2 [56-60].

When a single molecule is linked to source and drain electrodes, the electrical conductance of the resulting device is controlled by the quantum interference pattern formed within the molecule by the source's de Broglie waves of electrons [61]. Motivated by the goal to increase the performance of molecular-scale diodes [56–66], transistors [44,63], switches [67], and thermoelectric devices [60,68–70], current research has focused on harnessing such wave patterns within heterocyclic aromatic molecules.

The diversity of molecules (organic and organometallic) and their diverse properties may result in the discovery of novel physical phenomena. Additionally, molecular junctions may be useful for investigating the fundamental principles of electron transfer pathways. However, there are additional technological motives, one of which is the utilization of molecules as electronically active constituents in a variety of applications. One of these reasons is related to size, as the normal size of molecules (between 1 and 10 nm) enables a higher packing density on a device, resulting in cost, efficiency, and power dissipation advantages [14,15,66]. These and numerous other notions contribute to the appeal of molecular electronics as a subject of research.

The fundamental concept of molecular electronics lies at the heart of nanoscience, as it is predicated on the notion that innovative devices can be made using elements so small that novel properties arise. Due to the intrinsic quantum mechanical nature of molecules, molecular devices can display properties that are not possible at room temperature. Indeed, by synthesizing functional molecules such as switches, synthetic chemists impart a level of flexibility and structural control that is not possible with comparable solid-state electronics. The usage of gold-based nano-electrodes in particular has emerged as a potential technique due to AuNTs' intrinsic nanoscale size and the reduced electronic mismatch caused by having molecules and electrodes of different materials [15,16,34,38]. This thesis examines a variety of organic and organometallic compounds theoretically. The systems studied in this thesis were studied theoretically using two distinct techniques: (DFT), which are implemented in the Gaussian and SIESTA code [75,76], and the nonequilibrium Green's function formalism of transport theory, which is implemented in the GOLLUM code [77].

1.4 Literature Survey

Nowadays, molecular electronics is one of the most important fields of science that investigates the electronic transport and thermoelectric properties of structures in which a single molecule is utilized as a basic building blocks.

M. Kiguchi, et al. [78] in 2010, investigated the relationship between the anchor groups and the electrical properties of molecular junctions. They found the contact position between electrodes and molecule will affect the electric conductance of single molecule junctions.

In this context, single-molecule junctions formed from inorganic complexes and organometallic compounds within molecular junctions have attracted increasing attention. L. Luo, et al. [79] in 2011, investigated the electronic properties of two series of linear ruthenium (II) bis(σ-arylacetylide) molecular wires. They demonstrated the important role of the metal centers in the transport of molecular junctions, as well as they reported that the conductance of such molecules exhibited very weak length dependence due to a high degree of electronic coupling between the redox centers.

The previous work of H. M. Wen, et al. [80] in 2013, reported the organometallic based molecular junctions exhibited a high conductance in compare with their organic analogous. Their work has been supported by the results of J. Ponce, et al. [81] in 2014, were they gave insight into the effect the metal coordination on the room-temperature conductance of molecular wires.

The observations of A. C. Aragonès, et al. [82] in 2016 about the conductance switching in an organometallic single molecule wires open up a new door for the design and control of spin-polarized transport in nanoscale molecular devices at room temperature. This research encouraged other to

investigate the electrical properties of inorganic molecular junctions, where L. A. Zotti, et al. [83] in 2013 presented a theoretical study of electrical transport in nano-metallic devices. They demonstrated that the existence of Pt- metal cluster displays the quantum destructive interference.

A. Oday Al-Owaedi, et al. [84] in 2016 introduced a theoretical and experimental studies of trans-Ru complexes. They interpreted the electronic properties of such molecules in terms of the transport mechanisms (LUMO-dominated conductance). These results have significant implications for the future design of organometallic complexes for studies in molecular junctions. Therefore A. Oday Al-Owaedi, et al. [85] in 2017 presented an investigation about the important role of the metal complexes inhibiting orthogonal contacts, which explained the strange high conductance values of some of organometallic molecules.

P. Sam-ang and G. R. Matthew, [86] in 2017 show characterizing destructive quantum interference in electron transport. Destructive quantum interference in electron transport through molecules provides an unconventional route for suppressing electric current. In this work we introduce interference vectors' for each interference and use them to characterize the interference. An interference vector may be a combination of multiple molecular orbitals (MOs), leading to more robust interference that is likelier to be experimentally observable.

R. J. Davidson, et al.[87] in 2018, to develop a new design of molecular nano junction depending on organometallic molecules. They explored the ability to control the orientation of molecular conductors on the electrode surfaces, which showed only a single high conductance feature.

Z. Guang-Ping, et al.[88] in 2019, optimizing the conductance switching performance in photo switchable dimethyldihydropyrene/cyclophanediene

single-molecule junctions. Designing molecular switches with high stability and performance is still a great challenge in the field of molecular electronics. For this aim, key factors influencing the charge transport properties of molecular devices require to be carefully addressed.

A. A. Baraa Al-Mammory, et al. [89] in 2021, thermoelectric Properties of Oligoyne-Molecular Wires. Oligoynes are prototype molecular wires due to their conjugated system and the coherent tunneling transport, which aids this type of wires to transfer charges over long distances. The electric and thermoelectric characteristics for a series of Oligoyne molecular wires ((n) 3, 5, 7 and 9) are studied to explore the fundamental transport mechanisms for electrons crossing through single molecules, we probed both the electrical conductance and Seebeck coefficient for Au|molecule|Au configurations using (DFT).

The promising results of previous researches encouraged, M. Rasool Al-Utayjawee and A. Oday Al-Owaedi, [90] in 2021, Enhancement of Thermoelectric Properties of Porphyrinbased Molecular Junctions by Fano Resonances. Single-molecule porphyrin applications gain attention by using molecules as elementary blocks of electronic components involving metallic atoms. Theoretically, one type of molecular-scale porphyrin device is used in this article, consisting of organometallic single molecules with different metals (Zn, Mg, Cu and Fe), sandwiched between gold electrodes bound by thiol anchor groups. The transmission and Seebeck coefficients for Au|molecule|Au configurations were computed by using (DFT).

1.5 Aims of the Work

This research is aiming to investigate the electronic and thermoelectric properties of organometallic molecular junctions. Also, one of the main goals of this study is the exploring of some of optical characteristics such as HOMO-LUMO gap of these devices; Therefore, the goals of this work can be summarized as following:

- A study, of charge transport properties of three groups of organometallic compounds using four metals in each group , which are (Fe, Co, Ru and Pt) will be investigated using a combination of density functional theory (DFT) calculations, time-depending density functional theory (Td-DFT) . These molecules allow us to examine the relativistic effect of metal substitution on creating destructive quantum interference in a single molecule and its effect on the electronic properties of these devices.
- Optical and electronic structures, Seebeck's coefficient and other thermoelectric properties of a group of structurally related organometallic molecules will be studied. All particles will be performed using DFT (Gaussian and SIESTA) calculations.
- The different calculated properties of these nano-structures, will predicate their applications such as organometallic-electronic compounds in laser active media, dye-sensitized solar cells (DSSC), optical field effect transistors (OFET), organic light-emitting diodes (OLED) and in charge transport studies of single molecules.

2.1 Introduction

Quantum chemical calculations can assist researchers in designing and adapting target molecules while reducing the cost of tests. This is especially valuable for screening and monitoring high-energy materials (HEM). Molecular modeling is a collection of strategies for using a computer to examine chemical problems [91-94]. Clinicians and computational chemists can use one of four major approaches: Molecular Mechanics (MM), Semi-Empirical (SE), Ab initio, or Density Functional Theory (DFT) [95,96].

To predict the properties of the quantum mechanical system, an equation, describing how the wave function changes with time, is required. For one particle in one-dimensional system, this equation is the Schrödinger equation (Time dependent form) [97-100]:

$$i\hbar\frac{\partial}{\partial t}\Psi(\vec{r},t) = -\frac{\hbar^2}{2m}\nabla^2\Psi(\vec{r},t) + V(\vec{r})\Psi(\vec{r},t) = H(\vec{r},t)\Psi(\vec{r},t) \quad \text{.....(2.1)}$$

As

$$\hat{H}\,\Psi(\vec{r},t) = E\,\Psi(\vec{r},t) \quad \text{.....(2.2)}$$

Where $\hat{H}$ is the Hamiltonian operator, Ψ is the wave function and *E* is the system Eigen value. The Hamiltonian operator ($\hat{H}$) consists of two terms: the kinetic energy operator of the electrons and nuclei ($\hat{T}$) and potential energy components operator ($\hat{V}$), as follows:

$$\widehat{H} = \hat{T} + \hat{V} \quad \text{.....(2.3)}$$

The total Hamiltonian of the molecular system $\hat{H}$ containing M nuclei and N electrons can be expressed as follows [101,102]:

$$\hat{H} = \overbrace{-\frac{\hbar^2}{2m_i}\sum_{i=1}^{N}\nabla_i^2}^{electrons} - \overbrace{\frac{\hbar^2}{2M_A}\sum_{A=1}^{M}\nabla_A^2}^{nuclei} - \overbrace{\sum_{i=1}^{N}\sum_{A=1}^{M}\frac{Z_A}{r_{iA}}}^{electrons,nuclei} + \overbrace{\sum_{i=1}^{N}\sum_{j>i}^{N}\frac{1}{r_{ij}}}^{electrons} + \overbrace{\sum_{A=1}^{M}\sum_{B>A}^{M}\frac{Z_A Z_B}{r_{AB}}}^{nuclei} \quad \text{……..(2.4)}$$

Here ∇_i^2 is the Laplacian operator, in Cartesian coordinates is defined as:

$$\nabla_i^2 = \frac{\partial^2}{\partial x_i^2} + \frac{\partial^2}{\partial y_i^2} + \frac{\partial^2}{\partial z_i^2}$$

$$\hat{H}_{total} = \hat{T}_e + \hat{T}_n + \hat{V}_{ne} + \hat{V}_{ee} + \hat{V}_{nn} \quad \text{…..…….……(2.5)}$$

The total kinetic energy is defined in equations (2.4) and (2.5) as the sum of the electronic ($\hat{T}_e$) and nuclear ($\hat{T}_n$) kinetic energies. The total potential energy is comprised of three components: attractive interactions between nuclei and electrons ($\hat{V}_{ne}$), repulsive interactions between nuclei ($\hat{V}_{nn}$), and repulsive electron-electron interactions ($\hat{V}_{ee}$). $Z_{A,B}$ denotes the nuclear charges of atoms A and B, respectively; m_A denotes the mass of atom A; r_{iA} denotes the distance between nucleus A and electron i, r_{AB} denotes the distance between nuclei A and B; and r_{ij} denotes the distance between i and j electrons, and $r_{ij} = |\vec{r}_i - \vec{r}_j|$.

The Born-Oppenheimer Approximation allows for the separation of electronic and nuclear motions in molecules. The molecule's entire wave function is as follows [95, 96, 102]:

$$\Psi_{total} = \Psi_{electronic} \times \Psi_{nuclear.} \quad \text{...……...……..(2.6)}$$

Due to the fact that the nucleus is far heavier than electrons, nuclear motion is much slower than electronic motion. When the nucleus's kinetic energy is ignored, the nucleus's potential energy can be considered constant.

Additionally, the Hamiltonian operator can be devoid of the nucleus's potential and kinetic energies. The Hamiltonian operator $\hat{H}$ can be expressed as follows:

$$\hat{H}_e=\hat{T}_e + \hat{V}_{ne} + \hat{V}_{ee} \quad \text{.....(2.7)}$$

2.2 Hartree-Fock methods

To solve the Schrödinger equation for a system that employs the time-independent Schrödinger equation to describe the quantum mechanical behavior of all electrons in the system, it is necessary to calculate the multi-wave functions of the electrons, as solving the Schrödinger equation requires the solution of numerous simultaneous differential equations [102, 103].

In 1928, Hartree simplified the problem using an iterative self-consistent field "SCF" approach. Hartree speculated the shape of the multi-electron wave functions in order to simplify the challenge. These wave functions are characterized by the presence of simple plane waves. With this assumption in place, the covariance principle could be applied [101,102]. If an unknown collection of parameters describes a particular system, the set of parameter values can be stated as [94,96,102]:

$$E_{\emptyset} = \frac{\langle \emptyset | \hat{H} | \emptyset \rangle}{\langle \emptyset | \emptyset \rangle} \geq E_o \quad \text{.....(2.8)}$$

Where $E_{\emptyset}$ is the trial function's lowest-energy eigenvalue, ϕ is the trial function, and E_o is the ground-state energy. The Hartree-Fock method's wave function is more complicated than the Hartree product's wave function. It can, however, be expressed in a compressed form as a slater determinant. Because electrons are fermions with a spin of (1/2), the overall electronic wave

function will be anti-symmetric when any two electron coordinates are exchanged [93,94]. The determinant takes into account all electron spin and the Pauli Exclusion Principle, as well as whether electrons spin up ($+ ½ \; or \; \alpha$) or down ($- ½ \; or \; \beta$). For the N-electron system, the slater determinant is as follows [104, 105]:

$$\Psi = \frac{1}{\sqrt{N!}} \begin{vmatrix} \psi_1(1)\alpha(1) & \psi_1(1)\beta(1) & \psi_2(1)\alpha(1)\,\psi_2(1)\beta(1)\ldots & \psi_N(1)\alpha(1) & \psi_N(1)\beta(1) \\ \psi_1(2)\alpha(2) & \psi_1(2)\beta(2) & \psi_2(2)\alpha(2)\,\psi_2(2)\beta(2)\ldots & \psi_N(2)\alpha(2) & \psi_N(2)\beta(2) \\ \vdots & \vdots & \vdots & \vdots & \vdots \\ \psi_1(N)\alpha(N) & \psi_1(N)\beta(N) & \psi_2(N)\alpha(N)\,\psi_2(N)\beta(N)\ldots & \psi_N(N)\alpha(N) & \psi_N(N)\beta(N) \end{vmatrix} \quad \ldots\ldots\ldots\ldots\ldots(2.9)$$

Where Ψ is the electronic wave function; α and β is the spin of electrons, and $\frac{1}{\sqrt{N!}}$ is a normalizations factor [106]. The use of the iterative process of the self–consistent field producer yields the molecular orbitals to solve the Hartree–Fock equation $\Psi(\vec{r}_i)$ [107, 108].

$$\hat{F}\,\Psi_i(\vec{r}) = \epsilon_i \Psi_i(\vec{r}) \quad \ldots\ldots\ldots\ldots\ldots\ldots(2.10)$$

Where $\hat{F}$ delineates the Fock operator for a closed shell system.

$$\hat{F} = \hat{H}^{core}(1) + \sum_{L=1}^{n/2}(2\,\hat{J}_l - \hat{K}_l) \quad \ldots\ldots\ldots\ldots\ldots\ldots(2.11)$$

The one-electron Hamiltonian is the first operator of the Hartree-Fock Hamiltonian for an electron moving in the field of the bare nuclei $\hat{J}_l \; and \; \hat{K}_l$; its effect on $\Psi_i(\vec{r})$ and the exchange operator $\hat{K}_l$ is [94]:

$$\widehat{K}_l\Psi_i(r) = \int \frac{\Psi_l^*(\vec{r})\Psi_i(\vec{r})}{\left|\vec{r}-\overrightarrow{r'}\right|}\, dv'\, \Psi_l(\vec{r}') \qquad \text{…….……...(2.12)}$$

And Coulomb operator, $\widehat{J_l}$ is:

$$\widehat{J_l}\Psi_i(\vec{r}) = \int \frac{\Psi_l^*(\vec{r})\Psi_l(\vec{r})}{\left|\vec{r}-\overrightarrow{r'}\right|}\, dv'\, \Psi_i(\vec{r}) \qquad \text{…….……...(2.13)}$$

Equation (2.12) shows the quantum mechanical correction term. The linear combination atomic orbital (LCAO) method for an individual molecular orbital is defined as [94]:

$$\Psi_i = \sum_{\mu=1}^{N} C_{\mu i}\, \emptyset_\mu \qquad \text{…….……(2.14)}$$

$C_{\mu i}$ is the molecular orbital expansion coefficients. The basic functions ϕ_μ are chosen to be normalized.

The exact energy E_o of the ground state of the system within the selected limits, or the exact solution of the Schrodinger equation [109-112] is:

$$E(\emptyset_1, \emptyset_2, \dots\dots\dots, \emptyset_n) \geq E_o \qquad \text{……..(2.15)}$$

The equality sign shall be applied only when Ψ is the exact ground state function.

2.3 Density Functional Theory

It is vital to have a credible source of structural and electronic knowledge in order to comprehend the behavior of molecular electronic devices. In this section, a quick overview of (DFT) [103,113] is given, which was widely used during my PhD study as a theoretical tool for assessing the quality and quantity of molecular structures, charge density, and band structures.

DFT determines the system's ground state properties, with electron density playing a significant role. At the moment, it is the most successful method for calculating matter's electrical structure. It is applicable to a wide variety of particles, ranging from atoms through molecules, solids, and nuclei. It is capable of predicting a wide variety of molecular properties, vibrational frequencies, molecule structures, ionization energies, dissolution energies, interaction paths, electrical and magnetic properties, and so on [114,116].

(DFT) is a theory of quantum mechanics used in physics and chemistry to examine the electronic structure (primarily the ground state) of multi-body systems, including atoms and molecules. Using this theory, the parameters of a multi-electron system can be calculated using a functional, that is, functions of another function, which in this case is the spatially dependent electron density. Hence the term DFT from the application of functional electron density. DFT is among the most popular and adaptable techniques available in condensed matter physics, computational physics, and computational chemistry [117].

Methods in quantum mechanics can be classified into two categories: ab initio methods and semi-empirical methods. Hartree-Fock theory (HF), formation configuration interaction theory (CI), perturbation theory (PT), and density functional theory (DFT) are all examples of ab initio approaches (DFT). These methods begin with the Schrödinger equation and do complete integration without the need of empirical components derived from empirical measurement [118].

The DFT's fundamental premise is that an electronic system's energy can be expressed in terms of the electron's potential density. $\rho(r)$ signifies the

overall electron density at a particular point r in space for a system of n electrons. The electronic energy E is said to be a function of electron density and is indicated as E(ρ), indicating that there is only one corresponding energy for a given function ρ(r) [119].

Thomas and Fermi created the Thomas-Fermi model in 1927, which served as a functional precursor to density theory. Thomas and Fermi computed an atom's energy by plotting its kinetic energy against its electron density. They combined this with classical formulas for nuclear-electron and electron-electron interactions, both of which may be expressed in terms of the electron density [120].

DFT calculates the characteristics of a multiparticle system as a function of the electron density (r). The electron density of a given condition is defined as the number of electrons per unit volume. It is independent of the amount of electrons in the system and is hence [121]:

$$N = \int \rho(\vec{r}\,)\, d\vec{r} \qquad \text{.....(2.16)}$$

The basic concept of DFT, a tool for computing ground state properties of metals, insulators, and semiconductors [122], is based on ground state energy; All other electronic properties of the ground state are uniquely determined by the electron density. Today, DFT is one of the most important tools in this field.

The fundamental premise of DFT, a technique for determining the ground state properties of metals, insulators, and semiconductors [123], is that the ground state energy determines all other electronic properties of the ground state [103]. Today, DFT is a significant instrument in this sector.

2.3.1 The Schrödinger Equation and Variational Principle

The Schrödinger equation can be used to describe any system composed of several non-relativistic particles:

$$H\Psi_i(\vec{r}_1,\vec{r}_2..\vec{r}_N,\vec{R}_1,\vec{R}_2..\vec{R}_M) = E_i\Psi_i(\vec{r}_1,\vec{r}_2..\vec{r}_N,\vec{R}_1,\vec{R}_2..\vec{R}_M) \quad \text{……(2.17)}$$

Here, $\widehat{H}$ is the Hamiltonian operator for a system composed of N electrons and M nuclei that describes the interaction of particles, where Ψi denotes the wave function of the system's i^{th} state and E_i denotes the numerical value of the energy associated with the state denoted by Ψi. The Hamiltonian factor for such a system can be expressed as the sum of five terms defined in [123-126].

$$H = \overbrace{-\frac{\hbar^2}{2m_e}\sum_{i=1}^{N}\nabla_i^2}^{T_e} \overbrace{-\frac{\hbar^2}{2m_n}\sum_{n=1}^{M}\nabla_n^2}^{T_n} \overbrace{-\frac{1}{4\pi\varepsilon_o}\sum_{i=1}^{N}\sum_{n=1}^{M}\frac{Ze^2}{|\vec{r}_i-\vec{R}_n|}}^{U_{en}} + \overbrace{\frac{1}{8\pi\varepsilon_o}\sum_{i=1}^{N}\sum_{j\neq i}^{N}\frac{e^2}{|\vec{r}_i-\vec{r}_j|}}^{U_{ee}}$$
$$+ \overbrace{\frac{1}{8\pi\varepsilon_o}\sum_{n=1}^{M}\sum_{n\neq\acute{n}}^{M}\frac{Z_nZ_{\acute{n}}e^2}{|\vec{R}_n-\vec{R}_{\acute{n}}|}}^{U_{nn}} \quad \text{……(2.18)}$$

Here i and j denote the N-electrons while n and n' running on the M-nuclei in the system, m_e and m_n are the mass of the electron and nucleus respectively, e and Z_n are the electron and nuclear charge respectively. The position of the electrons and nuclei are denoted as $\vec{r}_i$ and $\vec{R}_n$ respectively.

In the equation (2.18), the first and second terms, T_e and T_n represent the kinetic energy of electrons and nucleus, respectively. The last three terms represent the potential part of the Hamiltonian; where U_{en} defines the

attractive electrostatic interaction between electrons and nucleus. Electron-electron, U_{ee} and nuclear-nuclear, U_{nn} describe the repulsive part of the potential respectively [127,128].

When solving the Schrödinger equation (equation 2.17) and knowing the wave function Ψ, all important physical quantities can be calculated. However, even for modest system sizes - even for a few atoms - the general problem is virtually impossible even on modern supercomputers [128].

The virtue of density functional theory is that it expresses the physical quantities in terms of the ground-state density. The electronic density of a general many body state, characterized by a wave function $\Psi(r_1,r_2\ldots..r_{n)}$, is defined as [129]:

$$\rho(r) = \int dr_1\, dr_2 dr_3 \ldots\ldots\ldots dr_i\, |\Psi(r_1, r_2, r_3 \ldots\ldots r_i|^2 \qquad \ldots\ldots\ldots\ldots\ldots\ldots(2.19)$$

2.3.2 The Hohenberg-Kohn Theorems

In 1964 [130], P. Hohenberg and W. Kohn developed the density functional theory, which established that the ground state of a many-electron system can be determined by its ground state electron density ρ(r) [103,131] or that there is a close and unambiguous relationship between the ground state energy and the density, ρ(r), of an interacting electron system. The Hohenberg-Kohn theorems are two extremely straight forward but extremely powerful statements:

Theorem (1): states that a multi-electron system's ground state energy is a unique and universal function of the ground state electron density ρ(r). E_{HK} is a function of the ground state density ρ(r).

Theorem (2): says that given a multi-electron system, the ground state energy function is reduced by the ground state electron density ρ(r). External potential V_{ext} is a one-of-a-kind function of density ρ(r). Given that V_{ext} is a Hamiltonian fix for system H, it is obvious that the multi-whole body's ground state is a unique function of ρ(r). E_v ground state energy function is as follows [104,132]:

$$E_V[\rho] = \int \rho(\vec{r})\, V_{ext}(\vec{r})d\vec{r} + F_{HK}[\rho] \qquad \text{.....(2.20)}$$

Where $F_{HK}[\rho]$ is a function of $\rho(\vec{r})$ to be determined; it consists of the kinetic energy and all electron-electron interactions; and $V_{ext}(r)$ is the external potential. The ground state energy anisotropy satisfies the following principle [132]:

$$\delta\{E_V[\rho] - K[\int \rho(\vec{r})\, d\vec{r} - N]\} = 0 \qquad \text{.....(2.21)}$$

Which gives

$$K = \frac{\delta E_V[\rho]}{\delta\rho(r)} = V_{ext}(\vec{r}) + \frac{\delta F_{HK}[\rho]}{\delta\rho(r)} \qquad \text{.....(2.22)}$$

Where K denotes the chemical potential and $F_{HK}[\rho]$ denotes a globally independent function of the external potential $V_{ext}(\vec{r})$. Hohenberg-Kohn theory from equation (2.21) and equation (2.22), was first proposed and meant to handle the non-spin polarized electron state, but was later extended to include the spin–polarized electron state, finite temperature, and relativistic conditions [130]. The Hohenberg–Kohn theorems established the fundamental concept that the ground state electron density serves as the foundation for all ground

state physics in a multi-electron system. However, these theories did not specify the kinetic, commutative, or associative functions. Simultaneously, no one knows how to generate a multi–electron system's ground state electron density ρ(r) [132].

The Hamilton operator of n-electron system within the Born-Oppenheimer approximation can be described by [133]:

$$\hat{H} = \hat{T} + \hat{V}_{ext} + \hat{V}_{ee} \quad \text{..... (2.23)}$$

The external potential $\hat{V}_{ext}$ is uniquely defined by the electron density ρ(r). The total energy can be written as:

$$E_T = T[\rho_o] + \int V_{ext}(\vec{r})\rho_o(\vec{r})dr + J[\rho_o] + E_{NC}[\rho_o] \quad \text{.....(2.24)}$$

Where $T[\rho_o]$ is the kinetic energy, $E_{NC}[\rho_o]$ is the non-classical electron–electron interaction energy and $J[\rho_o]$ is the classical coulomb energy defined as:

$$J[\rho_o] = \frac{1}{2} \iint \frac{\rho_o(\vec{r}_1)\rho_o(\vec{r}_2)}{|\vec{r}_1 - \vec{r}_2|} dr_1 dr_2 \quad \text{..... (2.25)}$$

V_{ext} directly depends on the system and it is simply the coulomb potential of the nuclei. Therefore, the total energy can be written as:

$$E_T = \int V_{ext}(\vec{r})\rho_o(\vec{r})dr + F_{HK}[\rho_o] \quad \text{..... (2.26)}$$

Where F_{HK} is a universal functional of the electron density:

$$F_{HK}[\rho] = T[\rho]+J[\rho]+E_{NC}[\rho] \quad \text{..... (2.27)}$$

Hohenberg-Kohn theorem assumes that F_{HK} exists, but the actual form of F_{HK} is unknown and must be approximated [133].

2.3.3 The Kohn-Sham Theorems

Thus far, shown that determining the ground-state density enables one to calculate the ground-state energy and other quantities. The precise form of the functional presented in equation:

$$E(\rho) = T(\rho) + E_{int}(\rho) + \int dr\, V_{ext}(\vec{r})\rho(\vec{r}) \qquad \ldots\ldots\ldots\ldots\ldots\ldots(2.28)$$

This is an unknown equation. In general, the kinetic term and internal energy of interacting particles cannot be represented as density-dependent functions. Kohn and Sham proposed the solution in 1965 [124]. According to Kohn and Sham, the original Hamiltonian of the system can be replaced with an effective Hamiltonian of non-interacting particles in an effective external potential with the same ground-state density as the original system. Due to the lack of a clear recipe for accomplishing this, it is significantly easier to solve a non-interacting problem.

According to Hohenberg and Kohn, the energy functional $F_{HK}[\rho]$ of an interacting many–electron system can be expressed as [133]:

$$F_{HK}[\rho] = T\,[\rho] + \frac{1}{2}\iint \frac{\rho(\vec{r})\,\rho(\overrightarrow{r'})}{\left|\vec{r}-\overrightarrow{r'}\right|}\, d\vec{r}\,d\overrightarrow{r'} + E_{XC}[\rho] \qquad \ldots\ldots\ldots\ldots\ldots\ldots(2.29)$$

Where T[ρ] represents the system's kinetic energy. The second term is the classical coulomb energy; and the third term, Exc[ρ], is the exchange correlation energy, which describes non–classical electron interactions, including all many–body effects.

However, a first principle computation could not be performed because the concrete expressions for functional T[ρ] and $E_{XC}[\rho]$ were not provided. To address this issue, Kohn and Sham suggested an approach based on the assumption of a non-interacting many–electron system with the same electron number N and ground state electron density ρ(r) as an interacting many–electron system under an external potential V_{ext}(r). The fundamental concept is as follows: for a non–interacting system, ρ(r) can be written as a set of auxiliary orthogonal functions $\Psi i(\vec{r})$ as [133,134]:

$$\rho(\vec{r}) = \sum_i \Psi_i^*(\vec{r})\,\Psi_i(\vec{r}) \qquad \text{…….……(2.30)}$$

With $\langle \Psi_i | \Psi_j \rangle = \delta_{ij}$ the Kohn-Sham kinetic energy was given by:

$$T_{KS}[\rho] = -\frac{\hbar^2}{2m} \int \sum_{i=1}^{N} \Psi_i^*(\vec{r})\,\nabla^2\,\Psi_i(\vec{r})\,dr \qquad \text{…….……..(2.31)}$$

Considering the many-body interaction, the true kinetic energy $T[\rho]$ in equation (2.31) is not equal to $T_{KS}[\rho]$. The difference between $T[\rho]$ and non–interacting electron system $T_{KS}[\rho]$ can be combined with non-classical energy $E_{NC}[\rho]$ of interacting electron system as [124]:

$$E_{XC}[\rho] = E_{NC}[\rho] + T[\rho] - T_{KS}[\rho] \qquad \text{.....……(2.32)}$$

Where $E_{NC}[\rho] = V_{ee}[\rho] - J[\rho]$

The ground state energy functional can be written as:

$$E_V[\rho] = T_{KS}[\rho] + \frac{1}{2} \iint \frac{\rho(\vec{r})\,\rho(\vec{r'})}{|\vec{r} - \vec{r'}|}\,d\vec{r}d\vec{r'} + E_{XC}[\rho] + \int \rho(\vec{r})\,V_{ext}(\vec{r})d\vec{r}$$

...……(2.33)

Applying the variational principle we get:

$$\frac{\delta}{\delta\Psi_i^*(\overrightarrow{r})}\{E[\rho] - \int d\vec{r}\ \sum_i \epsilon_i\ \Psi_i^*(\vec{r})\ \Psi_i(\vec{r})\} = 0 \qquad \text{.....(2.34)}$$

The Kohn- Sham equations:

$$\left\{-\frac{\hbar^2}{2m}\nabla^2 + \int \frac{\rho(\overrightarrow{r'})}{\left|\vec{r}-\overrightarrow{r'}\right|} d\overrightarrow{r'} + V_{Xc}[\rho] + V_{ext}(\vec{r})\right\}\Psi_i(\vec{r}) = \epsilon_i\ \Psi_i(\vec{r}) \text{ .....(2.35)}$$

Where, $V_{Xc}[\rho] = \frac{\delta E_{Xc}[\rho]}{\delta\rho(\overrightarrow{r})}$

Is the exchange–correlation potential that has been updated in equation (2.32) to include all changes in kinetic energy between interacting and non-interacting systems. It is worth emphasizing that the Kohn-Sham equation must be self–consistent when evaluating the influence of the electron density ρ(r) on the wave function $\Psi i(\overrightarrow{r})$. The total energy of a system can be determined by solving a set of Kohn-Sham equation (2.35) self-consistently.

$$E = \sum_i^N f_i\varepsilon_i - \frac{1}{2}\iint \frac{\rho(\vec{r})\,\rho\left(\overrightarrow{r'}\right)}{\left|\vec{r}-\overrightarrow{r'}\right|}\ d\vec{r}d\overrightarrow{r'} + E_{XC}[\rho] - \int d\vec{r}\ \rho(\vec{r})\,V_{ext}(\vec{r}) \text{ ...(2.36)}$$

The total energy is not equal to the sum of the energy of individual electrons ϵ_i. The energy required to transition from (i) to (j) states is not simply ϵ_i-ϵ_j; consequently, the physics of the Kohn-Sham equation is not identical to that of the Schrodinger equation [125,128].

2.4 The Exchange Correlation Functional

The literature has various proposals for the exchange and correlation of energy. The first successful - and still basic - form was the Local Density

Approximation (LDA) [135], which is a local functional that depends solely on the density. Then came the Generalized Gradient Approximation (GGA) [136], which, in addition to the density derivative, provides information about the neighborhood, making it semi-local.

LDA and GGA are the two most frequently used approximations in density functional theory for the exchange and correlation energy. Additionally, there are various additional functionalities that extend beyond LDA and GGA. Several of these functionals are tuned to the special requirements of the basis sets used to solve the Kohn-Sham equations (equation 2.35)and a sizable category are the so-called hybrid functionals (e.g. B3LYP , and Para hybrid GGA), which combine the LDA and GGA forms.

The Van der Waals density functional (Vd W-DF) [136, 137], one of the most recent and universal functionals, comprises non-local terms and has been shown to be extremely accurate in systems with significant dispersion forces [136].The following sections will discuss the Local Density Approximation and the Generalized Gradient Approximation in further detail.

2.4.1 Local Spin Density Approximation

The exchange correlation potential is described in terms of the density of and spins using the local spin density approximation (LSDA). It was created to do property calculations on open-shell systems [134].

$$E_{Xc}^{LDA}[\rho_\alpha , \rho_\beta] = \int \rho(\vec{r})\, \varepsilon_{Xc}\, (\rho(\vec{r})_\alpha , \rho(\vec{r})_\beta)\, d\vec{r} \qquad \text{.....(2.37)}$$

Where E_{XC} denotes the exchange-correlation energy associated with each particle. For some features such as vibrational frequencies, equilibrium

structures, and dipole moments, LSDA outperforms HF. In general, the LSDA delivers reliable information for systems that closely resemble a uniform electron gas, i.e. those with a slowly varying density with position. However, in fact, atomic and molecular systems do not have uniform electron concentrations, necessitating the development of more complicated models [138].

2.4.2 Generalized Gradient Approximation

GGA extends LDA by including the derivatives of the density into the functional form of the exchange and correlation energies. In this case there exists no closed form for the exchange part of the functional, hence it has to be calculated along with the correlation contributions using numerical methods. Just as in the case of the LDA there exist many parameterizations for the exchange and correlation energies in GGA [136].Generalized gradient approximations (GGA's) for the exchange-correlation energy improve upon the local spin density (LSD) description of atoms, molecules, and solids, presenting a simple derivation of a simple GGA, in which all parameters (other than those in LSD) are essential constants [138,139].

$$E_{xc}^{GGA}[\rho_\alpha, \rho_\beta] = \int f(\rho_\alpha, \rho_\beta, \nabla\rho_\alpha, \nabla\rho_\beta)\, d\vec{r} \qquad \text{.....(2.38)}$$

This functional generally offers an improvement over the LSDA because they account for the variation of density with position. To simplify the problem, (E_{xc}) is often written as the sum of an exchange (E_x) and correlation (E_c) terms [135]:

$$E_{xc} = E_x + E_c \qquad \text{.....(2.39)}$$

The exchange-energy functional can then be obtained from the HF exchange term with the Kohn-Sham orbitals. Various exchange and correlation functionals have been separately developed and can be combined in different ways. For instance, one popular (GGA) functional is B3LYP, where Becke's 1988 exchange functional is paired with the Lee-Yang-Parr correlation functional [138].

LDA and GGA are the two most commonly used approximations for the approximation of exchange-correlation energies in the DFT. Also, there are several other functionals, which go beyond LDA and GGA. In general, there is no robust theory of the validity of these functionals. It is determined via testing the functional for various materials over a wide range of systems and comparing results with reliable experimental data.

2.4.3 The Hybrid Functional

The hybrid functionals are extremely good at accurately representing a wide variety of molecular characteristics. Calculating the exact (Hartree-Fock) exchange in big molecules and solids, particularly in systems with metallic properties, is computationally expensive. The most widely used hybrid functional, B3LYP, employs Becke's 1988 exchange function (E_X^{B88}) and Lee Yang and Parr's correlation function (E_C^{LYP}) as gradient adjustments to the LSDA exchange and correlation functions, respectively [138-141].

$$E_{XC}^{B_3LYP} = (1 - a)E_X^{LSDA} + a\,E_X^{HF} + bE_X^{B88} + \mathrm{c}\,E_C^{LYP} + (1 - \mathrm{c})E_C^{LSDA} \quad \text{.....(2.40)}$$

The three parameters are: a=0.20, b=0.72 and c=0.81. Where'a' specifies the amount of exact exchange, and 'b' and 'c' control the contribution of exchange and correlation, respectively.

2.5 Pseudopotentials

I have demonstrated that by using the Kohn-Sham formalism to define an exchange-correlation functional, it is possible to break a large interacting problem into a big effective non-interacting problem. This significantly simplifies the situation from a physical standpoint. However, in typical molecular systems with a large number of atoms, the calculation is still quite large and may be computationally expensive. To reduce the amount of electrons in an atom, one can inject pseudopotentials that effectively eliminate the atom's core electrons. Fermi developed pseudopotentials in 1934 [139], and approaches have evolved since then, from constructing less realistic empirical pseudopotentials to more realistic ab-initio pseudopotentials [139, 140].

The electrons in an atom are classified into two types: core and valence electrons, with core electrons located within completely filled atomic shells and valence electrons located in partially filled shells. In addition to the fact that core electrons are spatially restricted around the nucleus, when atoms are brought together, only valence electron states overlap, implying that in most systems, only valence electrons contribute to the formation of molecular orbitals. This enables the core electrons to be removed and replaced with a pseudopotential, yet the valence electrons retain the same screened nucleon charge as if the core electrons remained. This significantly reduces the number

of electrons in a system, reducing the time and memory necessary to calculate the properties of molecules with a large number of electrons.

2.6 Time-Dependent Density Functional Theory (TD-DFT)

The time-dependent density functional theory (TD-DFT) extends the ground-state density functional theory by allowing for the examination of a system's excited-state features in the presence of time-dependent potentials, such as electric or magnetic fields. TD-DFT may be used to investigate the influence of fields on molecules by calculating representative excitation energies, oscillator strength, wavelength, molecular orbital character, and electronic transitions of the molecules [141].

The theoretical of TD-DFT based on the Runge-Gross theorem (R-G theorem) in 1984. The R-G theorem explained the association between the time-dependent external potential $\hat{V}_{ext}(\vec{r})$ and $\rho(\vec{r},t)$ of the system. R-G theorem designated that when two external potentials $\hat{V}_{ext}(\vec{r})$ and $\widehat{V'}_{ext}(\vec{r})$ have an alteration of more than a time-dependent function, their own electron densities $\rho(\vec{r},t)$ and $\rho'(\vec{r},t)$ are also dissimilar [142].

Runge and Gross discussed how excited states are obtained using TD-DFT. The starting point of studying time-dependent systems is the time-dependent Schrodinger equation. The TD-DFT is straight related to the Schrodinger equation $\left[\boldsymbol{i}\,\hbar\,\frac{\boldsymbol{\partial}}{\boldsymbol{\partial t}}\,\boldsymbol{\Psi}\,(\,\vec{\boldsymbol{r}}\,,\boldsymbol{t}\,)=\,\hat{\boldsymbol{H}}\,\boldsymbol{\Psi}\,(\,\vec{\boldsymbol{r}}\,,\boldsymbol{t}\,)\right]$ where the Hamiltonian is known to be [143]:

$$\hat{H} = \hat{T} + \hat{V}_{\text{elec.elec}} + \hat{V}_{\text{ext.}}(\vec{r}) \qquad \text{.....(2.41)}$$

Here, $\hat{H}$ consists of the kinetic energy operator $\hat{T}$ electron-electron repulsion $\hat{V}_{\text{elec.elec}}$ (Coulomb operator) and the external potential $\hat{V}_{\text{ext.}}(\vec{r})$. Where $\hat{V}_{\text{ext.}}(\vec{r})$ is given in the following operators:

$$\hat{V}_{\text{ext.}}(\vec{r}) = \sum_{i=1}^{N} \hat{V}\text{ext.}(\vec{r_i}) \qquad \text{…….……(2.42)}$$

The densities of the system rise from a fixed first state $\Psi(t_o) = \Psi(0)$. The first state, $\Psi(0)$ is arbitrary, it must not be the ground-state or some other eigen state of the first potential $\hat{V}\text{ext.}(\vec{r}) = \hat{V_o}(\vec{r})$. The R-G theorem indicates that there exists an one-to-one correspondence between the time-dependent external potential $\hat{V}\text{ext.}(\vec{r})$, and the time-dependent electron density $\rho(\vec{r}, t)$, for systems developing from a fixed first many-body state. Translation to it, the density determines the external potential, and next helps in obtaining the time-dependent many-body wave functions [145].

As this wave-function controls all observables of the system as an important, the saying point is that all observables are functionals of $\rho(\vec{r}, t)$. The statement of the theorem is the "densities $\rho(\vec{r}, t)$ and $\rho'(\vec{r}, t)$ evolving from the same initial state $\Psi(0)$ under the effect of two potentials $\hat{V}\text{ext.}(\vec{r})$ and $\widehat{V'}_{ext}(\vec{r})$ are always different provided that the potentials differ by additional than a chastely time-dependent function [141,143]:

$$\hat{V}\text{ext.}(\vec{r}, t) = \widehat{V'}_{ext}(\vec{r}, t) + C(t) \qquad \text{…….……..(2.43)}$$

Where the C(t) allows increase to wave functions that are different only by a phase factor $e^{-iC(t)}$, therefore, the same electronic density is stable. R-G theorem states that the density is a functional of the external potential and of

the first wave function on the space of potentials differing by more than the addition of C(t).

2.7 Basis Set

In theoretical physics and chemistry, a basis set is a collection of mathematical functions that are used to explain the form of molecular orbitals. Both ab-initio and DFT approaches make use of basis sets to specify the molecular orbitals in a system quantitatively. While it is possible to develop a basis set from scratch, the vast majority of calculations are performed using pre-existing basis sets. The correctness of the results is dependent on the type of calculation used and the basis sets used. Slater-type orbitals (STOs) and Gaussian-type orbitals (GTOs) are two forms of basis sets [143].

2.7.1 Slater Type Orbitals (STO's)

Slater type functions show a correct behavior near the nuclei at r → 0 with an intermittent behavior. The Slater type orbitals have the form [91]:

$$X^{STO} = N\, r^{n-1}\, e^{-\xi r}\, Y_{lm}(\theta, \varphi) \qquad \text{.....(2.44)}$$

Where, N is a major quantum number and ξ is a constant related to the effective charge of the nucleus. Y_{lm} is a spherical harmonic which describes the angular part of the wave function.

2.7.2 Gaussian Type Orbitals (GTO's)

The Gaussian type orbitals (GTOs) basis function is widely used in HF and related approaches because it enables the calculation of many-center

integrals analytically. In terms of Cartesian coordinates, Gaussian type orbitals can be written as [95]:

$$X^{GTO} = N\, x^{lx}\, y^{ly}\, z^{lz}\, e^{-\xi r^2} \quad \text{.....(2.45)}$$

N is a normalization factor; the sum of lx, ly and lz determines the type of orbitals; and ξ represents the orbital exponent that shows compact large ξ or diffuse small ξ is the resulting function, r^2 dependence in the exponential is insufficiency of the GTO's related to the Slater-type orbitals STO's.

One of the negative aspects of STO's is that many-center integrals such as Coulomb and HF-exchange terms are hard to compute with STO's. For this reason, it plays no role in modern wave function based quantum chemistry codes. As a result, for the calculations of Coulomb and HF-exchange terms, the analytical solution is available for the Gaussian functions. In order to improve the GTO basis sets, one usually. employs a contracted GTO basis set, in which several primitive Gaussian functions are mixed to give a contracted Gaussian function (CGF) as [134]:

$$X_j^{CGF} = \sum_i^M C_{ij}\, X_a^{GTO} \quad \text{.....(2.46)}$$

M is the number of Gaussian primitives employed in a linear combination in this case. Gaussian uses a variety of different basis sets, including minimum basis sets, split valence sets, polarization and diffuse functions, and others [103].

Extending a basis set is as simple as increasing the number of basis functions utilized per orbital. The valence double-zeta (VDZ) basis set employs two basis functions per valence orbital, the valence triple-zeta (VTZ) basis set employs three, and so forth. For example, the 6-31G basis set

employs a set of six primitives condensed to a single basis function for each core orbital and a split-valence of three primitives and one primitive for each valence orbital. While split valence basis sets improve the description of molecular orbitals, they are still incapable of producing their own balanced basis set [121].

Polarization functions are frequently utilized because they produce more accurate calculated geometries and vibrational frequencies [97]. To improve the results, the basis set must be supplemented by polarization functions [103]. Polarization functions with a greater angular momentum include the d- and f-type functions for heavy atoms and the p- and d-type functions for hydrogen and helium atoms. This increases the basis set's versatility by allowing the orbital's form to change (polarized in one direction). The relativistic Effective-Core Potentials (ECPs) of heavy metals, such as the Stuttgart Dresden triple zeta ECPs (SDD) basis set, are employed. For heavy metals, the Los Alamos National Laboratory's 2-double-zeta (LANL2DZ) and SDD basis sets are strongly suggested. Scalar relativistic corrections are more stringent than ECP corrections, and spin-free computations are not much more expensive [140,146].

2.7.3. SIESTA Basis Sets

It is self-evident that the Hamiltonian must be diagonalised in order to find the wave functions. This operation entails the inversion of a large matrix, the computing time of which scales according to the number of non-zero members. As a result, for efficient calculations, the Hamiltonian must be sparse with a large number of zeros. SIESTA makes use of a Linear Combination of Atomic Orbitals (LCAO) basis set, which is formed from the

atoms' orbitals and is required to be zero after a predetermined cut-off radius. As the overlap between basis functions decreases, the former produces the needed sparse form of the Hamiltonian, while the latter permits even a small basis set to yield properties similar to those of the examined system. The simplest basis set for an atom is called a single ζ basis, which corresponds to a single basis function, $\Psi_{nlm}(r)$ per electron orbital (i.e. 1 for an s-orbital, 3 for a p-orbital, etc.). In this case each basis function consists of a product of one radial wave function, $\emptyset_{nl}^{1}$ and one spherical harmonic Y_{lm}:

$$\Psi_{nlm}(r) = \emptyset_{nl}^{1}(r)\, Y_{lm}(\theta, \emptyset) \qquad \text{.....(2.47)}$$

The radial part of the wave function is found by using the method proposed by Sankey [147,148], where the Schrodinger equation is solved for the atom placed inside a spherical box. It is under the constraint to vanish at a cut-off radius r_c. This constraint produces an energy shift δE within the Schrödinger equation such that the eigen functions first node occurs at r_c:

$$\left[-\frac{d^2}{dr^2} + \frac{l(l+1)}{2r^2} + V_{nl}^{ion}(r)\right]\emptyset_{nl}^{1}(r) = (\varepsilon_{nl} + \delta E)\emptyset_{nl}^{1}(r) \qquad \text{.....(2.48)}$$

For higher accuracy basis sets (multiple-ζ), additional radial wave functions can be included for each electron orbital. The additional radial wave functions, phi_{nl}^{i} for $i > 1$, are calculated using a split-valence method. This involves defining a split valence cut off for each additional wave function r_s^i , so it is split into two piecewise functions: a polynomial below the cut-off and the previous basis wavefunction above it:

$$\emptyset_{nl}^{i}(r) = \begin{cases} r^{l}(a_{nl} - b_{nl}r^{2}) & r < r_{s}^{i} \\ \emptyset_{nl}^{i-1} & r_{s}^{l} < r < r_{s}^{l-1} \end{cases} \qquad \text{……..(2.49)}$$

The additional parameters are found at the point r_s^i where the wavefunction and its derivative are assumed continuous.

Further accuracy (multiple-ζ polarized) can be obtained by including wave functions with different angular momenta corresponding to orbitals which are unoccupied in the atom. This is done by solving (equation 2.49) in an electric field such that the orbital is polarized or deformed due to the field (see [149] for details) so a different radial function is obtained. This is now combined with the appropriate angular dependent spherical harmonic which increases the size of the basis. Table (2.1) shows the number of basis orbitals for a selected number of atoms for single-ζ, single- ζ polarized, double- ζ and double- ζ polarized.

Table 2.1: Examples of the radial basis functions per atom as used within the SIESTA for different degrees of precisions.

Basis Set	H	C	Au
Single-ζ (SZ)	1= (1 × 1s)	4= (1×2s+3×2p)	6 = (1 × 6s + 5 × 5d)
Double-ζ (DZ)	2= (2 × 1s)	8 = (2×2s +6×2p)	12 = (2 × 6s + 10 × 5d)
Single-ζ Polarised (SZP)	4=(1×1s+3×2p)	9 = (1×2s+3×2p+5×3$\tilde{d}$)	9 = (1× 6s+5×5d+3×6$\tilde{p}$)
Double-ζ Polarised (DZP)	5=(2×1s+3×2p)	13 = (2×2s+6×2p+5×3$\tilde{d}$)	15 = (2×6s+10×5d+3×6$\tilde{p}$)

2.8 Theory of Quantum Transport

The purpose of molecular electronics is to gain an understanding of the electrical properties and behavior of molecular junctions. One of the difficulties is delivering molecular structures of electrode blocks for the purpose of examining their electrical properties. Connection In general, the force between the molecule and the metal electrode has a significant role. In determining the transport properties of a lead | molecule | lead frame as a result of scattering processes within the lead | molecule | lead frame. The primary theoretical way for understanding scattering in this System is using the Green's function formalities [148].

Our objective in this section is to gain a general understanding of Landauer's formalism, and we will begin with a simple derivation of the Landauer formula. A one-dimensional construction is presented to demonstrate the overall methods utilized in the description. Transport in arbitrarily complex-geometry intermediate conductors. Assume this procedure. The interaction between carriers and inelastic processes is negligible, which is a well-known fact for molecules less than 3nm in length at ambient temperature [143].

2.8.1 Green’s Function Scattering Formalism

We apply a Green function scattering formalism to determine the transmission coefficient of a molecule coupled to semi-infinite leads. This is a continuation of the next chapter's discussion of calculating the electronic structure of an isolated molecule using DFT. The isolated molecule's properties and the interaction between the molecule and the electrodes have an

effect on the open system's electronic properties. As a result, transport models must account for both aspects in order to comprehend the electron scattering process between the two electrodes [147].

To begin, it is necessary to determine the scattering matrix for a basic one-dimensional system. This section will detail the approach employed. Due to the fact that Green's function will be employed in the derivation, I will first describe the form of Green's function for a basic one-dimensional lattice (Section 2.8.1.1) then we'll calculate the scattering matrix in one dimension, Scattered (Section 2.8.1.2).

2.8.1.1 Perfect One-Dimensional Lattice

In this section will discuss what the Green's function looks like for a simple one dimensional lattice with on-site energies ε_o and real hopping parameters as shown in Fig. (2-1).

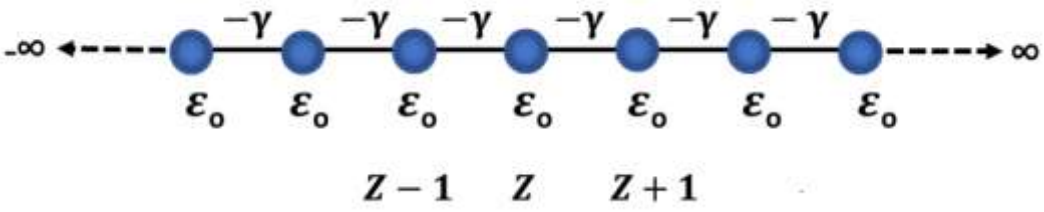

Figure (2-1): One-dimensional periodic lattice tight-binding approximation with on-site energies ε_o and hopping parameters γ[147].

The Schrödinger equation describes the wave function of the system with Hamiltonian H [147,148],

$$\hat{H}\,\psi = E\,\psi \qquad \text{…….……(2.50)}$$

Wave function Ψ_z it is expanded into a one-dimensional orthogonal localized basis set $|z'\rangle$:

$$|\psi\rangle = \sum \psi_{z'} |z'\rangle \qquad \text{.....(2.51)}$$

Substituting equation (2.51) in equation (2.50) and multiply the result by $|z\rangle$ we get:

$$\sum H_{z,z'} \psi_{z'} = E\psi_z \qquad \text{.....(2.52)}$$

Hence,

$$H_{z,z'} = \langle z|\widehat{H}|z'\rangle \qquad \text{.....(2.53)}$$

The matrix form of the Hamiltonian can be simply written:

$$H = \begin{pmatrix} \ddots & -\gamma & 0 & 0 \\ -\gamma & \varepsilon_o & -\gamma & 0 \\ 0 & -\gamma & \varepsilon_o & -\gamma \\ 0 & 0 & -\gamma & \ddots \end{pmatrix} \qquad \text{.....(2.54)}$$

the Schrödinger equation (equation 2.50) can be expanded at a lattice site z in terms of the energy and wave function ψ_z equation (2.51).

$$(E - H)\psi = 0 \qquad \text{.....(2.55)}$$

$$\varepsilon_o \psi_z - \gamma\psi_{z+1} - \gamma\psi_{z-1} = E\psi_z \qquad \text{.....(2.56)}$$

By using the wave function as given by Block's theorem for the perfect lattice chain which has the form $\psi_z = \frac{1}{\sqrt{v_g}} e^{ikz}$, where $-\pi \leq k < \pi$. The Schrödinger equation (eq. 2.56) can be solved to give the dispersion relation:

$$E = \varepsilon_o - 2\gamma\, cosk \qquad \text{.....(2.57)}$$

Where we introduced the quantum number, k, commonly referred to as the wavenumber [145,147].

To calculate the retarded Green's function $g(z,\ z')$, which is closely related to the wave function, the following equation is solved:

$$(E - H)g(z, z') = \delta_{z,z'} \qquad \text{.....(2.58)}$$

Physically, the lagging Green's function, $g\ (z,\ \acute{z})$, describes the response of a system at point z due to a source at point $\acute{z}$. Intuitively, we would expect such excitation to give rise to two waves, which travel outward from the excitation point, with amplitudes A and B as shown in Fig. (2-2).

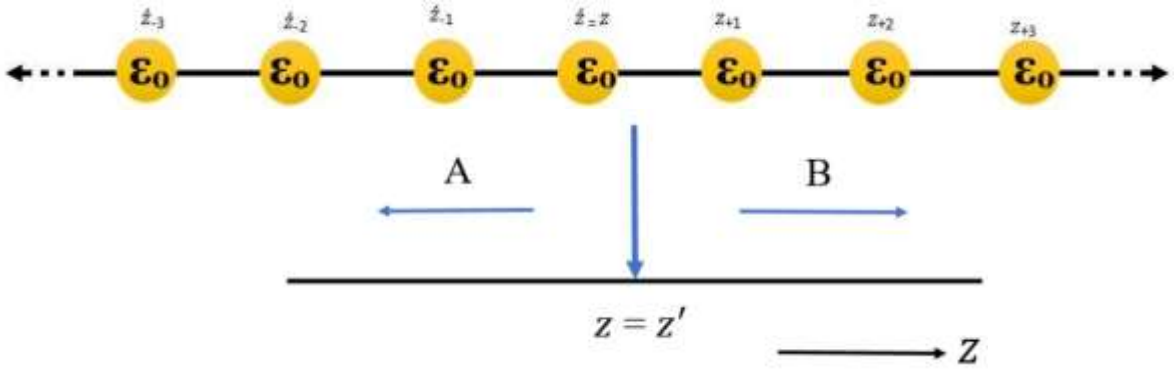

Figure (2-2): Retarded Green's function of an infinite one-dimensional lattice. The excitation at z = z ′ causes waves to propagate left and right with amplitudes A and B respectively[147].

These waves can be expressed simply as:

$$g(z, z') = Be^{ikz} \qquad z > z'$$

$$g(z, z') = Ae^{-ikz} \qquad z < z' \qquad \text{.....(2.59)}$$

In this equation, the solution satisfies equation (2.58) at every point except $z = z'$. To overcome this, the Green's function must be continuous equation (2.60), so the two are equal at $z = z'$:

$$[g(z,z')]_{z=z'\ left} = [g(z,z')]_{z=z'\ right} \quad \text{.....(2.60)}$$

$$Be^{ikz} = Ae^{-ikz} \implies A = Be^{2ikz} \quad \text{.....(2.61)}$$

By substituting equation (2.61) into the Green's function equation (2.59), we will find as shown:

$$g(z,z') = Be^{ikz} = Be^{ikz'}\, e^{ik(z-z')}\ z > z'$$

$$g(z',z) = Be^{2ikz'}e^{-ikz} = Be^{ikz'}\, e^{ik(z'-z)}\ z < z' \quad \text{.....(2.62)}$$

We can rewrite equation (2.62) as:

$$g(z',z) = Be^{2ikz'}e^{ik|z-z'|} \quad \text{.....(2.63)}$$

To find the value of the constant B, we use equation (2.58) and use equation (2.56) which for $z = z'$ given:

$$(\varepsilon_o - E)B - \gamma Be^{ik} - \gamma Be^{ik} = 1 \quad \text{.....(2.64)}$$

$$\gamma B\left(2cosk - 2e^{ik}\right) = 1$$

$$B = \frac{1}{2i\gamma sink} = \frac{1}{i\hbar v_g}$$

where the group velocity, found from the dispersion relation equation (2.57), is:

$$v_g = \frac{1}{\hbar}\frac{\partial E(k)}{\partial k} = \frac{2i\gamma sink}{\hbar} \quad \text{.....(2.65)}$$

We can rewrite the retarded Green's function as shown:

$$g^R(z - z') = \frac{1}{i\hbar v_g} e^{ik|z-z'|} \quad \text{.....(2.66)}$$

The literature [150,151] shows a more extensive derivation. The next step is to submit a file defect in the lattice to create a scattering area and then the transmission coefficient can be calculated.

To Calculate the Green's function for in this problem, we can get the scattering amplitudes. So, form a solution equation (2.58), which is given as follows:

$$G = (E - H)^{-1} \quad \text{.....(2.67)}$$

This equation can be singular if the energy E is equal to the Hamiltonian eigenvalues H, to deal with this, it is practical to consider the limit:

$$G_{\mp} = \lim_{\eta \to 0}(E - H \pm i\eta)^{-1} \quad \text{.....(2.68)}$$

Here η is a positive number and G+, G- is the retarded (advanced) Green's function. The sign of the positive infinitesimal η determines the type of solution which is either a retarded (-) or advanced (+) Green function. Generally, the methodology of computing electron transport is focused on computing a Green function for the infinite system, which includes the leads and the scattering region [150,151].

In the case where there is no coupling between the molecule and the leads, α = 0, the Green's function can be given as:

$$g = \begin{pmatrix} -\frac{e^{ik}}{\gamma} & 0 \\ 0 & -\frac{e^{ik}}{\gamma} \end{pmatrix} = \begin{pmatrix} g_L & 0 \\ 0 & g_R \end{pmatrix} \qquad \text{.....(2.69)}$$

If we consider a switch on of the interaction, then to obtain the Green's function of the coupled leads of this system, G, Dyson's equation is written:

$$G^{-1} = (g^{-1} - V) \qquad \text{.....(2.70)}$$

where V is the operator that describes the interaction connecting the leads, which has the form:

$$V = \begin{pmatrix} 0 & V_c \\ V_c^{\dagger} & 0 \end{pmatrix} = \begin{pmatrix} 0 & \alpha \\ \alpha^* & 0 \end{pmatrix} \qquad \text{.....(2.71)}$$

The solution to Dyson's equation, (Eq. 2.70) reads:

$$G = \frac{1}{|\alpha|^2 - \gamma^2 e^{-2ik}} \begin{pmatrix} \gamma e^{-ik} & \alpha \\ \alpha^* & \gamma e^{-ik} \end{pmatrix} \qquad \text{.....(2.72)}$$

The only step left is to calculate the transmission, t, and reflection, r, amplitudes from the Green's function equation (2.72). This is done by taking advantage of the Fisher-Lee relation [147] that relates the scattering amplitudes of a scattering problem to Green's function of the problem. Since $A = B = 1/i\hbar v g$, the equation (2.73) gives a definition for the transmission and reflection coefficients, equations (2.74) and (2.75): The Fisher-Lee relations in this case state that:

$$G_{1,1} = \frac{1}{i\hbar v_g} (1 + r)$$

$$G_{2,1} = \frac{1}{i\hbar v_g}\, t\, e^{ik} \qquad \text{…….……..(2.73)}$$

$$r = i\hbar v_g\, G_{1,1} - 1 \qquad \text{…….……(2.74)}$$

And

$$t = i\hbar v_g\, G_{2,1} e^{ik} \qquad \text{……..……(2.75)}$$

Therefore, these amplitudes will be corresponded to particles incident from the left. On the other hand, particles are travelling from the right side, which means these expressions could be used for transmission t' and reflection r' amplitudes. According to these coefficients above, the probability can be defined: T = tt*, R = rr*. Consequently Thus, the transmission probability for this case can be given as:

$$T = \frac{\sigma^2}{(\gamma^2 - \alpha^2)^2 + \sigma^2} \qquad \text{…….……(2.76)}$$

The parameters in this equation are $\sigma = 2\gamma\alpha sink$, and if α = γ that means the transmission T=1. In the case when α is greater or smaller than γ, which leads to create scattering region, and could be resulted to the transmission T ≤ 1.

2.8.2 The Landauer formula

Standard theoretical model to describe the transport phenomenon in ballistic mesoscopic the systems are Landauer's formula [153], a method applicable to phase cohesive systems. First of all, we assume that the system connects two large Scattering tanks, as shown in Fig. (2-3), in this case all are inelastic relaxation processes are limited to tanks [147]. Therefore, the

electron is transferred passage through the system is formed as a quantum mechanical scattering problem. The second important assumption is that this system is connected to external tanks by an ideal quantum wire, which acts as a waveguide for electron waves.

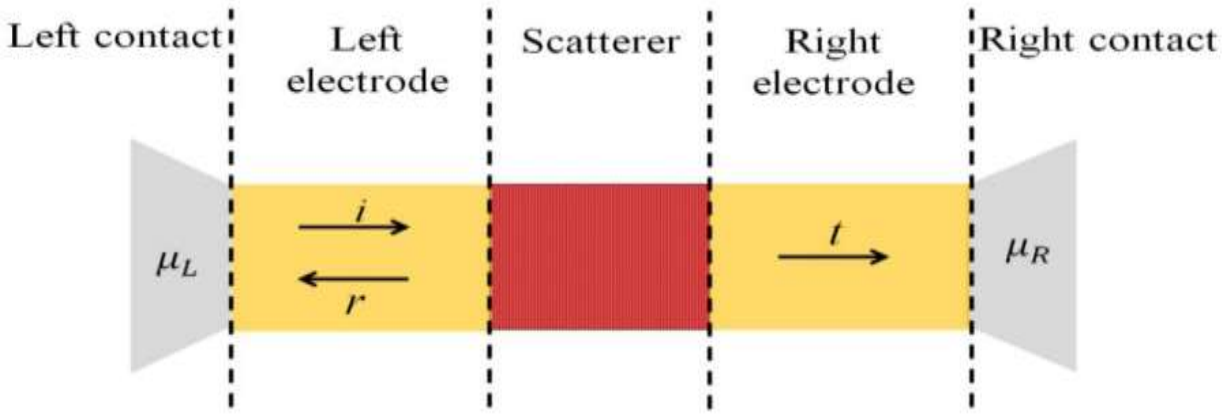

Figure (2-3): Shows a mesoscopic scatterer connected to the contacts by ballistic filaments. The μ_L and μ_R represent the chemical potential at the contacts. When the incident wave packet hits the scatterer on the left, it will be sent with probability $T = tt^*$, it is reflected with probability $R = rr^*$ where, t, t^*, r and r^* represent the transmission and reflection amplitudes from left to the right and vice versa. It requires the conservation of charges T + R = 1[154].

Mesoscopic scattered as shown in Fig. (2-3), connected to two electron tanks, and these reservoirs have slightly different chemical potentials $\mu_L - \mu_R = \delta E > 0$, and it causes electrons to move from the left to the right tank. We will discuss the solution to one channel open to one electron: the incident electric current δI which is generated by the chemical potential gradient, as indicated by:

$$\delta I = e v_g \frac{\partial n}{\partial E} \delta E = e v_g \frac{\partial n}{\partial E} (\mu_L - \mu_R) \qquad \text{.....(2.77)}$$

The charge of the electron is (e), the group velocity is v_g. i.e. the velocity of electron, and $\partial n/\partial E$ is density of states per unit length in the lead in the energy window that can be determined by the chemical potentials from contacts:

$$\frac{\partial n}{\partial E} = \frac{\partial n}{\partial k}\frac{\partial k}{\partial E} = \frac{\partial n}{\partial k}\frac{1}{v_g \hbar} \qquad \text{..}\ldots\ldots\ldots\ldots\ldots\ldots(2.78)$$

As in one-dimension, after including a factor of 2 of the rotation dependency $\frac{\partial n}{\partial k} = \frac{1}{\pi}$. When we substitute into equation (2.78), we will find that $\frac{\partial n}{\partial E} = \frac{1}{\pi}\frac{1}{v_g \hbar}$, which simplifies the equation (2.77) to:

$$\delta I = \frac{2e}{h}(\mu_L - \mu_R) = \frac{2\,e^2}{h}\,\delta V \qquad \ldots\ldots\ldots\ldots\ldots\ldots(2.79)$$

Where δV is the voltage generated by the chemical potential mismatch. From Eq.(2.79) it is clear that in the absence of a scattering region, the conductance of a quantum wire with one open channel is $\frac{2\,e^2}{h}$. If now we consider a scattering region, the current collected in the right contacts will be:

$$\delta I = \frac{2\,e^2}{h}\,T(\mu)\delta V \implies \frac{\delta I}{\delta V} = G = \frac{2\,e^2}{h}\,T(\mu) \qquad \ldots\ldots\ldots\ldots\ldots\ldots..(2.80)$$

This equation is the Landauer formula, which relates the conductivity G of a mesoscopic scatterer to the transmission probability T of the electrons passing through it. Where $T(\mu)$ is the transmission coefficient as a function of the chemical potential μ and the quantum conductance G_0 represented by

$2e^2/h$. The quantity G_0 includes the factor of 2 in the formula to include spin degeneracy [147,155].

Landauer's formula has been generalized in more than one open case Buttiker channel [153]. In this case, the transmission coefficient is replaced by the sum of all the transmission amplitudes describing electrons coming from the left-hand contact and arriving to the right contact. Landauer's formula equation (2.80) for many open channels and then it becomes:

$$\frac{\delta I}{\delta V} = G = \frac{2\,e^2}{h} \sum_{i,j} \left|t_{i,j}\right|^2 = \frac{2\,e^2}{h}\, Tr(tt^{\dagger}) \qquad \text{.....(2.81)}$$

Here, $t_{i,j}$ represents the transmission amplitude that describes the scattering from j^{th} channel from the left leads to i^{th} channel is for the right lead and G is the electric conductance. According to the definition of transmission amplitude, reflection amplitudes $r_{i,j}$ can be entered to describe the scattering processes where the particle is scattered to the same lead from which it came, here $r_{i,j}$ distinguish probability a particle arriving at channel j is reflected back on channel i of the same lead. By combining the transmission and reflection amplitudes, we can produce the scattering matrix we call the S matrix, which connects the states coming from the left lead to the right and vice versa as follows:

$$S = \begin{pmatrix} r & t' \\ t & r' \end{pmatrix} \qquad \text{.....(2.82)}$$

In this equation, r and t denote left-handed electrons, while r' and t' denote right-handed electrons. When we return to equation (2.81), we see that r, t, r', and t' are matrices of multiple open channels that can be complicated in

the presence of a magnetic field. The following section calculates S for the system's retarded Green function G(E). G(E) is derived by coupling the Green function of the leads to the Green function of the scattering region using Dyson's equation. The S matrix is an important component of scattering theory. In other words, it is useful not only in describing linearity transport, but also in other problems such as adiabatic pumping [154,155].

3.1 Introduction

The theoretical methods and programs presented in this chapter are very powerful, and they have been used in many areas of mesoscopic transport in the past decade. It has been successfully applied to molecular electronics [109], spintronics [92] and mesoscopic superconductivity [93]. The method was also extended to limited bias using the non-equilibrium Green's function technique [94].

3.2 Building of Atomic Configuration: Avogadro Software

To obtain the structure of all the systems in the thesis, the Avogadro program was used. Avogadro is an advanced molecular editor and visualizer designed for cross-platform use in computational chemistry, molecular modeling, bioinformatics, materials science and related fields see Fig. (3-1). It provides high-quality flexible rendering and a robust additional structure [152]. Avogadro offers a semantic chemical generator and platform for visualization and analysis. For users, it offers an easy-to-use generator, integrated support for downloading from popular databases such as Pub-Chemistry and Protein Data Bank, extraction of chemical data from a variety of formats, including computational chemistry output, and native semantic support for the CML file format. For more theoretical details about Avogadro and what it offers, see [156].

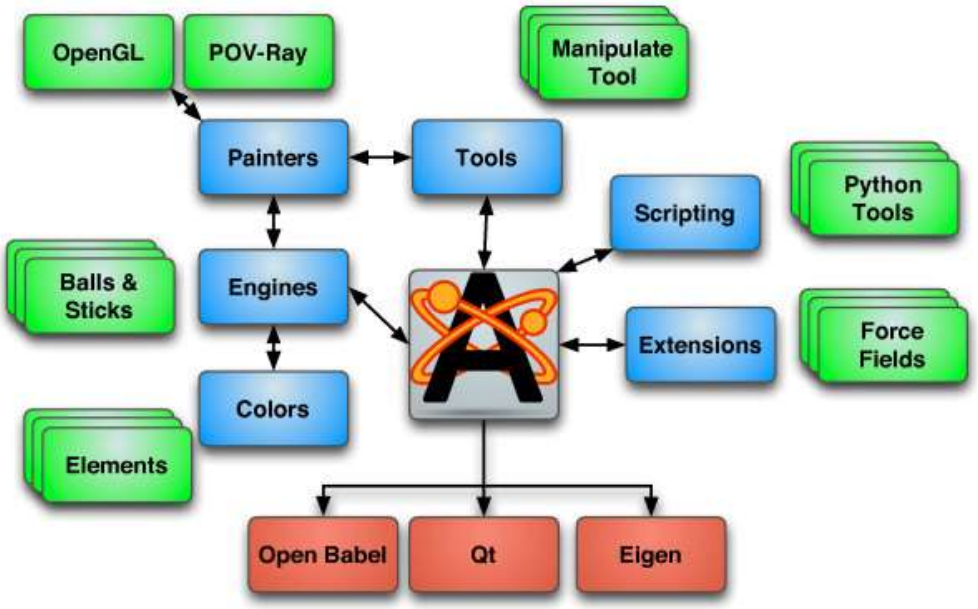

Figure (3-1): Atomic building capabilities and tools using Avogadro[152].

3.3 Iso-Surfaces Calculations

To gain a better understanding of the patterns in conduction behavior, we studied the electronic characteristics of the molecules and the electrical behavior of the junctions using DFT-based approaches. All molecules' electronic structures were initially studied at the theoretical level of B3LYP [126] with a base group of SDD [127]. The following chapter contains plots of the high occupied and low unoccupied molecular orbitals (HOMO and LUMO, respectively), as well as a summary of the energy analysis and distribution of the frontier molecular orbitals.

3.4 Electronic properties

Koopmans theory (KT) was used to calculate the electronic characteristics of the molecules in this investigation. The following is a description of the calculated properties:

3.4.1 HOMO, LUMO and H-L Gap

The most significant molecular orbitals are HOMO and LUMO, where HOMO denotes the highest occupied molecular orbital and LUMO denotes the lowest unoccupied molecule orbital. The most significant molecular MOs orbitals are referred to as frontier orbitals since they are found at the molecules' electrons' extremes. HOMO, the highest energy orbital containing electrons, is the electron donor orbital. LUMO, on the other hand, is the lowest energy orbital with space for electrons. The energy (H-Lgap) is defined as [145,158]: the difference in energies between the HOMO and LUMO levels.

$$(H-L)_{E\,gap} = E_{HOMO} - E_{LUMO} \qquad \text{..... (3.1)}$$

Not only do HOMO and LUMO and their associated energy gap determine the method by which molecules interact with other species, but the energy gap also helps characterize the chemical reaction and kinetic stability of the molecule. A molecule with a small frontier orbital gap is highly polarizable and is often associated with strong chemical reactivity and low kinetic stability; this type of molecule is sometimes referred to as a soft molecule [158,159]. When an electron is transported to a higher energy state, there by filling the empty molecular orbitals, the ensuing state is referred to as the excited state can be see Fig. (3-2). The energy difference between the HOMO and LUMO states is referred to as the HOMO - LUMO gap [158].

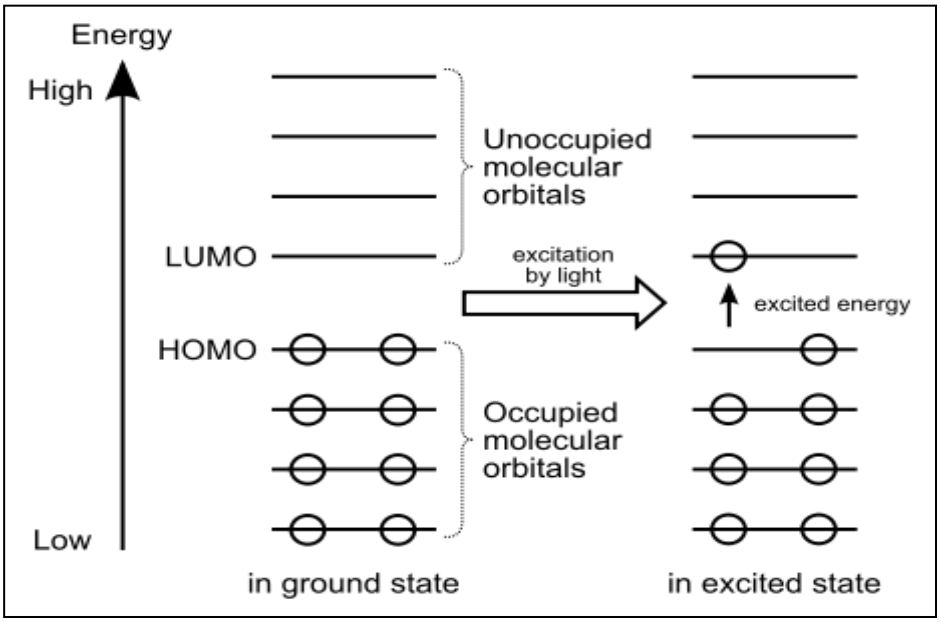

Figure (3-2): HOMO and LUMO levels of a single molecule[158].

The circle represents an electron in an orbital when light of a high enough frequency is absorbed by an electron in the HOMO, it is excited to the LUMO.

3.4.2 Fermi energy and Fermi level

The Fermi energy is a quantum mechanical notion that often refers to the energy difference between the highest and lowest occupied single-particle states in a quantum system of non-interacting fermions at absolute zero temperature. The lowest occupied state in a Fermi gas is assumed to have zero kinetic energy, but the lowest occupied state in a metal is commonly regarded to be the bottom of the conduction band [143]. Intriguingly, the word Fermi energy is frequently used interchangeably with another but closely related notion, the Fermi level (also called electrochemical potential), there are some critical distinctions between the Fermi level and Fermi energy, at least in the context of this article. While the Fermi energy is specified exclusively at absolute zero, the Fermi level is defined at any temperature. The Fermi energy

is a difference in energy levels (often equal to kinetic energy), whereas the Fermi level is a total energy level that includes both kinetic and potential energy. The Fermi energy can be defined only for non-interacting fermions (for which the potential energy or band edge is a static, well-defined quantity), whereas the Fermi level (for which the electrochemical potential of an electron remains well defined even in complex interacting systems at thermodynamic equilibrium) cannot be defined equilibrium.

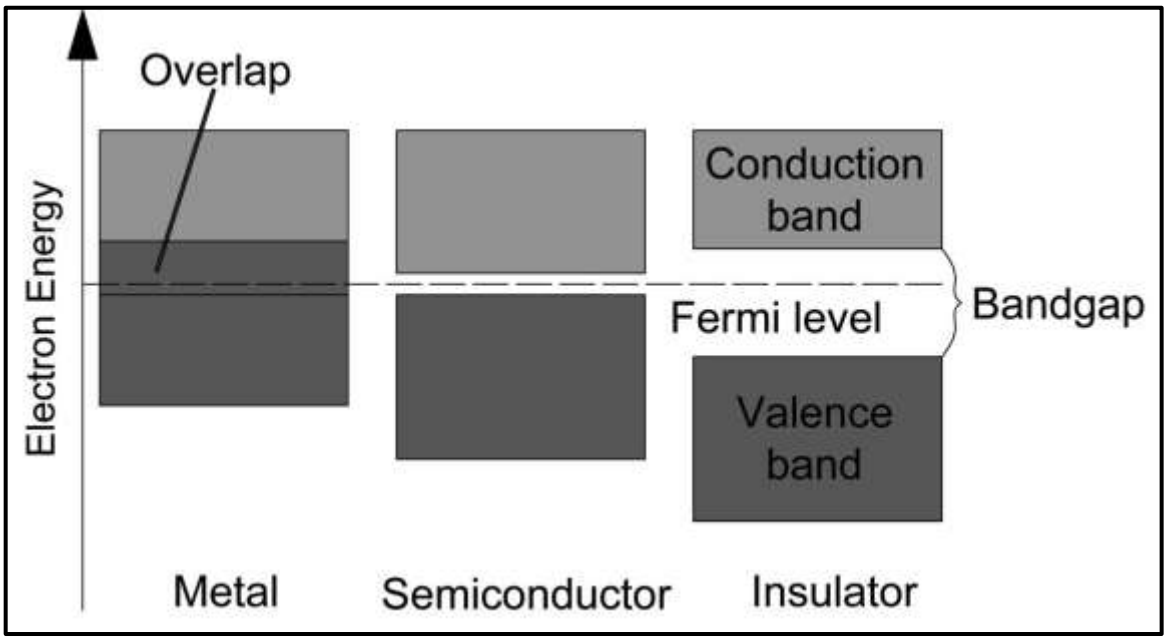

Figure (3-3): Fermi energy level of the metal, semiconductor and insulator[143].

Given that the energy of the highest occupied single particle state in a metal at absolute zero is the Fermi level, the Fermi energy in a metal is the energy difference between the Fermi level and the lowest inhabited single particle state at zero temperature, as seen in Fig. (3-3). Fermi energy level at temperature is given by: $f(\mathrm{E}) = [e^{\beta(E-E_F)} + 1]^{-1}$ Where f (E) is the Fermi function, $\beta = 1/k_B T$, E_F is the Fermi energy, k_B is Boltzmann constant, T is the temperature.

The Fermi energy, which is the fundamental anisotropy principle in DFT, is utilized to determine the direction of an electron cloud's departure. It is constant over all dimensions and may be calculated using the following equation [160]:

$$E_F = \left[\frac{\partial E}{\partial N}\right] v_{(\vec{r})} \quad \text{.....(3.2)}$$

Where E is the energy and N is the number of electrons. Theoretically, Fermi energy is relating as in the following equation [159]:

$$E_F \approx \frac{1}{2} (E_{HOMO} + E_{LUMO}) \quad \text{.....(3.3)}$$

Band theory can be used to explain the electrical conductivity of materials. In band theory, each electron's energy level is represented by a horizontal line. Due to the fact that any solid substance has a significant number of electrons with varying energy levels, the combinations of these energy levels form two continuous energy bands referred to as the valence band and the conduction band. The energy difference between the two bands denotes the electron-restricted zone. In band theory, the electrons bound to particular atoms or interatomic bonds are considered to be in the valence band. When an electric field is applied, electrons that may freely flow within the core are said to be in the conduction band. The pattern of bands in a solid in Fig.(3-3) identifies three distinct types of materials: insulators, semiconductors, and metals.

3.5 Electronic Transitions

UV or visible ray absorption results in the stimulation of external electrons. There are three types of electronic transitions: those involving p, s,

and n electrons, those involving charge transfer electrons, and those involving d and f electrons. When an atom or molecule absorbs energy, the electrons in its ground state are promoted to the excited state. Atoms in a molecule can rotate and vibrate in relation to one another. Additionally, these vibrations and rotations have distinct energy levels, which might be thought of as a dense existence atop each electrical level. UV and visible rays are absorbed by some functional groups in organic compounds that contain valence electrons with a low excitation energy. The spectrum of the chromosphere-containing molecule is complicated [131,133]. The electronic transitions between p, s, and n electrons are depicted in Fig. (3-4).

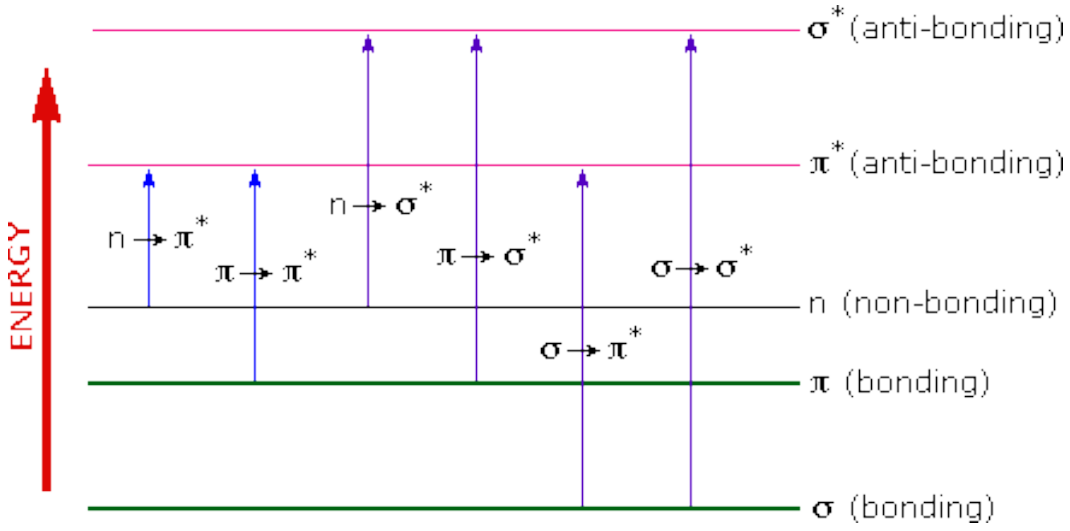

Figure (3-4): The electronic transitions of p, s, and n electrons [133].

3.6 Self-Consistency Process

After establishing the system's atomic configuration, we require the appropriate pseudo-potentials for each element, which can vary for each cross-correlation function. Additionally, a suitable base set selection must be made for each item in the account.

In the event of comprehensive optimization, the three alternatives can be combined to obtain the system's least energy and equilibrium network parameters. The process for relaxing the atomic locations allows the atoms to migrate until the remaining force between all the atoms is less than the needed affinity tolerance in eV/A, as seen in Fig. (3-5). Force is the essential quantity in structural optimization, and it may be numerically determined by taking the approximate numerical derivatives of the total power with respect to positions. SIESTA implements this strategy using the Hellmann-Feynman theorem [154,155]. We can enhance the computational accuracy and cost by doing two test calculations. Other input parameters affect the calculation's accuracy, such as the precision and density of the k-grid points used to evaluate the integration. Then, assuming that there is no interaction between the atoms, we generate the initial charge density.

Due to the fact that the pseudopotentials are known, this step is straightforward, and the total charge density is equal to the sum of the atomic densities. The self-consistent computation Fig. (3-5) begins with the Hartree-potential and exchange correlation potentials being calculated. Due to the fact that the density is represented in real space, the Hartree-potential is determined by solving the Poisson equation using either the multiple mesh approach [139] or the rapid Fourier transform method [145]. We begin the next iteration after solving the Kohn-Sham equations and obtaining a new density (r). Iteration is complete when the required convergence requirements are met. SIESTA offers extra density matrix mixing choices per cycle. I employ the Pulay [154] mixing approach in particular, in which the new density is mixed not just with the old, but also with a linear mixture of the preceding n densities. As a result, we obtain the ground state Kohn-Sham

orbitals and energy of a certain atomic arrangement. The operation described above is repeated in another loop, which is controlled by the conjugate gradient method [154,155], which is used to determine the minimal ground state energy and related atomic configuration. After achieving self-consistency, an additional subroutine is called to extract the Hamiltonian and nested matrices from the LCAO basis for use in scattering calculations.

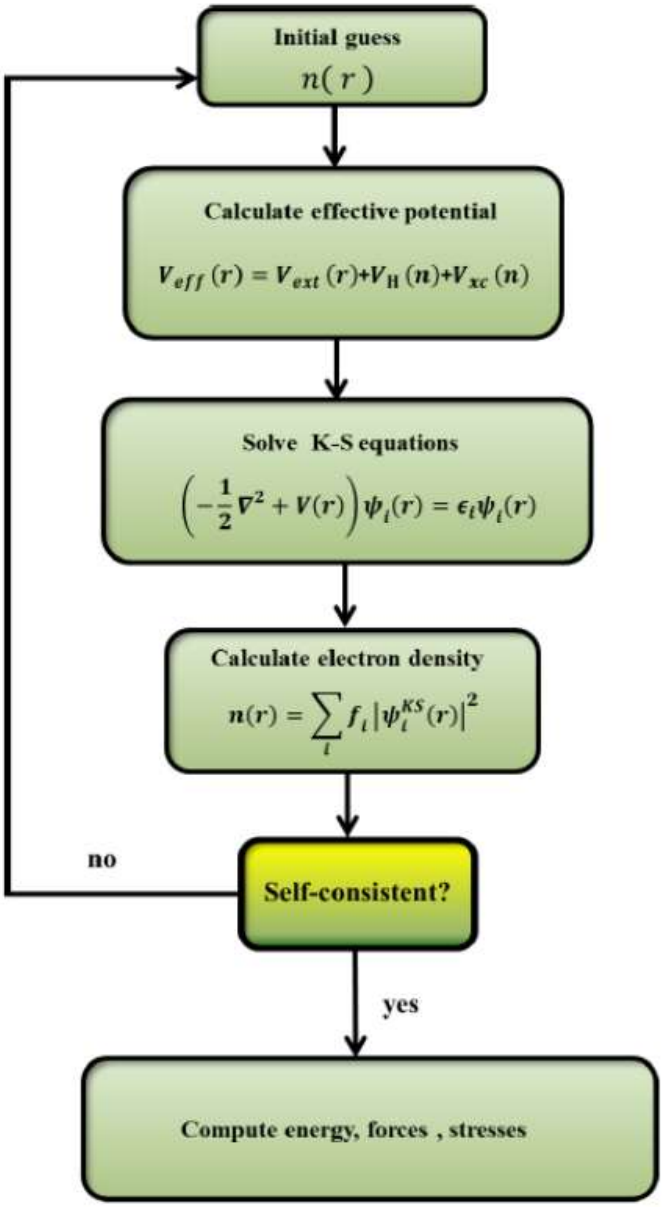

Figure (3-5): Schematic of the self-consistency process within SIESTA.

3.7 Calculations in Practice

To determine the electrical conductivity of the molecular, it was placed between two pyramidal gold electrodes and then allowed to relax to form the necessary shapes.

The transmission coefficient of a structure can be defined as the amplitude and intensity of the transmitted wave in comparison to the incident wave when waves propagate in a non-contact medium [128]. In non-relativistic quantum mechanics, the transmission coefficient and its corresponding reflection coefficient are used to describe the behaviour of a wave incident on a barrier. The transfer coefficient quantifies the likelihood of a particle tunnelling through a barrier. The transmission coefficient expresses the probability flow of the transmitted wave in comparison to the incident wave's flow [162,163].

The structure's transmission coefficient is positioned between two electrodes. T(E) is a transmission coefficient that quantifies the transfer of energy from E electrons to another electrode. The Hamiltonian H and the interference matrices S [164] were used to determine T(E).

T(E), which characterizes the spread of energy electrons from left to right electrode, was determined by first collecting their Hamiltonian and related nested matrices using SIESTA and then using and Gollum's code [76,77] to calculate T(E) using the relationship:

$$T = Trace\{\Gamma_R(E)G^R(E)\Gamma_L(E)G^{R\dagger}(E)\} \quad \text{..... (3.4)}$$

In this expression,

$$\Gamma_{L,R}(E) = i\left(\sum_{L,R}(E) - \sum_{L,R}{}^{\dagger}(E)\right) \quad \text{..... (3.5)}$$

Equation (3.5) describes the level broadening due to the coupling between left (L) and right (R) electrodes and the central scattering region, $\sum_{L,R}(E)$ are the retarded self-energies associated with this coupling and:

$$G^R = (ES - H - \sum_L - \sum_R)^{-1} \quad \text{..... (3.6)}$$

G^R is the retarded Green's function, where *H* is the Hamiltonian and *S* is the overlap matrix (both obtained from SIESTA). Electrical conductivity means flow of electric current through a material. When a current of one Ampere passes through a component across which a voltage of one Volt exists, then the electrical conductance ($G = I/E$) of the component is one Siemens (S) [123,153,155].

The electrical conductance *G(T)* and the thermopower as a function of the temperature T was computed from the formula:

$$L_n^{\sigma}(T) = \int_{-\infty}^{\infty}(E - E_F)^n T^{\sigma}(E)\left(-\frac{df(E)}{dE}\right) dE \quad \text{..... (3.7)}$$

Where

$$f(\mathrm{E}) = [e^{\beta(E-E_F)} + 1]^{-1} \quad \text{..... (3.8)}$$

where $T^{\sigma}(E)$ is the transmission coefficient, and σ represents spin [↑, ↓] of transport of electrons passing through the single-molecule from one electrode to another [196], *f (E,T)* is the Fermi distribution function, $\beta = 1/k_BT$, E_F is the Fermi energy, k_B is Boltzmann constant, *T* is the temperature. The electrical conductance *G(T)* has been calculated by using Landauer formula:

$$G = G_o \int_{-\infty}^{\infty} dE\, T(E)[-df(E)/dE] \quad \text{.....(3.9)}$$

Substitute an equation (3.7) into an equation (3.9) we get:

$$G(T) = G_{\circ}L_{\circ}(T) \quad \text{..... (3.10)}$$

where

$$G_0 = \left(\frac{2e^2}{h}\right) \quad \text{..... (3.11)}$$

Is the quantum of conductance, h is the Planck's constant, e is the electron charge. Since the quantity (*-df(E)/dE)* is the a probability distribution peaked at E = E_F with a width on the order K_BT, the previous expression shows that G/G_o is obtained by averaging T(E) over an energy range on the order K_BT in the vicinity of E = E_F[139,165]. It is well known that the Fermi energy predicted by DFT is not reliable, and therefore, the plots G/G_o have been shown later as a function of $E_F - E_F^{DFT}$. Then, the thermopower *S*(T) is given by[167-168]:

$$S(T) = -\frac{L_1}{eTL_{\circ}} \quad \text{.....(3.12)}$$

3.8 Thermal conductivity

Thermal conductivity is described as a material's ability to conduct heat within; it varies with temperature. It is calculated primarily using Fourier's law of thermal conductivity. Heat is transported more slowly through low thermal conductivity materials used as thermal insulation than through high thermal conductivity materials utilized in heat sink applications. Thermal conductivity is expressed in SI units as watts per meter Kelvin (W/m • K). The term "thermal resistance" refers to the reciprocal of the term "thermal conductivity" [165].

3.8.1 Thermoelectric coefficients

When a system is subjected to a temperature difference ΔT and a voltage difference ΔV, the thermoelectric effect occurs. This results in the passage of an electric current I and a heat current $\dot{Q}$ through a device. According to Buttiker, Imry, Landauer, et al. [165,166], the electric current I and heat current $\dot{Q}$ passing through a device are proportional to the voltage difference ΔV and temperature differential ΔT. Thus, the thermoelectric coefficients G, L, M, and K are used to connect both currents to temperature and potential differences [167]:

$$\begin{pmatrix} I \\ \dot{Q} \end{pmatrix} = \begin{pmatrix} G & L \\ M & K \end{pmatrix} \begin{pmatrix} \Delta V \\ \Delta T \end{pmatrix} \qquad \text{…..……(3.13)}$$

We can write the equation in another form:

$$\begin{pmatrix} I \\ \dot{Q} \end{pmatrix} = \frac{1}{h} \begin{pmatrix} e^2 L_o & \frac{e}{T} L_1 \\ e L_1 & \frac{1}{T} L_2 \end{pmatrix} \begin{pmatrix} \Delta V \\ \Delta T \end{pmatrix} \qquad \text{.....……(3.14)}$$

Here, T represents the reference temperature, as well as the transport at room temperature through the single molecules are coherent in phase, with moments $L_n = L_n^{\uparrow} + L_n^{\downarrow}$. (n = 0,1,2), where L_n is written as equation (3.7).

We can rewrite equation (3.14) in the terms of the electrical conductance (G) (electrical resistance $R = 1/G$), thermopower ($S = -\Delta V/\Delta T$) , Peltier coefficient (Π), and the electronic contribution to the thermal conductance (k_e), as shown:

$$\begin{pmatrix}\Delta V\\ \dot{Q}\end{pmatrix}=\begin{pmatrix}\frac{1}{G} & -\frac{L}{G}\\ \frac{M}{G} & K-\frac{LM}{G}\end{pmatrix}\begin{pmatrix}I\\ \Delta T\end{pmatrix}=\begin{pmatrix}R & S\\ \Pi & k_e\end{pmatrix}\begin{pmatrix}I\\ \Delta T\end{pmatrix} \qquad \text{……(3.15)}$$

The electrical conductance, G is given by the Landauer formula: $G(T)=\left(\frac{2e^2}{h}\right)L_{\circ}(T)$,This parameter is described in an equation (3.10).

Thermal energy is given in this case: Seebeck's modulus is a measure of how much of the thermoelectric potential is induced in response to temperature difference across a substance. It can also be defined as the thermal energy and thermoelectric sensitivity of a material, and is measured in volts per kelvin (V/K) in SI units. The Seebeck modulus of a substance is calculated from equation (3.12) when a small temperature gradient is applied to a substance such as [57]:

$$S=-\frac{\Delta V}{\Delta T}=\frac{1}{eT}\frac{L_1}{L_o} \qquad \text{……(3.16)}$$

where ΔT is the small temperature difference between the two ends of a material and ΔV is the thermoelectric voltage visible at the ends.

Furthermore, the Peltier modulus is the inverse of the Seebeck modulus, as it is determined by flowing current through two junctions, resulting in a temperature difference. The Peltier effect was discovered in 1834 by physicist Peltier. This is not the same as Joule heating, despite appearances. In joule heating, the current simply raises the temperature of the material through which it passes, whereas in Peltier effect devices, a temperature differential is generated, with one junction being colder and the other becoming hotter. Peltier coolers, while not as efficient as some other types of coolers, are

precise and simple to control and adjust. Peltier effect devices are used in a variety of microelectronic devices, including microcontrollers and central processing units in computers (CPUs). The Peltier effect occurs when an electric charge flows through a junction between two different conductors and generates or absorbs heat [56]. It is mostly used by computer enthusiasts to bypass microprocessors in order to increase performance without triggering CPU overheating or process failures. The Peltier coefficient is defined as the amount of heat that is transported solely as a result of the charge current in the absence of a temperature difference:

$$\Pi = \left(\frac{\dot{Q}}{I}\right)_{\Delta T=0} = \frac{1}{e}\frac{L_1}{L_o} = -ST \qquad \text{.....(3.17)}$$

And the electronic contribution to the thermal conductance (k_e) (and the thermal conductance k_e is defined as the heat current due to the temperature drop in the absence of an electric current) is given:

$$k_e = -\left(\frac{\dot{Q}}{\Delta T}\right)_{I=0} = \frac{1}{hT}\left(L_2 - \frac{L_1^2}{L_o}\right) = -K\left(1 + \frac{S^2\,GT}{K}\right) \text{.....(3.18)}$$

Therefore the evaluation of S or Π gives an idea of how well the device will act as a heat driven current generator or a current driven cooling device. An additional quantity, the thermoelectric figure of merit, ZT [168] can also be defined in terms of these measurable thermoelectric coefficients, from the above equations, the figure of merit $ZT = \frac{S^2\,GT}{K}$ [169] can be written as:

$$ZT_e = \frac{1}{\frac{L_o L_2}{L_1^2} - 1} \qquad \text{.....(3.19)}$$

From classical electronics, ZT is derived by finding the maximum induced temperature difference produced by an applied electrical current in the presence of Joule heating. Let us consider a current carrying conductor placed between two heat paths with temperatures T_L and T_R, and electrical potentials V_L and V_R respectively. The thermoelectric figure of merit can be determined by finding the maximum induced temperature difference of the conductor due to an electrical current. Define $\dot{Q}$ as the heat gain from the path L to R, and then from equation (3.15) i.e.:

$$\dot{Q} = \Pi I - K \Delta T \qquad \text{.....(3.20)}$$

$\dot{Q}$ This heat transfer will cause the left path to cool and the right path to heat, with a result that ΔT increases. The amount of Joule heating can be expressed as $\dot{Q_J} = R I^2$, which is proportional to the electrical resistance and the square of the current. This Joule heating will also affect the temperature difference induced by the heat transfer, and therefore in the steady state case [56]:

$$\Pi I - K \Delta T = \frac{R I^2}{2} \qquad \text{.....(3.21)}$$

where, $R/2$ is the sum of two parallel resistances (internal and external resistances). After rearranging this, the temperature difference is:

$$\Delta T = \frac{1}{K} (\Pi I - \frac{R I^2}{2}) \qquad \text{.....(3.22)}$$

This expression shows how the temperature difference depends on the current. To find the maximum temperature difference a differentiation equation (3.22) with respect to the electric current is made:

$$\frac{\partial \Delta T}{\partial I} = \frac{\Pi - IR}{k} = 0 \qquad \text{....……(3.23)}$$

Finally by writing back I = Π/R and substituting equation (3.17) into equation (3.22), for the maximum of the temperature different we get [166,167]:

$$(\Delta T)_{max} = \frac{\Pi^2}{2kR} = \frac{S^2 T^2 G}{2k} \qquad \text{.……(3.24)}$$

$$\frac{(\Delta T)_{max}}{T} = \frac{S^2 T^2 G}{2k} = \frac{1}{2} ZT \qquad \text{.……(3.25)}$$

$$\therefore \quad ZT = \frac{2\, S^2\, T^2\, G}{2K} \qquad \text{……(3.26)}$$

Yielding a dimensionless number that can be used to characterize the efficiency of a molecular device.

3.9 The Software

All calculations in this study have been performed by using the (Gaussian 09) package of Programs, SIESTA code and other assistant programs. These programs are described as below:

3.9.1 Gaussian 09 (G09) Program

The Gaussian program is a computational software package initially published by John Pople in 1970. Gaussian program is a very high-end quantum mechanical software package. The “09” mentions to the year 2009 in which the software was published [170].

Gaussian is capable of running all of the major methods in molecular modeling, including molecular mechanics, ab-initio, semi-empirical, HF and DFT. Moreover, excited state computes can be done by different methods in this program[110].

The name originates Gaussian comes from the use of the Gaussian Type Orbitals that Gaussian's originator, John Pople, used to try to overcome the computational difficulties that get up from the use of Slater Type Orbitals. A number of researchers, such as S.F. Boys and Isaiah Shavitt, Pople, quite brilliantly, recognized that the (relatively) simple, substitution of a series of Gaussian functions for the Slater function, would greatly simplify the rest of the calculation of the Schrödinger equation. Pople (1998) was awarded the Nobel Prize in chemistry (along with Walter Kohn) for this work [110,134].

3.9.2 SIESTA

All computations in this thesis were performed using the DFT implementation of the SIESTA code. It is utilized to obtain a convenient geometry for the structures presented and to perform calculations verifying their electrical properties. The word SIESTA is an abbreviation for the **S**panish **I**nitiative for **E**lectronic **S**imulations Using **T**housands of **A**toms. It is a self-consistent density functional theoretical technique that performs efficient computations by utilizing norm-conserving pseudopotentials and a Linear Combination of Atomic Orbital Basis set (LCAOB). For additional theoretical details on the SIESTA code and its capabilities, read [76].

There are two distinct methods for running DFT simulations with SIESTA: one is to solve the Kohn-Sham equations using the traditional self-

consistent field diagonalization approach, and the other is to directly reduce a modified power function [154].

The SIESTA code is used to determine the ground state energy of various atomic configurations and then to determine the systems' relaxed structure. This means that SIESTA can calculate our energy in terms of atomic coordinates (the location of atoms). Three types of structure optimization exist: relaxation in atomic coordinates, which allows for the modification of the forms and sizes of periodic cells [155].

SIESTA is both a method and a computer program for efficiently computing the electronic structure of molecules and solids and performing ab-initio molecular dynamics simulations. The efficiency of SIESTA is due to the use of tightly localized basis sets and the construction of linear-scaling algorithms that may be used to suitable systems. SIESTA employs fully non-local (Klein man-Bylander) norm-conserving pseudopotentials. It enables an infinite number of multiple-zeta and angular momenta, as well as polarization and on-site orbitals, by using atomic orbitals as a basis set. The finite-support basis sets are critical for calculating the Hamiltonian and overlap matrices in the procedures. Apart from the usual Rayleigh-Ritz eigen state method, it enables the employment of localized linear combinations of occupied orbitals (valence-bond or Wannier-like functions), effectively scaling the computer's time and memory linearly with the number of atoms. With modest workstations, simulations with several hundred atoms are possible. It routinely calculates total and partial energies, electric dipole moment, electron density, atomic forces, geometry relaxation, stress tensor, constant-temperature molecular dynamics, variable cell dynamics (Parrinello-Rahman), Brillion

zone k-sampling, local and orbital-projected DOS, band structure, vibrations (phonons), and ballistic electron transport [154,155].

3.9.3 GOLLUM 1.0 Program

GOLLUM is a program written by Fortran that computes the electrical and thermal transport properties of multi-terminal nano-scale systems. The program can compute transport properties of either user-defined systems described by a tight-binding (or Huckel) Hamiltonian. The program has been created to interface easily with any DFT code and uses a localized basis [77]. It currently reads information from SIESTA [76]. Plans to produce interfaces to other codes like FIREBALL are underway. GOLLUM is based on equilibrium transport theory, meaning that it consumes much less memory than NEGF (non-equilibrium Greens function) codes. The program has been designed for user-friendliness and takes a considerable leap towards the realization of ab initio multi-scale simulations of conventional and more sophisticated transport functionalities. GOLLUM delivers functionalities, reads either Tight-Binding or DFT Hamiltonians, simulates multi-terminal devices, computes the full scattering matrix and charge transport, number of open scattering channels, transmission and reflection coefficients, shot-noise, computes heat transport, thermal conductance and thermo power (Seebeck coefficient), peltier coefficient, computes spin transport, computes zero-voltage as well as I-V curves, computes band-structure of the leads and DOS in the scattering region [57,59,77].

4.1 Introduction

The twelve suitable structures of the various proposed series of organometallic compounds that *have* been investigated in this thesis are illustrated in Fig. (4-1). This chapter is divided into three sections; the first section discusses the electronic characteristics of compounds for three different correlation groups. The molecular design combines three key structural characteristics: (i) The molecules have terminal pyridyl, thiol, and thiomathyl anchoring units (Bicyclobentedine metal-2pyridyl), (Bicyclobentedine metal-2benzothiol), and (Bicyclobentedine metal-2benzthiomathyl); (ii) Each molecule contains one of twelve different core units, with metals (Fe, Co, Ru, and Pt) in the center and (iii) meta-meta conjugation occurs between the core unit and anchor group, resulting in two isomeric series that are isolated; we studied the electronic properties of the compounds in their ground state and excited state; we studied the relaxed structures to obtain the best geometric optimization of the structures; and we studied the excited state to obtain the absorptiometry and emission spectra.

The recommended compounds are initially generated using the Avogadro program and then relaxed using the three parameters. The Lee-Yang-Parr B3LYP density functional theory DFT approach was used in conjunction with SDD basis sets in the Gaussian 09 package of programs to investigate the ground state and spectroscopic features of these molecules. The properties of the excited states and transition states of relax structures are investigated using time dependent density functional theory, TD-DFT.

The second section of this thesis examined the electric and thermoelectric properties of inverted necklace organometallic molecular junctions in terms of

quantum interference, specifically electrical conductance, transmission coefficient, Seebeck's coefficient, and figure of merit. The DFT algorithm SIESTA was used in this investigation, with a generalized gradient approximation (PBE functional), a double-zeta polarized basis set, a force tolerance of 0.01 eV/A, and a real-space grid determined by a plan wave cut-off energy of 250 Ry.

While the third section included a comparative study of the three groups (and the intention is that these are the groups associated with the gold electrodes), where the electrical and thermoelectric properties of each metal linked in the center of these particles were investigated, as well as an understanding of the difference that occurs when the anchor groups are changed. We have investigated the spectral, electronic, electrical, and thermoelectric properties of all three phases and will discuss our findings in depth in this chapter.

Part I

4.2 Structural and Geometrical Optimisation

It is evident in Fig. (4-1) that (the pyridyl rings and phenyl with thiol and thiomethyl) are present on both sides of the dicyclobentedine-metal, as is the π-electron delocalization between the molecular units and aromatic rings. The effect of introducing an anchor group into phenyl rings is investigated. To investigate the effect of asymmetry in comparison to symmetry compounds, several compounds belonging to various subgroups are designed. We investigate the influence of electron accepting and electron donating groups. All geometrical parameters were determined using the B3LYP method in

conjunction with SDD basis sets in the Gaussian 09 program. The geometrical parameters derived from DFT calculations coincide well with those obtained from x-ray data C-C=1.421 Å, C-C-C=120 degree [114]. The relax structures of the compounds in Fig. (4-1) demonstrate that they all exhibit a quasi-planar conformation.

Bicyclobentedine-Pyridyl-metal

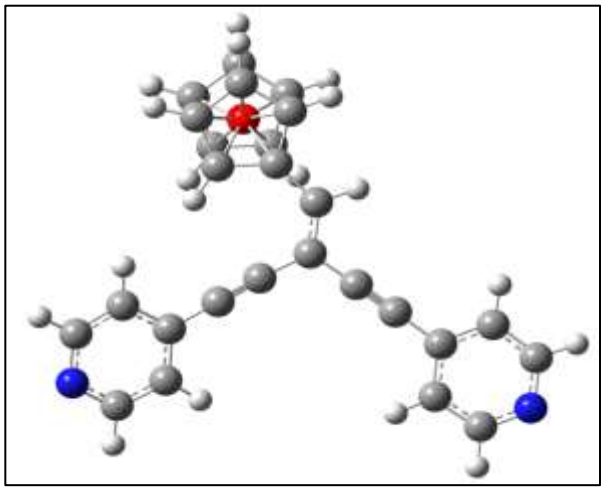

Bicyclobentedine-Thiol-metal

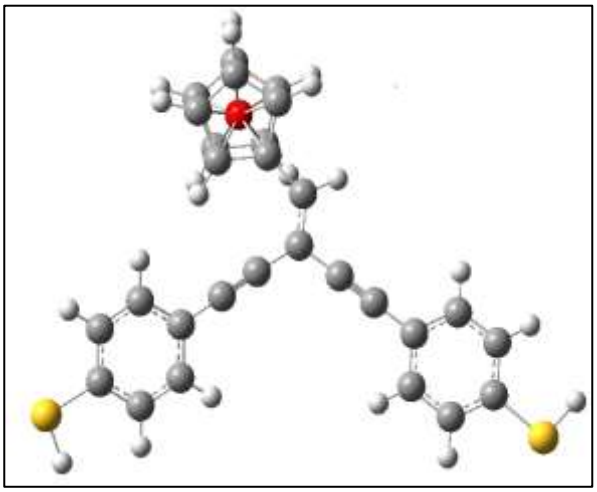

Bicyclobentedine-ThioMethyl-metal

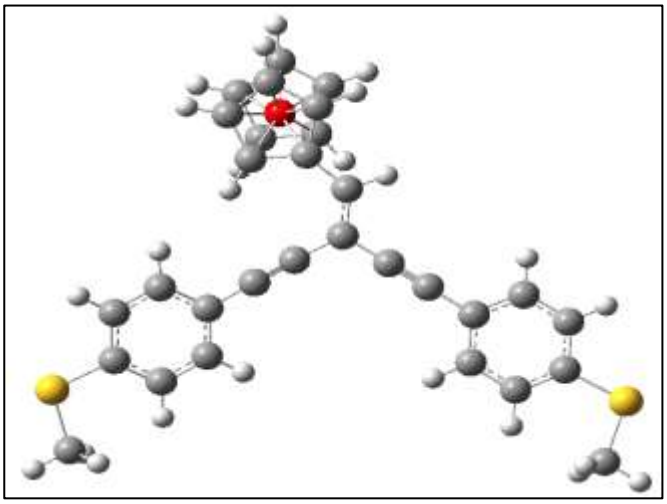

= Fe, Co, Ru and Pt

Figure (4-1): The relaxed geometries of all molecules.

The relaxed geometries of all molecules in the gas phase with varied metallic and anchor groups are illustrated in Fig. (4-1), as the figure demonstrates that there are three groups of Bicyclobentedine-metal based on the anchor groups linked to the molecules. The first group contains Bicyclobentedine-metal connected to phenyl rings via pyridyl anchor groups on both sides, while the second group has Bicyclobentedine-metal with an additional thiol anchor group. Additionally, the third group contains Bicyclobentedine-metal bonded to phenyl rings via thiomethyl anchor groups on both sides.

4.3 The Electronic Structure Properties

To gain a better understanding of the electronic characteristics of molecules and the electrical behaviour of junctions, DFT-based theory has been used [127]. To investigate the distribution and composition of the frontier molecular orbitals, first analyses of the electronic structures of all organometallic compounds were conducted at the B3LYP level of theory [131] using the SDD basis set. Fig. (4-2) shows plots of the highest occupied and lowest unoccupied molecular orbitals (HOMO and LUMO, respectively).

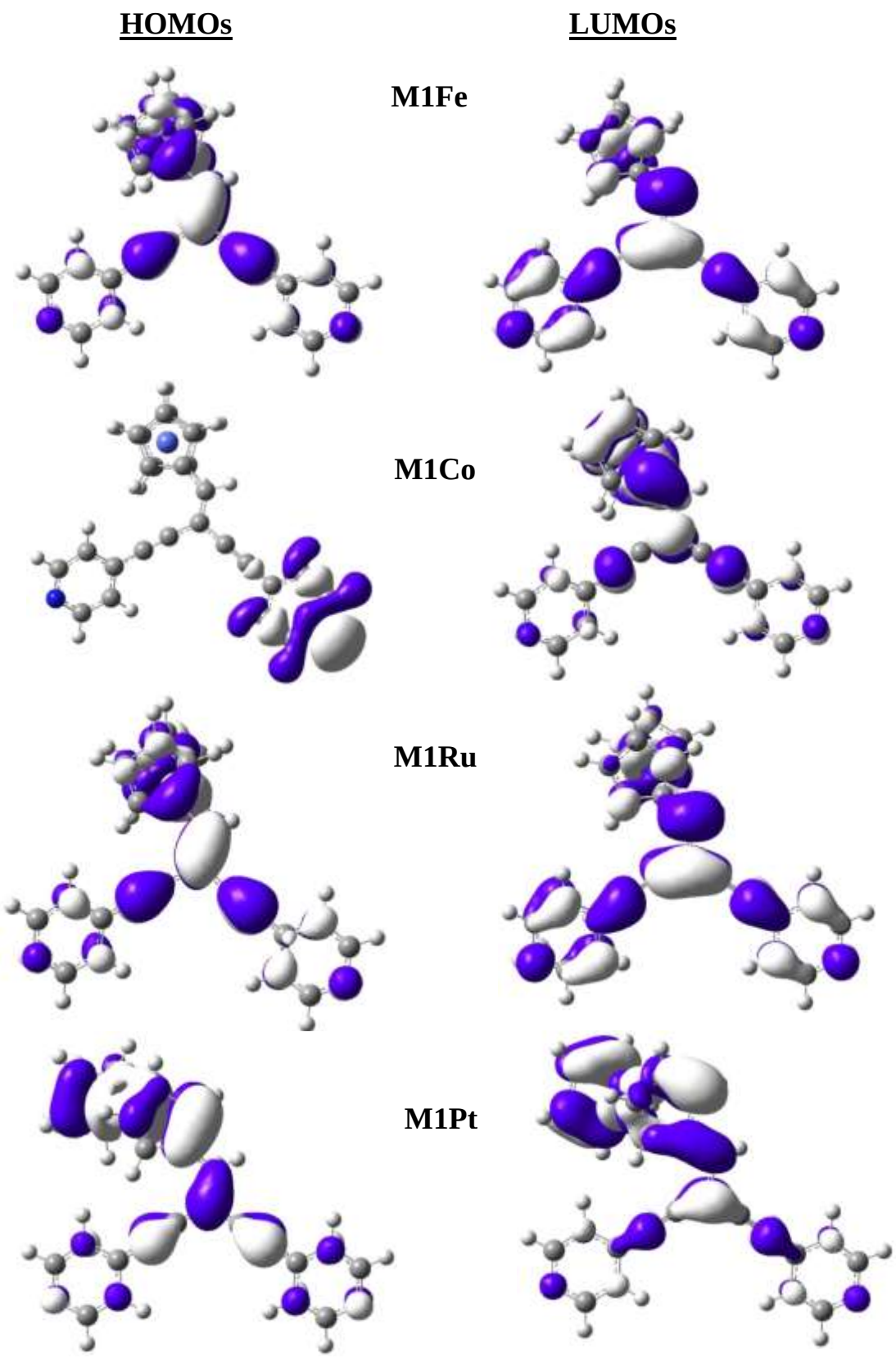
HOMOs
LUMOs
M1Fe
M1Co
M1Ru
M1Pt

HOMOs **LUMOs**

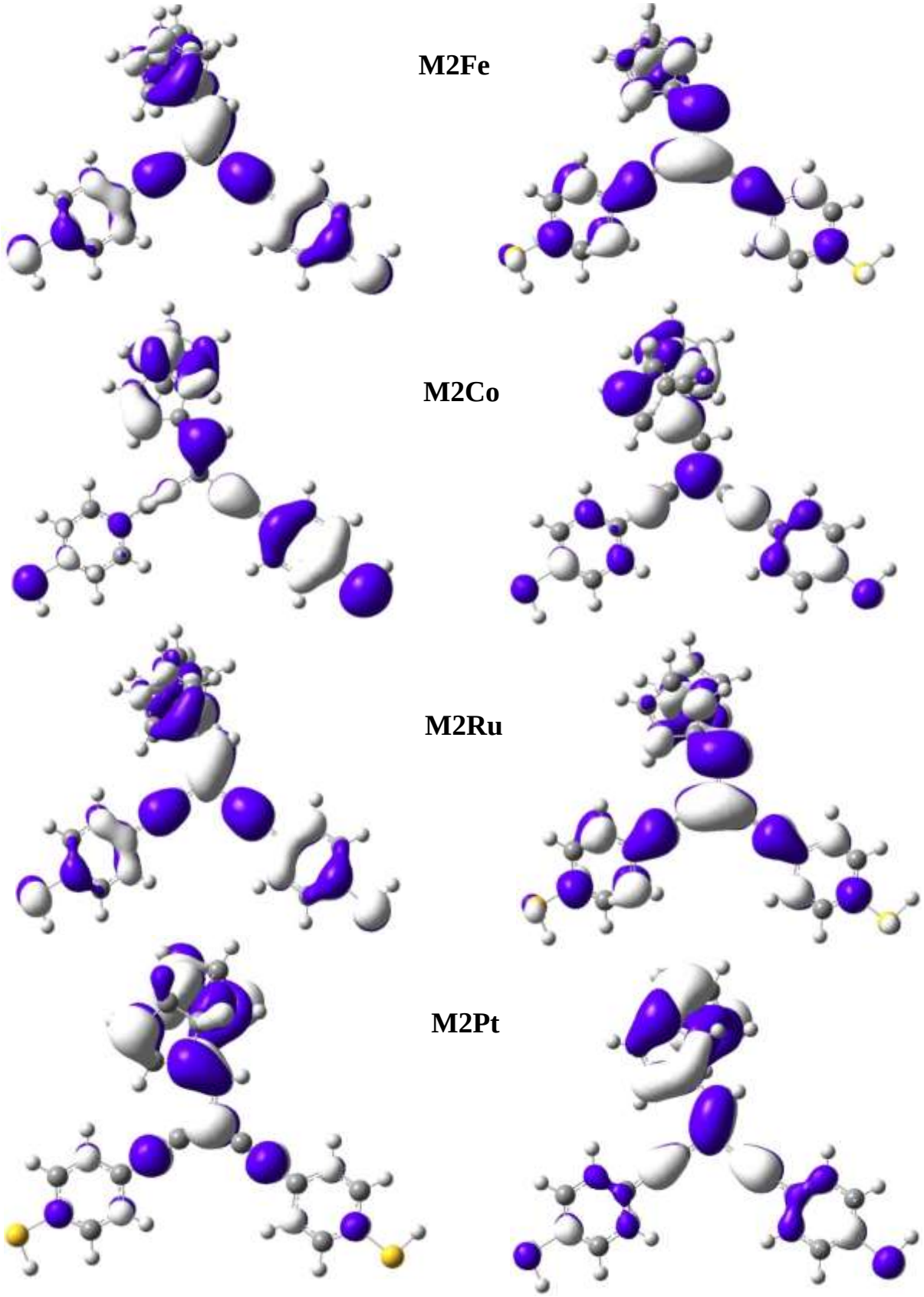

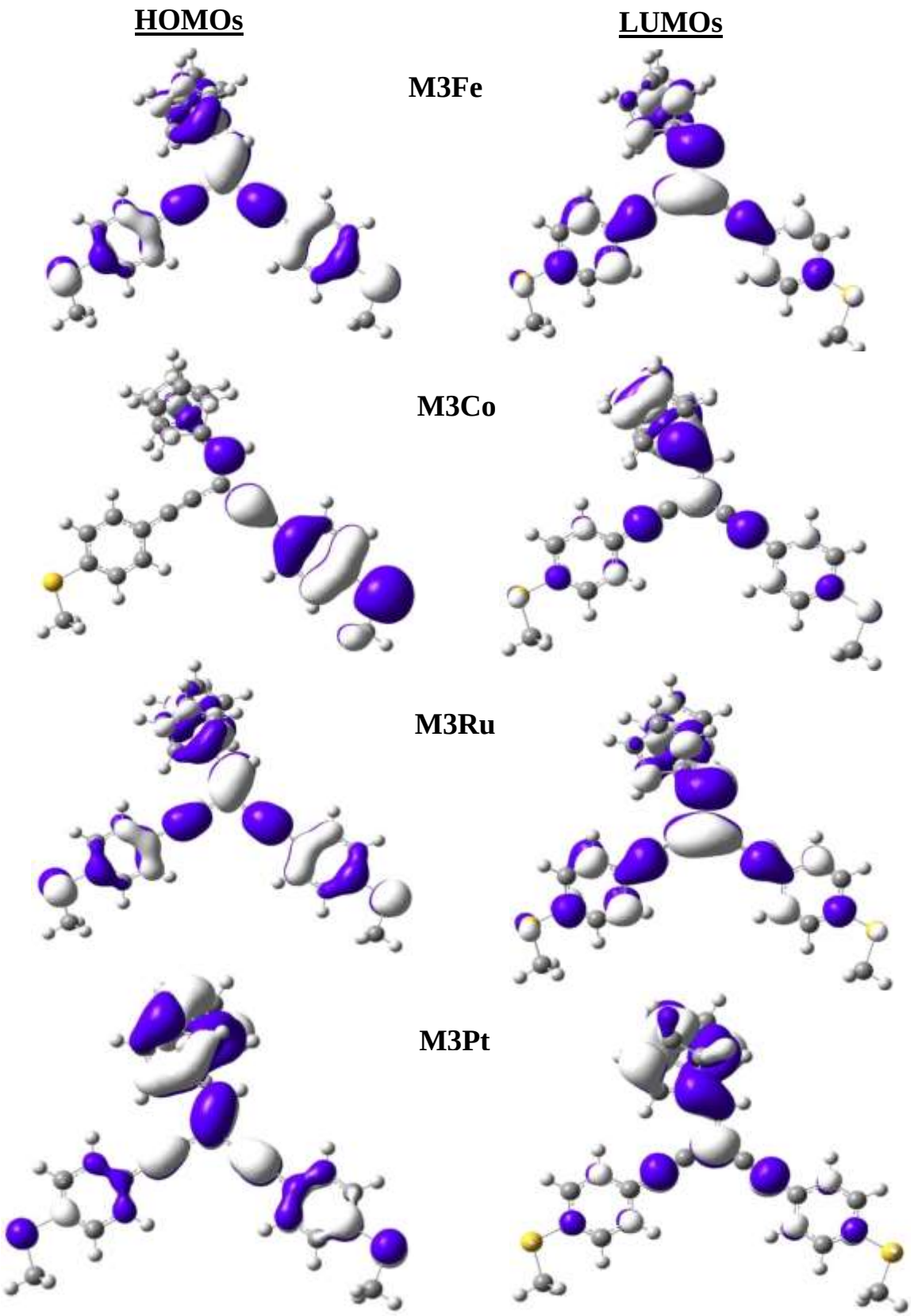

Figure (4-2): The iso-surfaces (±0.02 (e/bohr^3)$^{1/2}$) of the HOMOs and LUMOs for all molecules isolated.

Table 4.1: The HOMO, LUMO and H-L gap for all compounds.

Compounds	HOMO (eV)	LUMO (eV)	H-L gap(eV)
Group 1			
BCP-Fe	**-5.728**	**-2.477**	**3.251**
BCP-Co	**-8.984**	**-6.428**	**2.556**
BCP-Ru	**-5.721**	**-2.486**	**3.235**
BCP-Pt	**-5.344**	**-3.085**	**2.259**
Group 2			
BCPT-Fe	**-5.268**	**-1.995**	**3.273**
BCPT-Co	**-8.255**	**-6.438**	**1.817**
BCPT-Ru	**-5.232**	**-1.988**	**3.244**
BCPT-Pt	**-5.211**	**-3.339**	**1.872**
Group 3			
BCPTM-Fe	**-5.145**	**-1.891**	**3.254**
BCPTM-Co	**-7.775**	**-5.824**	**1.951**
BCPTM-Ru	**-5.111**	**-1.883**	**3.228**
BCPTM-Pt	**-5.103**	**-3.252**	**1.851**

To analyze and understand the behavior of the compounds' absorption spectra, it is required to study their electronic structures. The frontier orbital energies (HOMO and LUMO) and H-L gap for isolated compounds are listed in Table (4.1). According to the data in Table (4.1), some of the compounds investigated exhibit delocalization of the LUMO and localization of the HOMO. It's energies of the investigated compounds are significantly altered as shown in Table (4.1). The results demonstrated that HOMO and LUMO are clearly distinct, implying that differing structures have a significant effect on the electronic properties and that the anchor group and metal have an effect on the HOMO and LUMO energies.

The results indicated that the presence of an electron attracted to N or S in the various anchor groups on both sides of the compounds results in a decrease in the LUMO and hence a decrease in the H-Lgap or energy gap. Additionally, the existence of triple and double C-C bonds results in a decrease in the LUMO energy and a reduction in the energy gap due to the delocalization of both the HOMO and LUMO energies [127,131].

Frontier molecular orbitals FMOs play an important role in determining the charge separated states of compounds. As demonstrated, each organometallic investigated has respectable electron separated states. According to the distribution of HOMO and LUMO in Fig. (4-2), strong localization of the HOMOs occurs on the Bicyclopentadiene-metallic donor subunits to the backbone in the compounds, whereas strong delocalization of the LUMOs occurs on the bridges between the metal and Bicyclopentadiene in the center molecules, indicating that the electron density moves along the backbone in the compounds. Because the electron density of LUMO is predominantly concentrated on the acceptor units, electronic transitions of the

studied compounds from HOMO to LUMO may result in intra-molecular charge transfer from the donor units to the anchor groups on the acceptor units via the conjugated bridge between the two sides.

These findings provide as an excellent jumping-off point for the debate and serve as a basis for comparing HOMO and LUMO molecular orbitals, respectively. Unsurprisingly, the lower and higher energy structures are defined by an electronic structure with boundary orbitals nearly evenly distributed across the molecule center and metal, backbone, and anchor groups on both sides forming a linear p-type path conjugated between atoms (N or S) on either side of the molecules studied. It is worth noting that the weight of LUMO on pyridine anchor groups, as well as on other anchor groups, is significantly more than that of HOMO. This outcome is indicative of two points. The first is the charge carrier transport mechanism, which could be dominated by LUMO except for the thiol group, which is in the HOMO domain. The second argument is that the possibility of this sort of molecule forming a molecular junction is quite great, as is the junction's stability.

4.4 Density of States

The density of states (DOS) is a measure of the number of electronic states in a band per unit energy. It may be computed using the formula $D(E)=\Sigma_i\ \delta(E-\varepsilon_i)$, where ε_i is the system's eigenvalues and δ is the Kronecker delta. The DFT calculated DOS spectra for the isolated molecule versus energy are shown in Fig. (4-3), along with the value of the gap in DOS, which is the distance between the first onset of electron density from left to right between the HOMO and LUMO peaks, which is approximately (3.273-1.817) eV for meta-linked molecules.

M1Fe Pyridyl

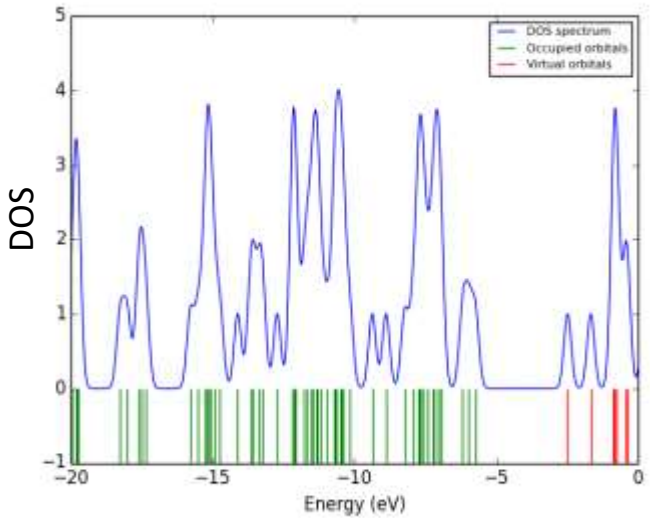

M1Co Pyridyl

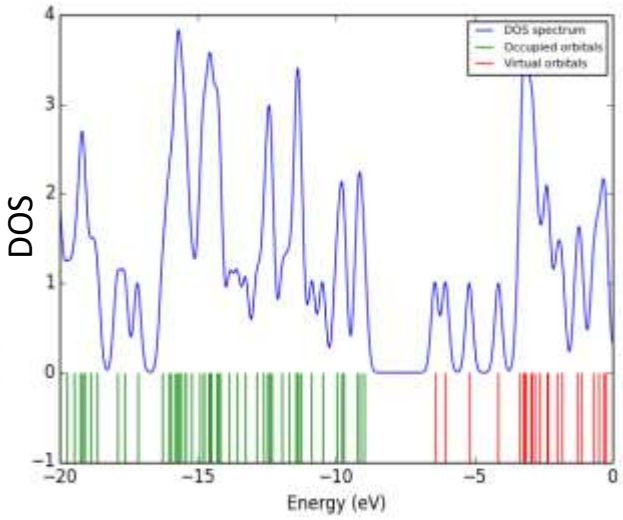

M1Ru Pyridyl

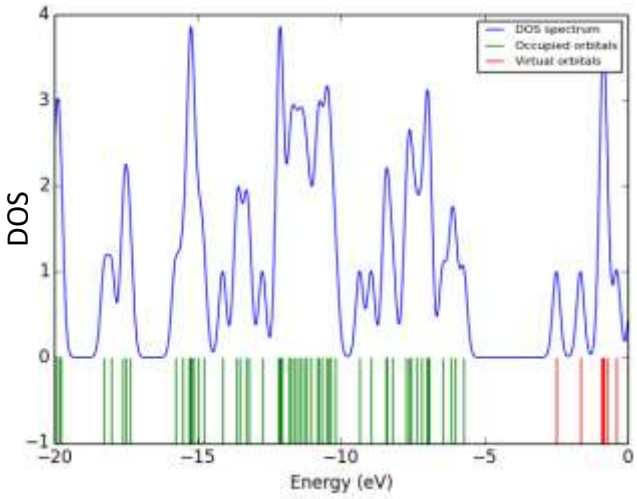

M1Pt Pyridyl

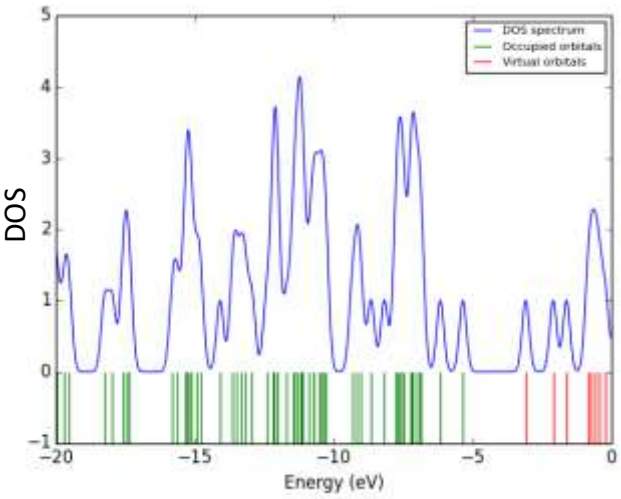

M2Fe Thiol

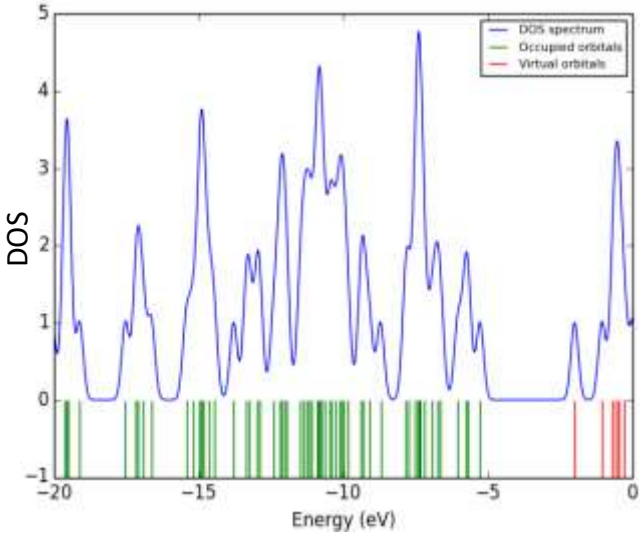

M2Co Thiol

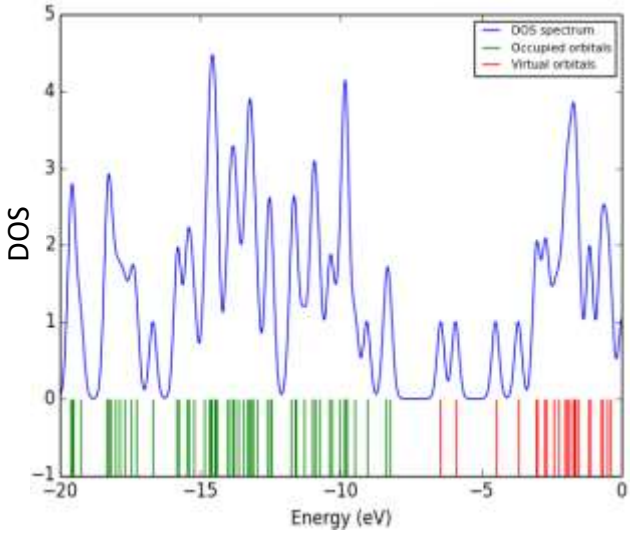

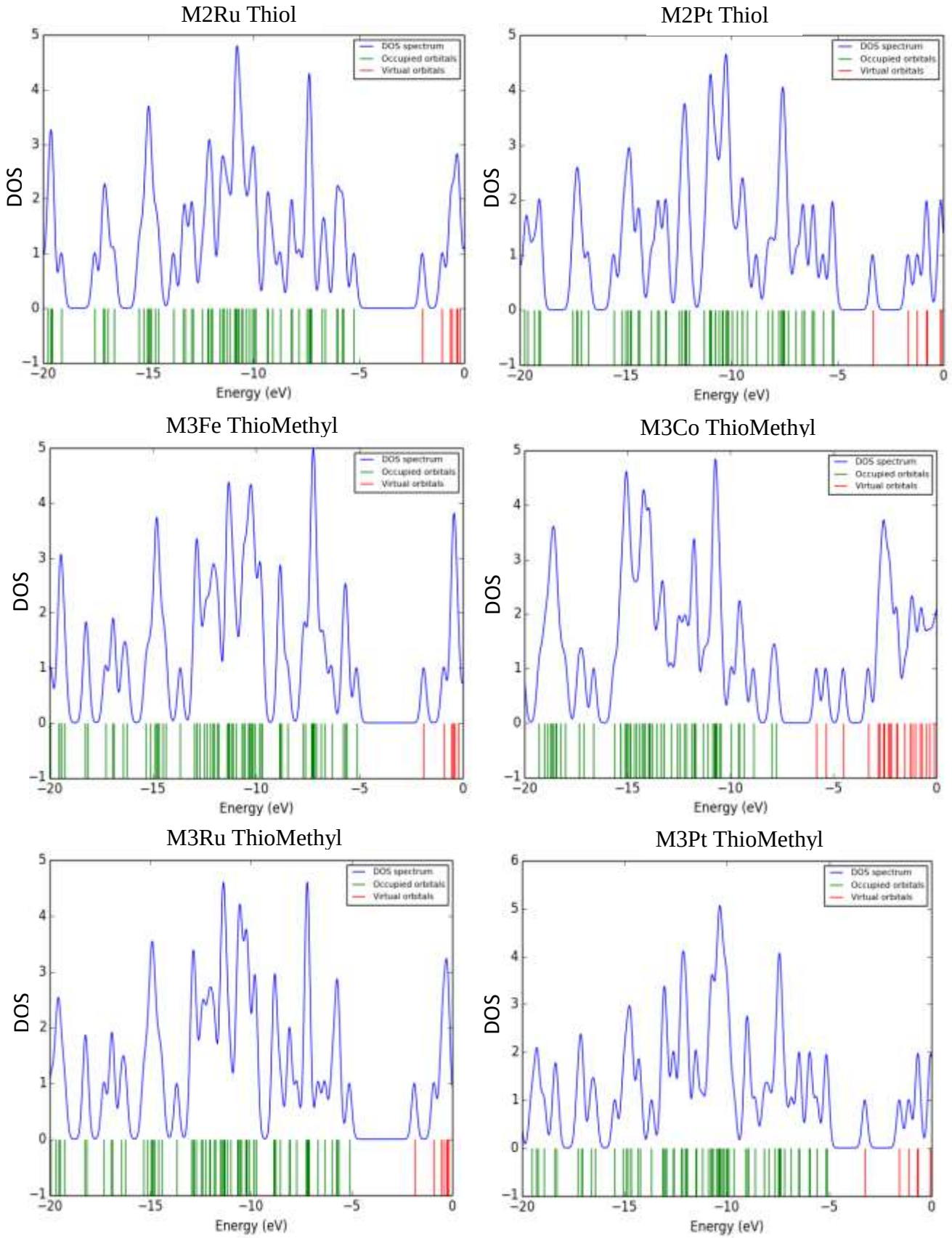

Figure (4-3): Density of state versus energy for meta calculated by DFT, in the gas phase.

As shown, the degeneracy of occupied molecular orbitals is more than that of virtual molecular orbitals in all compounds, indicating that the HOMO was localized and the LUMO was delocalized, and an indicator that the DOS was distributed more in the conduction band than in the valence band. The electronic transmissions in compounds (M1Fe Pyridyl, M1Fe Thiol, and M1Fe ThioMethyl) are feeble because the percentage of direct transmissions is relatively low, around 18%, 10%, and 8%, respectively. While electron transfer is extremely straightforward in the molecule (M1Co ThioMethyl), dependent on the ratio of the transition from HOMO to LUMO, which is approximately 95%. Additionally, the transitions between the compounds (M1Ru Pyridyl, M2Ru Thiol, and M3Ru ThioMethyl) are good, with transfer rates of (50%, 35%, and 43%), respectively.

Finally, we see that the electronic transitions of the compounds containing platinum (M2Pt Thiol and M3Pt ThioMethyl) are good and at a transmission rate of 43% and 41%, respectively. Except when the Pyridyl anchor group is present, it is a weak molecule with a low electronic transmission rate (12%). In comparison to other compounds, the electron in compounds can readily transition from the valence to the conduction band due to the fact that the DOS degeneracy of occupied molecular orbitals is more than that of virtual molecular orbitals. These compounds have the ability to behave appropriately in electronic applications when they interact with other molecules or species.

4.5 UV- Vis Spectra

The Ultraviolet-Visible and UV-V spectra of the substances under research were investigated and evaluated using the time dependent-self-consistent field TD-SCF approach with the same hybrid functional and basis sets as in the B3LYP/SDD-DFT method. The critical factor in determining if a compound can be used as a photovoltaic material is the compound's absorption spectrum being equal to the solar spectrum. As illustrated in figure (4-4), the compounds exhibit both direct and indirect transitions from the valence band to the conduction band at absorption wave lengths of (690.82, 576.08, 471.31, and 449.03)nm, respectively for group1; within this group, direct and indirect transmissions occur in varying proportions, as indicated by the proportion of direct transmissions in red in Table (4.2). The compounds in group2 transition directly or indirectly from valence to conduction at absorption wave lengths of (684.42, 1318.10, 442.3, and 821.48)nm, respectively. Compound M3Co also exhibits a direct transition HOMO to LUMO with a wavelength of 684.46nm; this molecule exhibits the highest direct transmission of up to 95%, which is not observed in the other molecules. The values of intensity (ε =a.u) or absorption energy E_{abs}(eV), absorption wave length λ_{max}(nm), oscillator strength O.S, molecular orbital character MOC %, and transition states are shown in Table (4.2).

Table 4.2: The Absorption spectra calculations of the compounds.

Compounds	E_{abs} (ε= a.u)	λ_{max} (nm)	O.S	MO character %
Group 1				
BCP-Fe	**661**	**690.82**	**0.0139**	H-2->L+3 (13%), H-1->L+4 (27%), **HOMO->LUMO (18%)**, HOMO->L+3 (21%), H-2>LUMO(9%), H-2->L+7 (3%), HOMO->L+7 (6%)
BCP-Co	**4268**	**576.08**	**0.1051**	**H-11->L+1 (22%), H-10->LUMO (38%), H-1->LUMO (28%),H-10->L+2 (5%), H-9->L+1 (2%)**
BCP-Ru	**5958**	**471.31**	**0.1203**	**H-2->LUMO (24%), HOMO->LUMO (50%), H-3 >LUMO (4%), H-3->L+2 (3%), H-2->L+2 (5%), H-1->L+3 (3%), HOMO->L+2 (6%)**
BCP-Pt	**21988**	**449.03**	**0.4899**	**HOMO->LUMO (12%), HOMO->L+1 (76%) H-7->LUMO (4%), H-1->LUMO (3%), H-1->L+1 (2%)**
Group2				
BCPT-Fe	**630**	**684.42**	**0.0131**	**H-2->LUMO (15%), H-2->L+5 (25%), H-1->L+4 (30%), HOMO->LUMO (10%), HOMO->L+5 (13%), H-2->L+7 (3%)**
BCPT-Co	**52**	**1318**	**0.0008**	**H-7->L+1 (27%), H-3->L+1 (18%), H-2->L+1 (14%), HOMO->L+1**

				(19%) H-13->L+1 (4%), H-10->L+1 (7%), H-4->L+1 (6%)
BCPT-Ru	**12040**	**442.3**	**0.1729**	**H-2->LUMO (16%), H-1->LUMO (32%), HOMO->LUMO (35%), H-4->LUMO (3%), H-2->L+4 (3%), H-1->L+4 (4%)**
BCPT-Pt	**5340**	**821.48**	**0.1123**	**H-3->LUMO (32%), H-2->LUMO (14%), HOMO->LUMO (40%), H-6->LUMO (9%), H-1->LUMO (4%)**
Group3				
BCPTM-Fe	**648**	**683.87**	**0.0134**	**H-2->LUMO (15%), H-2->L+5 (26%), H-1->L+4 (30%), HOMO->L+5 (11%), H-2->L+7 (2%), HOMO->LUMO (8%)**
BCPTM-Co	**29788**	**684.46**	**0.5014**	**HOMO->LUMO (95%), H-11->LUMO (2%)**
BCPTM-Ru	**13919**	**442.19**	**0.2358**	**H-2->LUMO (18%), H-1->LUMO (19%), HOMO->LUMO (43%), H-4->LUMO (3%), H-4->L+4 (2%), H-2->L+4 (4%), H-1->L+5 (2%), HOMO->L+4 (2%)**
BCPTM-Pt	**5678**	**825.12**	**0.1185**	**H-5->LUMO (10%), H-4->LUMO (27%), H-2->LUMO (14%), HOMO->LUMO (41%), H-3->LUMO (3%)**

M1Fe

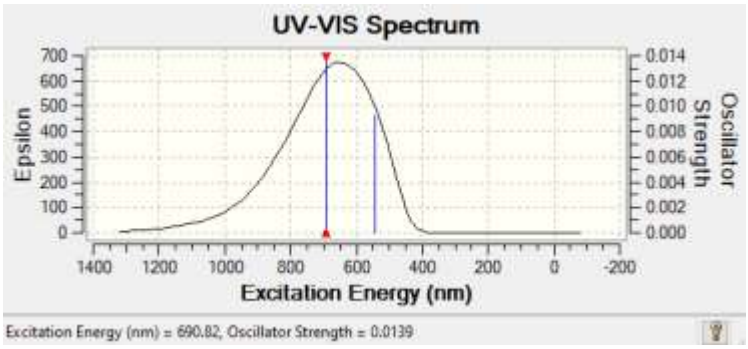

Absorption Spectra **Emission Spectra**

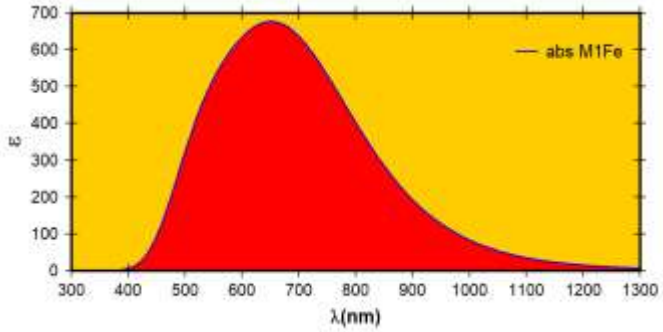

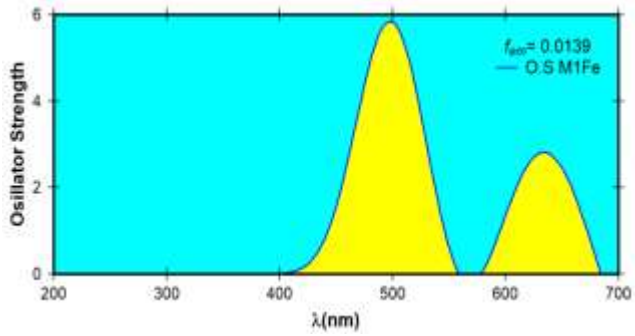

M1Co

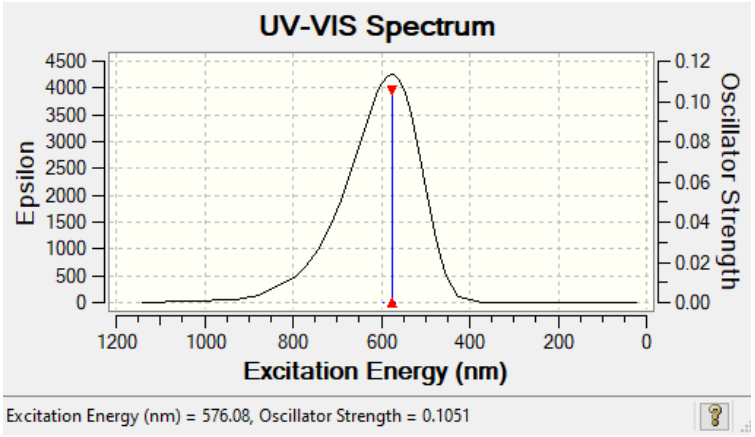

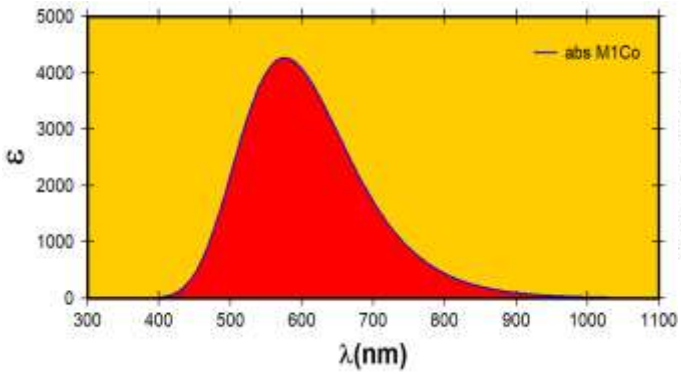

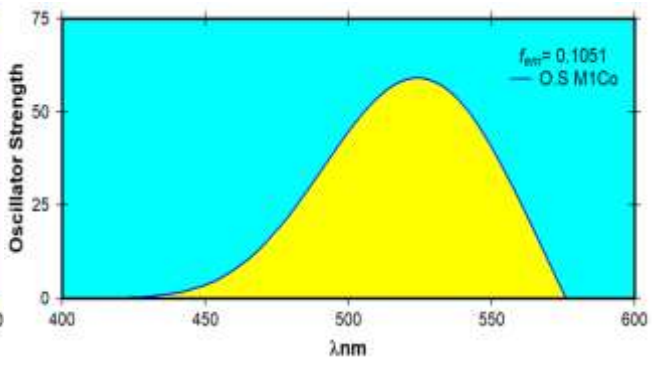

M1Ru

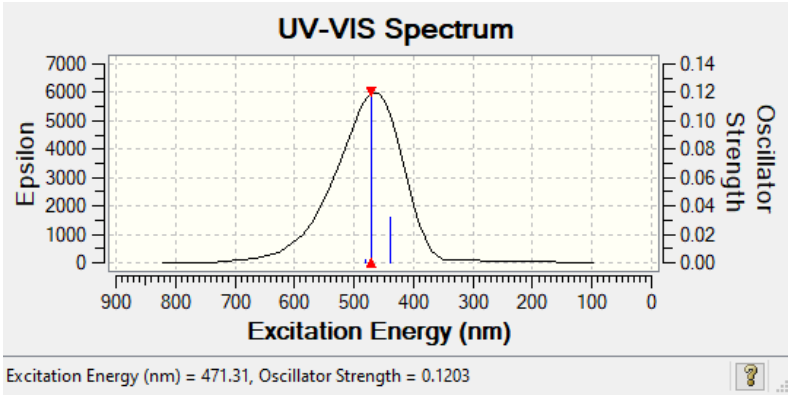
UV-VIS Spectrum
Epsilon
Oscillator Strength
Excitation Energy (nm)
Excitation Energy (nm) = 471.31, Oscillator Strength = 0.1203

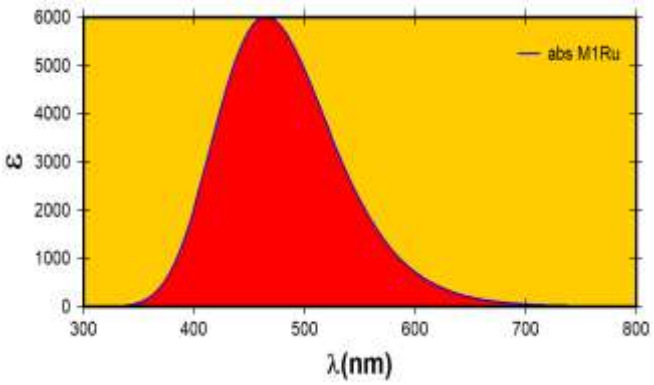
abs M1Ru
ε
λ(nm)

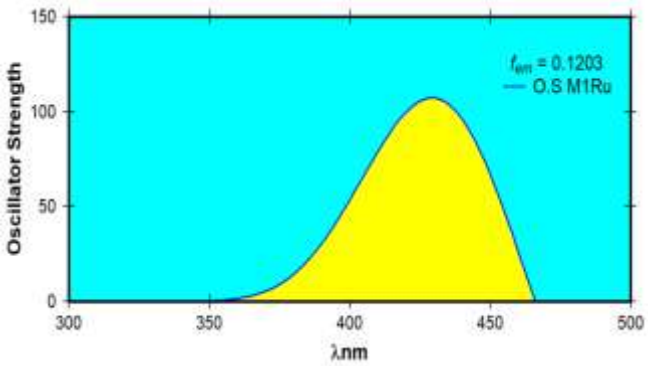
f_{em} = 0.1203
O.S M1Ru
Oscillator Strength
λnm

M1Pt

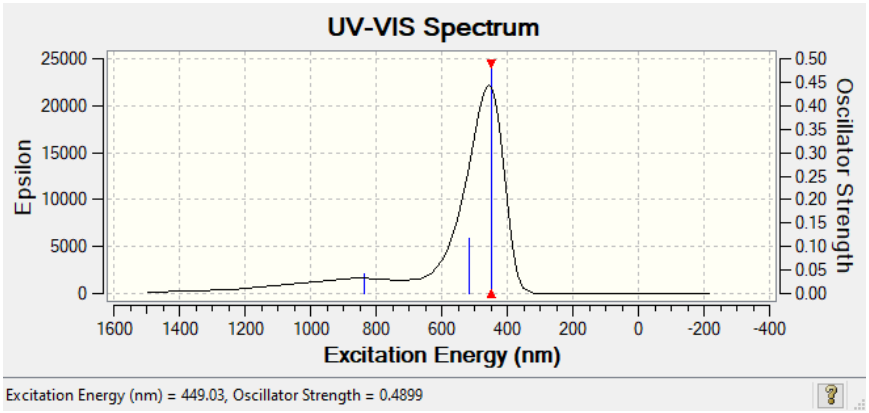
UV-VIS Spectrum
Epsilon
Oscillator Strength
Excitation Energy (nm)
Excitation Energy (nm) = 449.03, Oscillator Strength = 0.4899

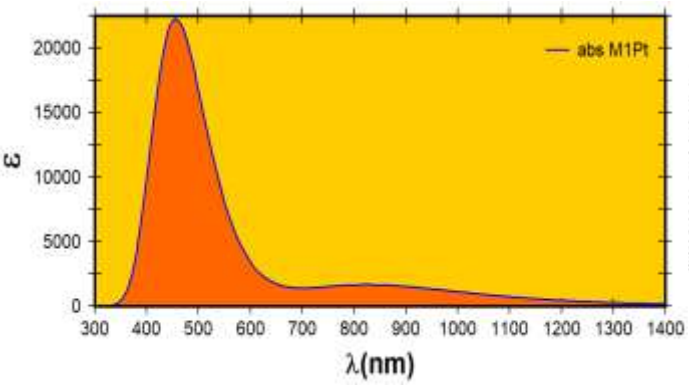
abs M1Pt
ε
λ(nm)

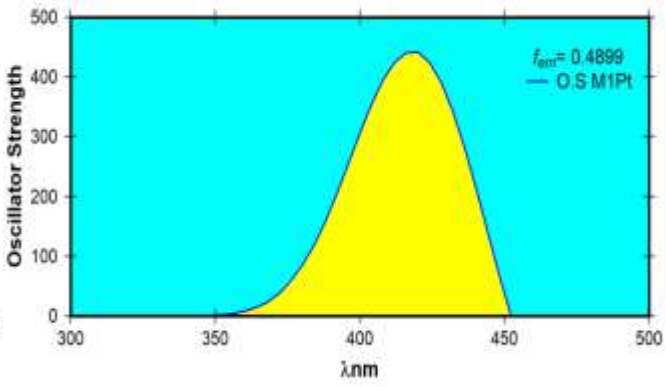
f_{em}= 0.4899
O.S M1Pt
Oscillator Strength
λnm

M2Fe

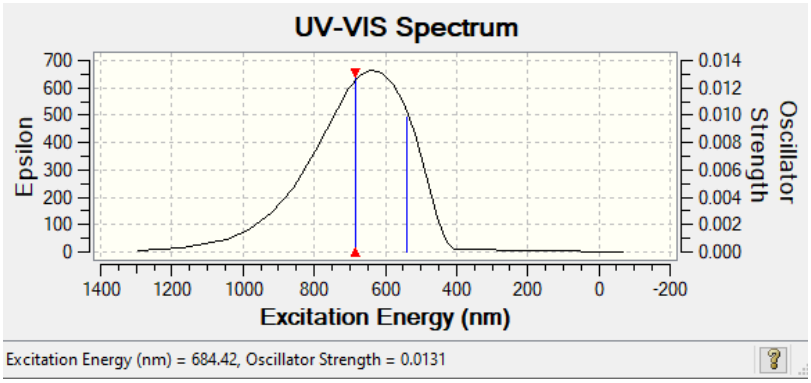

Absorption Spectra

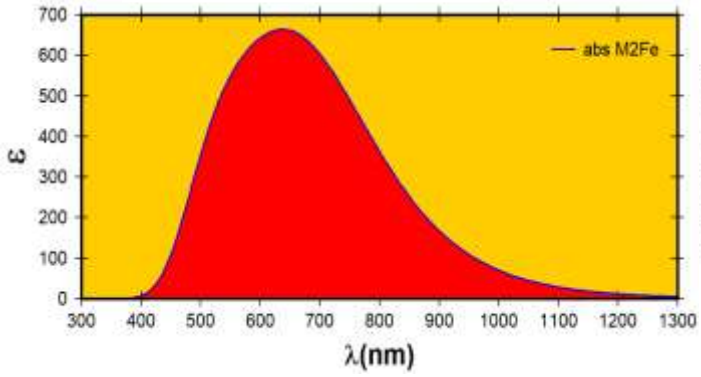

Emission Spectra

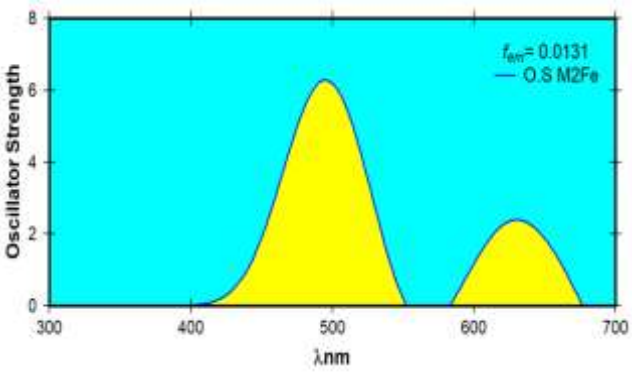

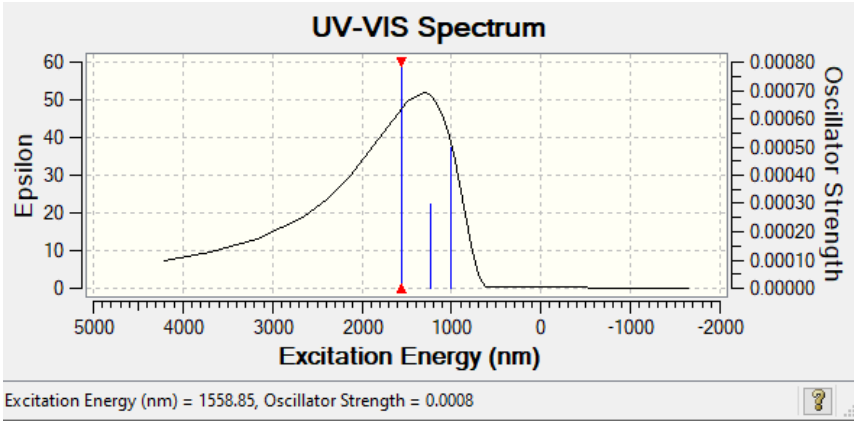

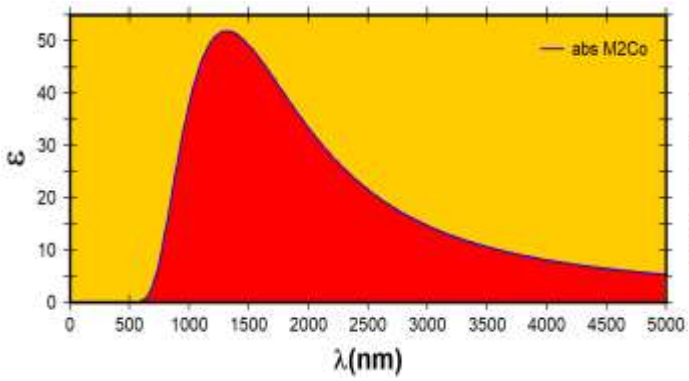

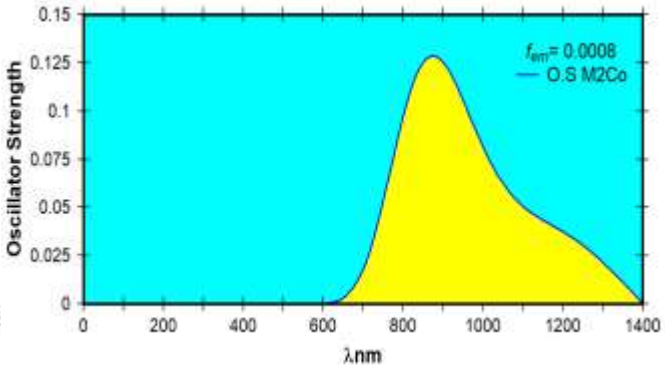

M2Ru

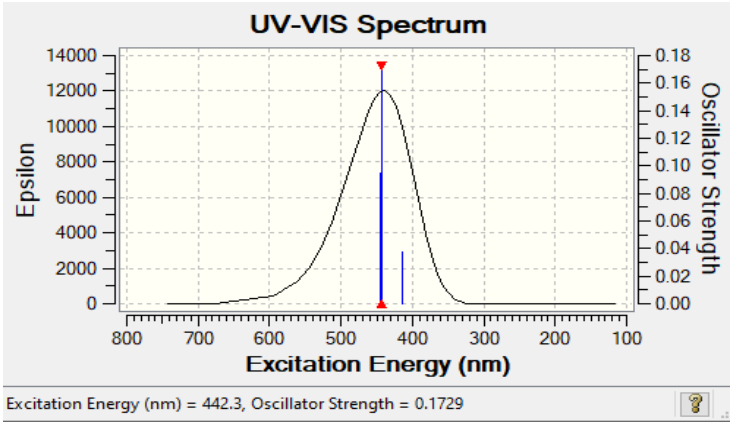
UV-VIS Spectrum
Epsilon
Oscillator Strength
Excitation Energy (nm)
Excitation Energy (nm) = 442.3, Oscillator Strength = 0.1729

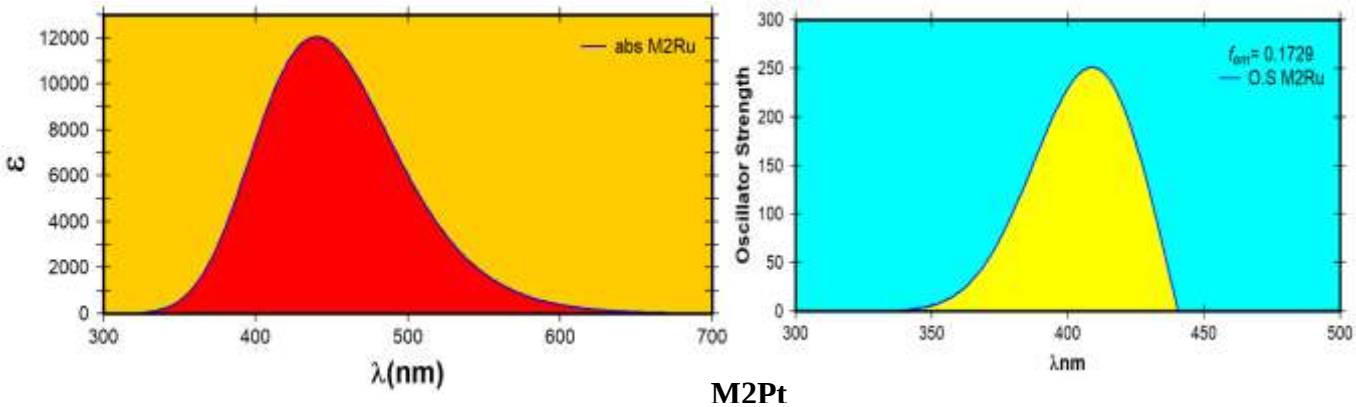
abs M2Ru
ε
λ(nm)
f_{em}= 0.1729
O.S M2Ru
Oscillator Strength
λnm

M2Pt

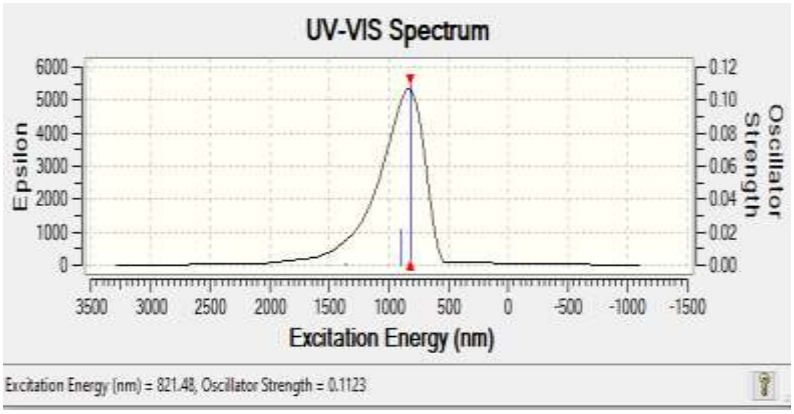
UV-VIS Spectrum
Epsilon
Oscillator Strength
Excitation Energy (nm)
Excitation Energy (nm) = 821.48, Oscillator Strength = 0.1123

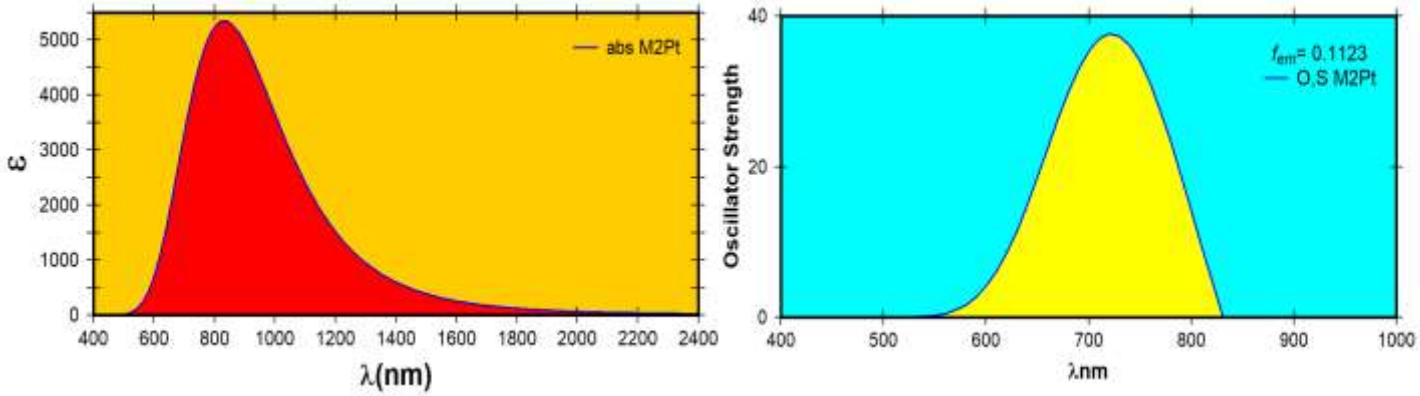
abs M2Pt
ε
λ(nm)
f_{em}= 0.1123
O.S M2Pt
Oscillator Strength
λnm

M3Fe

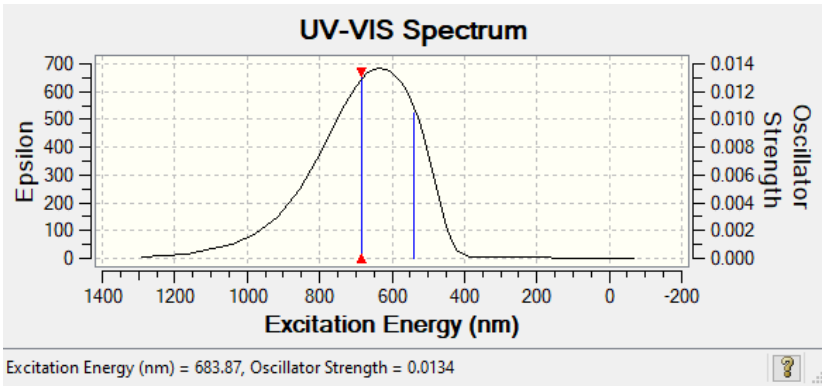

Absorption Spectra

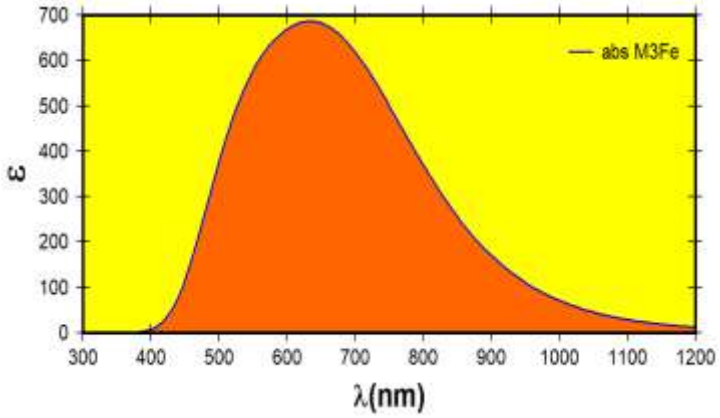

Emission Spectra

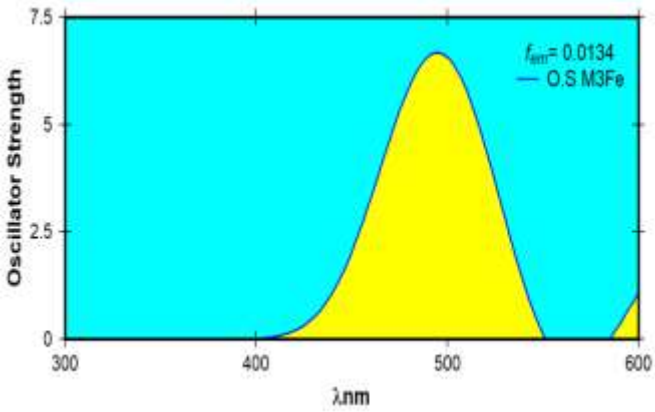

M3Co

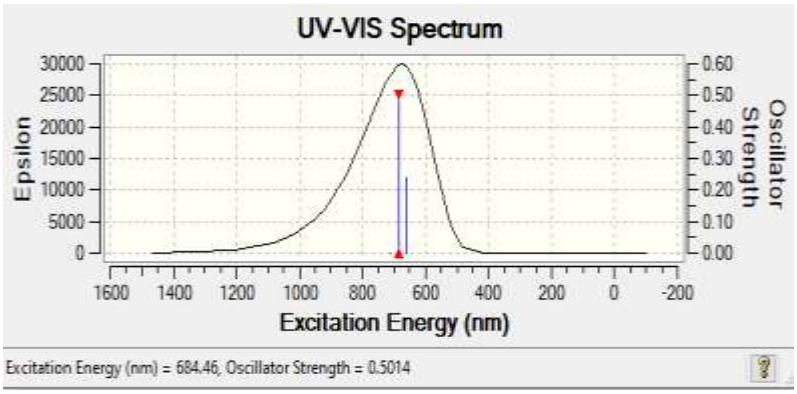

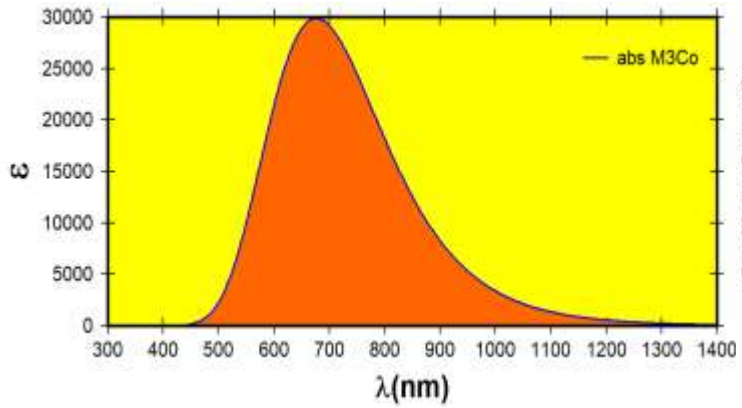

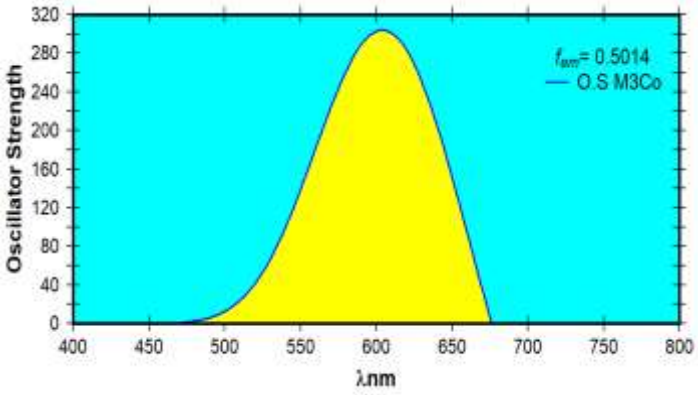

M3Ru

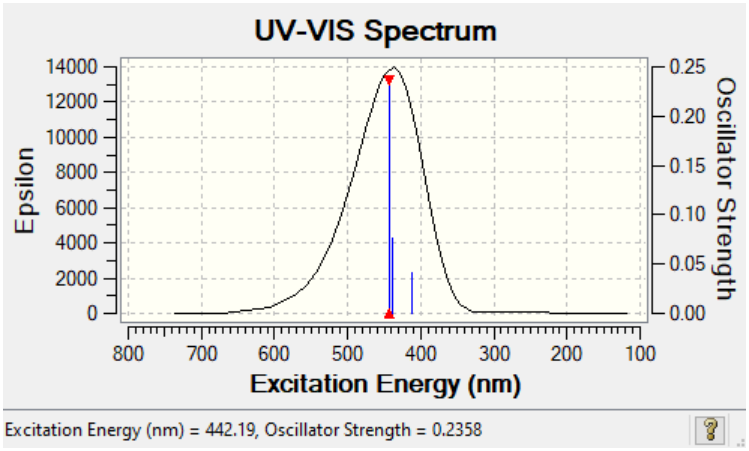
UV-VIS Spectrum
Epsilon
Oscillator Strength
Excitation Energy (nm)
Excitation Energy (nm) = 442.19, Oscillator Strength = 0.2358

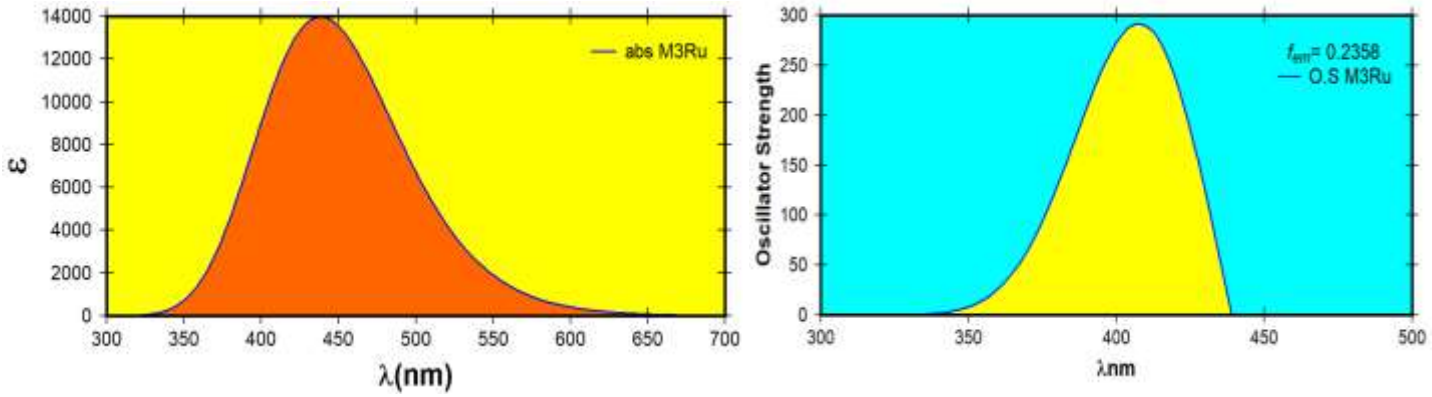
abs M3Ru
ε
λ(nm)
Oscillator Strength
f_{em}= 0.2358
O.S M3Ru
λnm

M3Pt

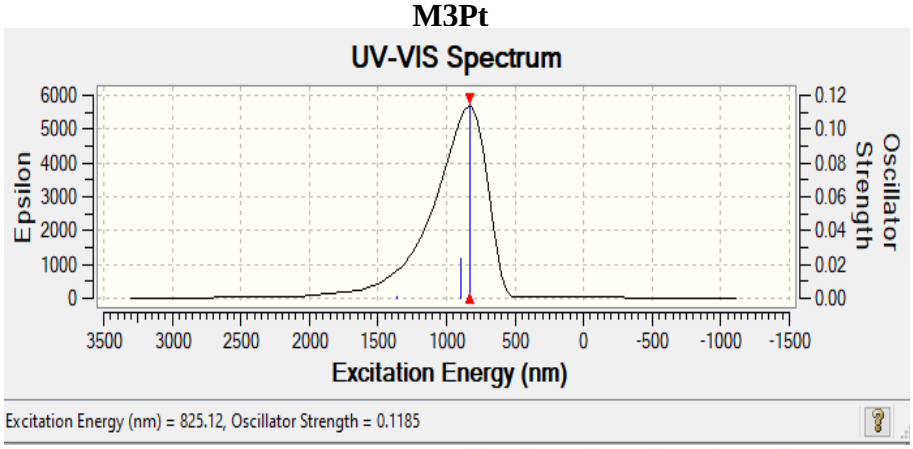
UV-VIS Spectrum
Epsilon
Oscillator Strength
Excitation Energy (nm)
Excitation Energy (nm) = 825.12, Oscillator Strength = 0.1185

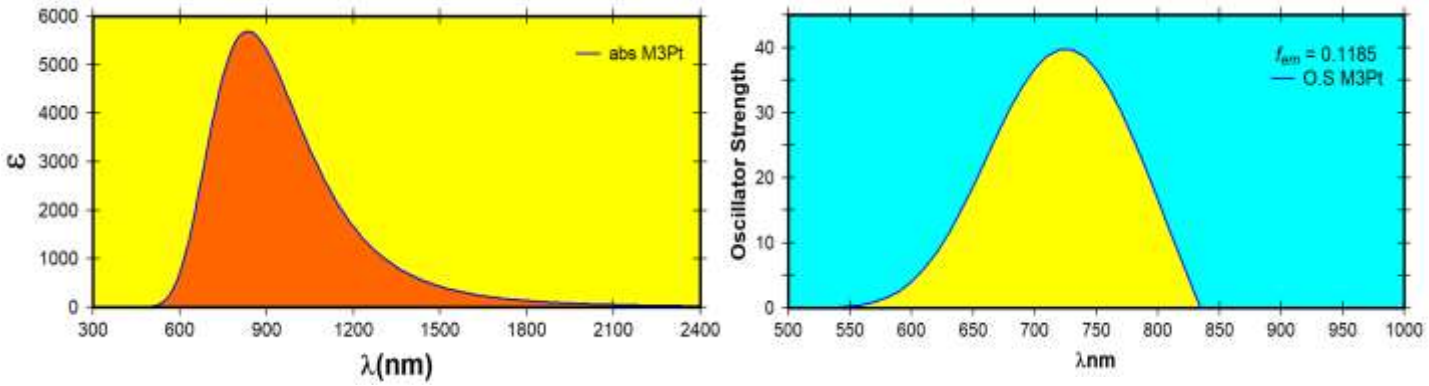
abs M3Pt
ε
λ(nm)
Oscillator Strength
f_{em} = 0.1185
O.S M3Pt
λnm

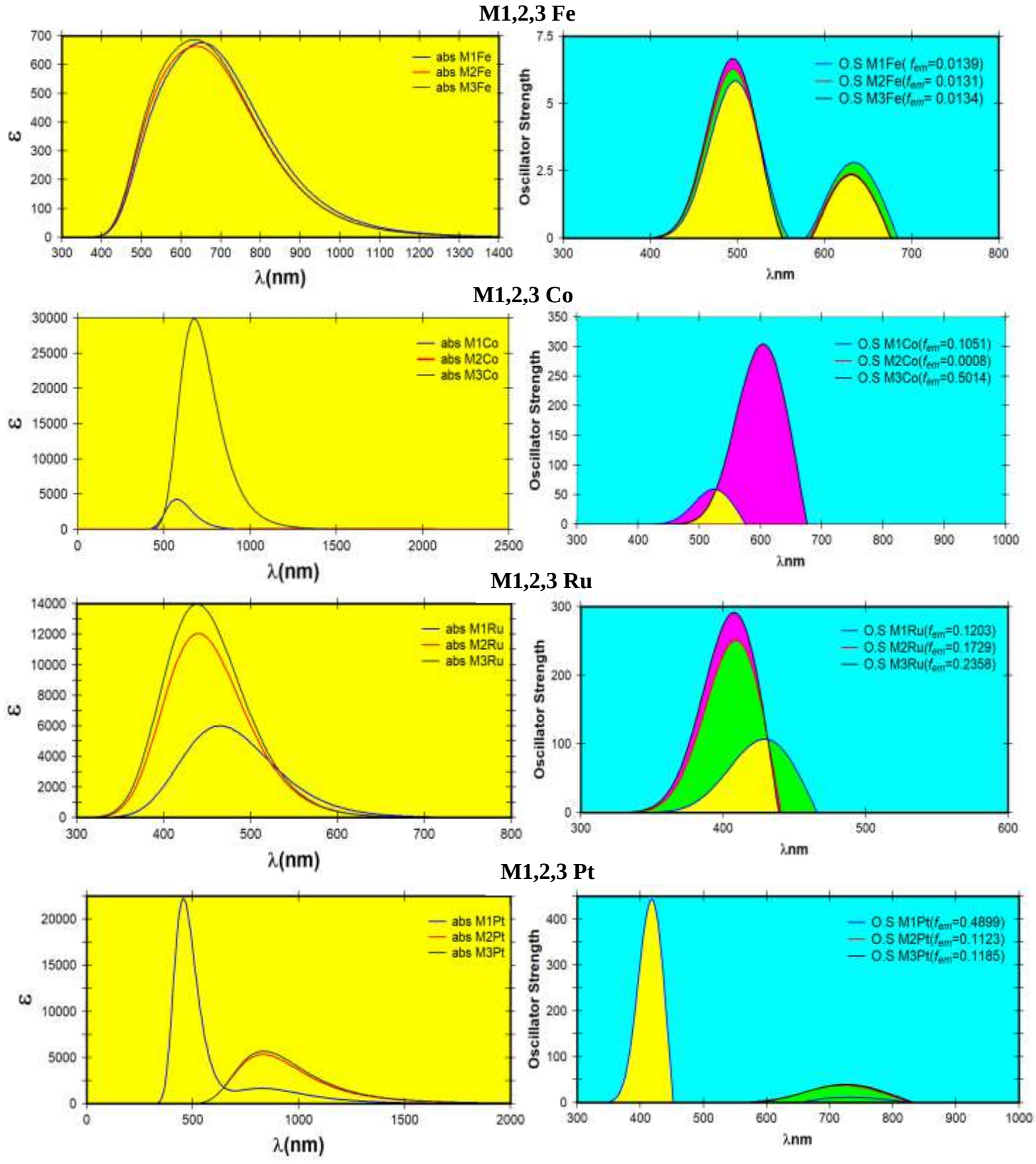

Figure (4-4): the Absorption and Emission spectra for all compound's.

Figure (4-4) highlights numerous significant findings. The first is shown in all figures, and it illustrates the absorption intensity as a function of wavelengths. It demonstrates that the absorption intensity increased substantially as the oscillation strength increased. The absorption intensity (ε) of three groups (Pyridyl, Thiol, and ThioMethyl) varies according to the group of the anchor and the metal used, with the cobalt metal in the second group (thiol) having the lowest absorption intensity (52 a.u) and the cobalt metal in the third group having the highest absorption intensity (29788 a.u) (thiomethyl). Not only that, but we can see a sharp change in the absorption peaks, with the maximum absorption occurring at 684.46 nm. In comparison, the molecule's lowest absorption intensity (ε) was at 1318 nm, indicating a fast transition from the visible to the infrared domain. As a result of these findings, we may assume that altering the anchor group and metallic composition not only influences absorption intensity, but also results in an effective displacement at wavelengths.

The second important result is exhibited in Fig. (4-4), which shows the emission oscillator strength (f_{em}) as a function of the wavelengths. Interestingly, the anchor group Co-ThioMethyl produces the highest f_{em} (0.5014), while Co-Thiol gives the lowest f_{em} (0.0008). The order of the absorption intensity (ε) for three groups ($\boldsymbol{\varepsilon_{M1Fe} > \varepsilon_{M3Fe} > \varepsilon_{M2Fe}}$) and the emission oscillator strength (f_{em}) order is ($\boldsymbol{f_{em\ M1Fe} > f_{em\ M3Fe} > f_{em\ M2Fe}}$), ($\boldsymbol{\varepsilon_{M3Co} > \varepsilon_{M1Co} > \varepsilon_{M2Co}}$) and the emission oscillator strength (f_{em}) order is ($\boldsymbol{f_{em\ M3Co} > f_{em\ M1Co} > f_{em\ M2Co}}$), ($\boldsymbol{\varepsilon_{M3Ru} > \varepsilon_{M2Ru} > \varepsilon_{M1Ru}}$) and the emission oscillator strength (f_{em}) order is ($\boldsymbol{f_{em\ M3Ru} > f_{em\ M2Ru} > f_{em\ M1Ru}}$) and

($\varepsilon_{M1Pt} > \varepsilon_{M3Pt} > \varepsilon_{M2Pt}$) and the emission oscillator strength (f_{em}) order is ($f_{em\ M1P} > f_{em\ M3Pt} > f_{em\ M2Pt}$) as shown in Table (4.2)

These findings provide a potential theoretical technique for the selection of structures and materials suitable for use as active laser medium, light-emitting diodes, and solar cells.

To explain the Fig. (4-4) and Table (4.2) for the four metals used in the three groups and the role of each metal in causing changes in those molecules in terms of absorption intensity and oscillation strength, we find that iron (Fe) metal is present in all three groups, the wavelength of which falls within the visible spectrum, and the absorption intensity of which ranges between (600-700) a.u., which encourages the use of these molecule. We observe that the greater the oscillation strength in the production of light-emitting diodes, as well as the greater the absorption intensity.

To explain the role of cobalt metal in these single molecules linked to various anchor groups, it was discovered that this metal has a high absorption intensity and oscillation strength in these molecules linked to the pyridyl anchor group and all of its transfers are indirect, whereas the thiol anchor group linked to these monomeric molecules has a low absorption intensity and oscillation strength. The absorption intensity and oscillation strength are very weak, which is due to the cobalt metal's high resistance to heat, and most importantly, the cobalt metal's presence with thiomethyl, the anchor group, which has a very high absorption intensity and oscillation strength due to the strong interaction between cobalt and this group. As is evident from the fact that nearly all electrical transitions are direct. Additionally, because these molecules have a high oscillation strength, they may be employed as an

effective medium for the laser and as light-emitting diodes due to their wavelength being in the visible area of the spectrum. High-intensity molecules can be employed in the construction of solar cell devices.

In light of the results obtained from the presence of ruthenium metal in these monomers molecules, we determined that it plays an active role in the third group (the thiomethyl group), as it has a high absorption intensity and strong oscillation strength, which contribute to its use in light-emitting diodes due to its wavelengths falling within the visible spectrum's three groups, as well as the high intensities, which contribute to the use of these molecules in the formation of solar cells.

Finally, we discover that the platinum metal used in the center of these molecules in the first group (pyridyl) has a high absorption intensity and an excellent oscillation strength, allowing it to be used as an effective medium for lasers, whereas the other groups have a lower absorption intensity and oscillation strength, indicating that the used pyridyl anchor group has good physical properties.

Part II

4.6 Structural and Geometrical Properties

To gain a better understanding of the conduction behavior, we used DFT to analyze the electronic characteristics of the molecules and the electrical behavior of the junctions. All molecules' electronic structures were preliminary studied at the B3LYP theoretical level using the SDD basis set. The study and control of electrical and electronic properties by single molecules coupled to two electrodes has generated considerable interest. Experiments and theoretical calculations shed light on the charge transfer mechanisms in custom-designed nanoscale junctions and on the interplay of the single molecule's chemical structure, electronic structure, and conductivity. In this investigation, the molecules were first geometrically relaxed in isolation to obtain the geometries depicted in Fig. (4-1). Geometric optimizations were performed using the DFT code SIESTA, which utilizes a generalized gradient approximation (PBE functional), a double-zeta polarized basis set, a force tolerance of 0.01 eV/A, and a real-space grid determined by a plan wave cut-off energy of 250 Ry.

The geometric formations before and after molecules are bonded to the electrodes are depicted in Fig. (4-5). Take note that different molecular binding groups have been utilised in the various molecular formulations. These various anchor groups enable us to investigate the thermal and electrical properties, as well as the effect of the anchor and metallic groups on these variables. The geometrical and structural properties of all molecules are depicted in Fig. (4-5), both before and after they bind to the gold electrodes. To begin, there is the molecular junction, which is the distance between each

molecule's nitrogen and sulfa atoms' centers. Clearly, this work contains molecules with a variety of metallic and anchor groups. This presents an ideal opportunity to investigate the effect of molecular structure on these compounds' electrical and thermoelectric properties. Additionally, it is demonstrated that there is a significant difference in the molecular lengths of all molecular junctions (which is the center to center distance of the apex atoms of the two opposing gold pyramids in the relaxed structure). Additionally, these results demonstrated that the bond length, defined as the distance between the top gold atoms of the pyramidal electrode and the anchor (N and S) atoms, is constant for all molecular junctions, equaling (0.25 and 0.23nm), as is the angle between [Carbon-Nitrogen and Gold is 180^{o} and Carbon-Sulfa and Gold is 120^{o}], which is consistent with references [8, 9, 14]

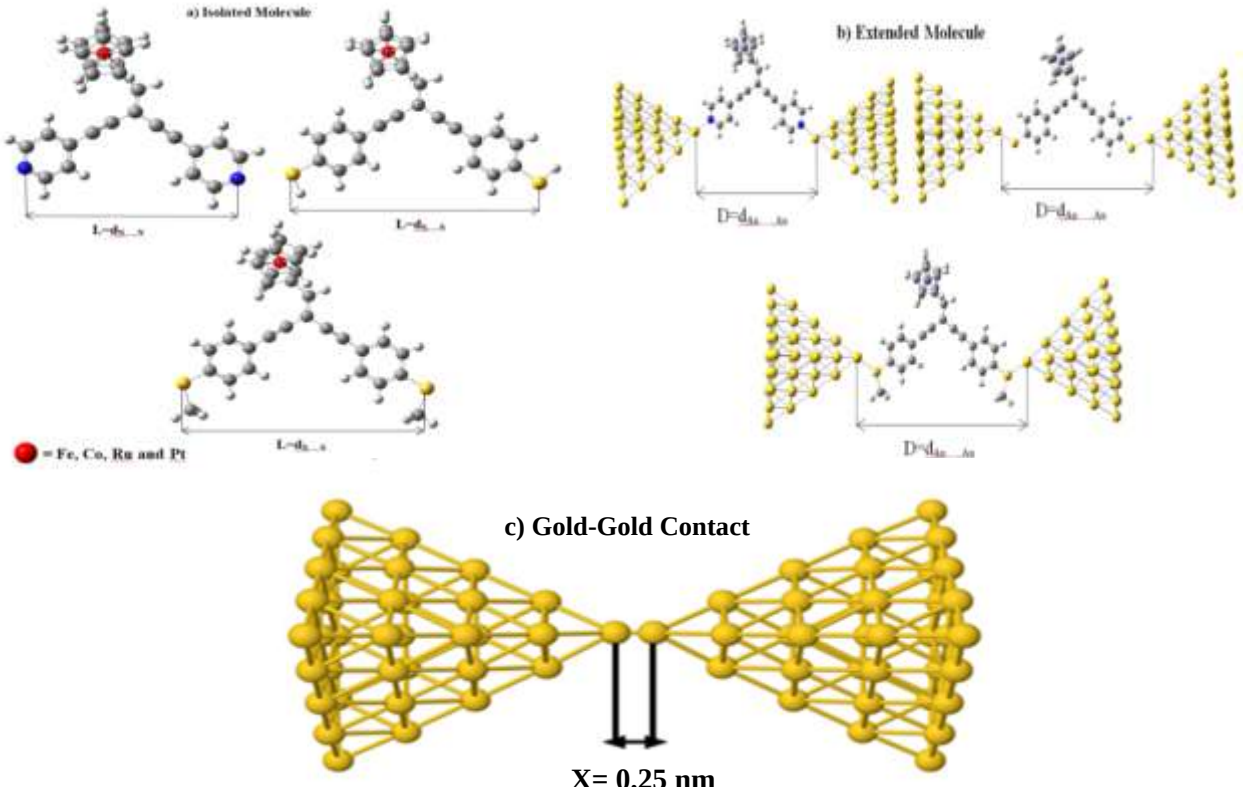

Figure (4-5): Schematic representation of the extended molecule of Au-M-Au;(a) shows an isolated molecule; (b) shows the extended molecule; (c) shows the gold contact.

4.7 The Electronic and Electric Properties

The electronic properties of the molecular necklace can be interpreted and comprehended by examining the behavior of electrons in these molecules. The isolated molecule's properties and the interaction between the molecule and the electrodes have an effect on the open system's electronic properties. As a result, transport models must account for both aspects in order to comprehend the electron scattering process between the two electrodes. This entails developing a method for resolving the problem of interacting electrons.

4.7.1 Transmission Coefficient and Electrical Conductance

The transmission coefficient T(E) at a molecular junction of electrons with energy travelling from one electrode to another will be described using a one-dimensional structure with a randomly spread region. The various types of resonance that describe conductance will next be addressed within the context of a general theory of electronic transmission. T(E) is a property of the entire system, which includes the leads, the molecule, and the contact between the leads and the molecule. Nonetheless, if the contact between the electrodes is poor, a graph of T(E) vs E will reflect the isolated molecule's energy-level structure. If the isolated molecule possesses energy levels E, T(E) will exhibit a succession of peaks (i.e. resonances) at energies around the levels E. The transmission coefficient and conductance were estimated in this thesis by first getting the relevant Hamiltonian and overlap matrices using SIESTA and then utilizing the GOLLUM code. This section discusses the effect of altering the metal core of the molecule and the anchor groups (at the ends of the molecule) on the results reported in Figures (4-6), (4-7), and (4-8).

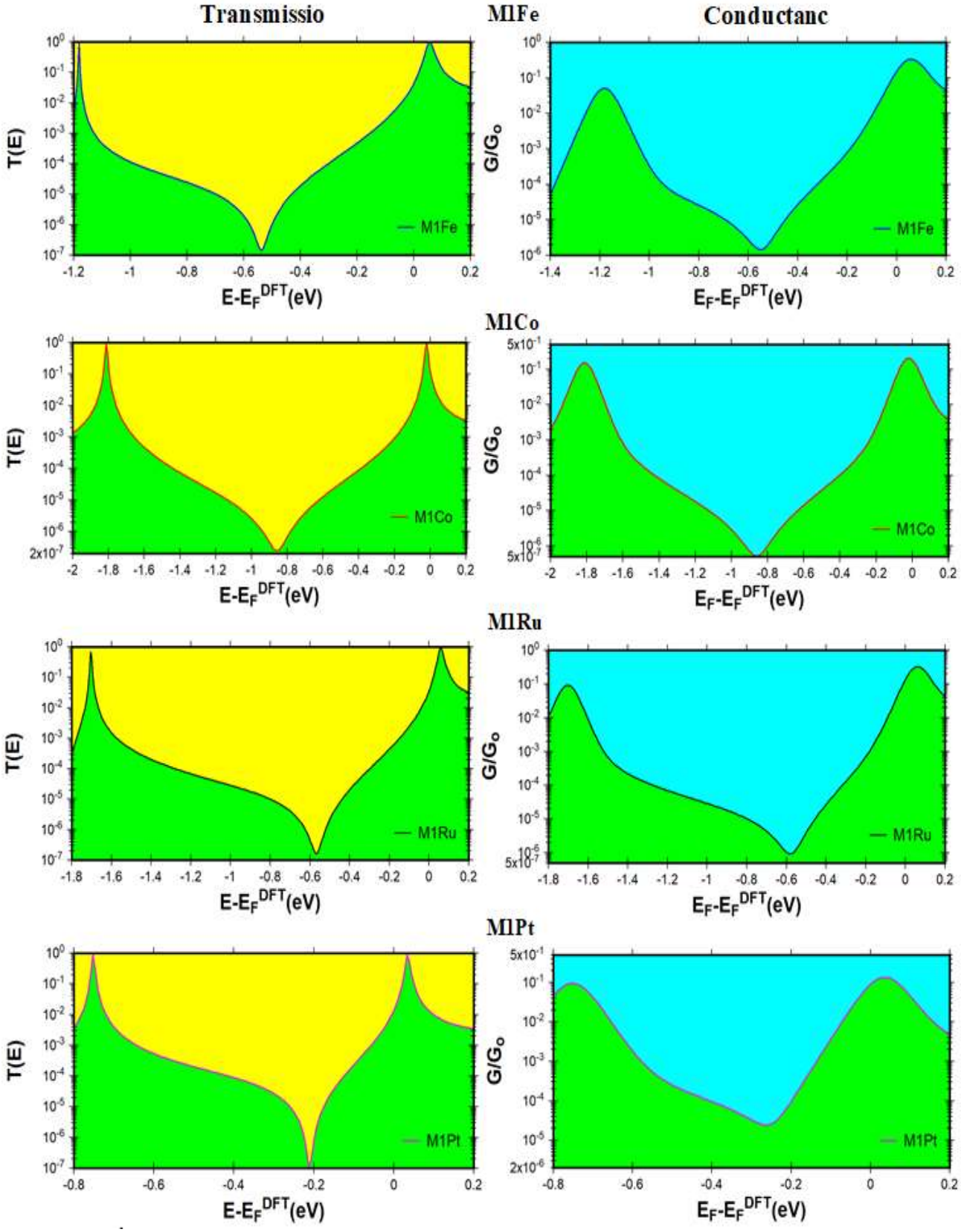
Transmissio
MIFe
Conductanc
T(E)
G/G$_o$
M1Fe
E-E$_F^{DFT}$(eV)
E$_F$-E$_F^{DFT}$(eV)
MICo
M1Co
MIRu
M1Ru
MIPt
M1Pt

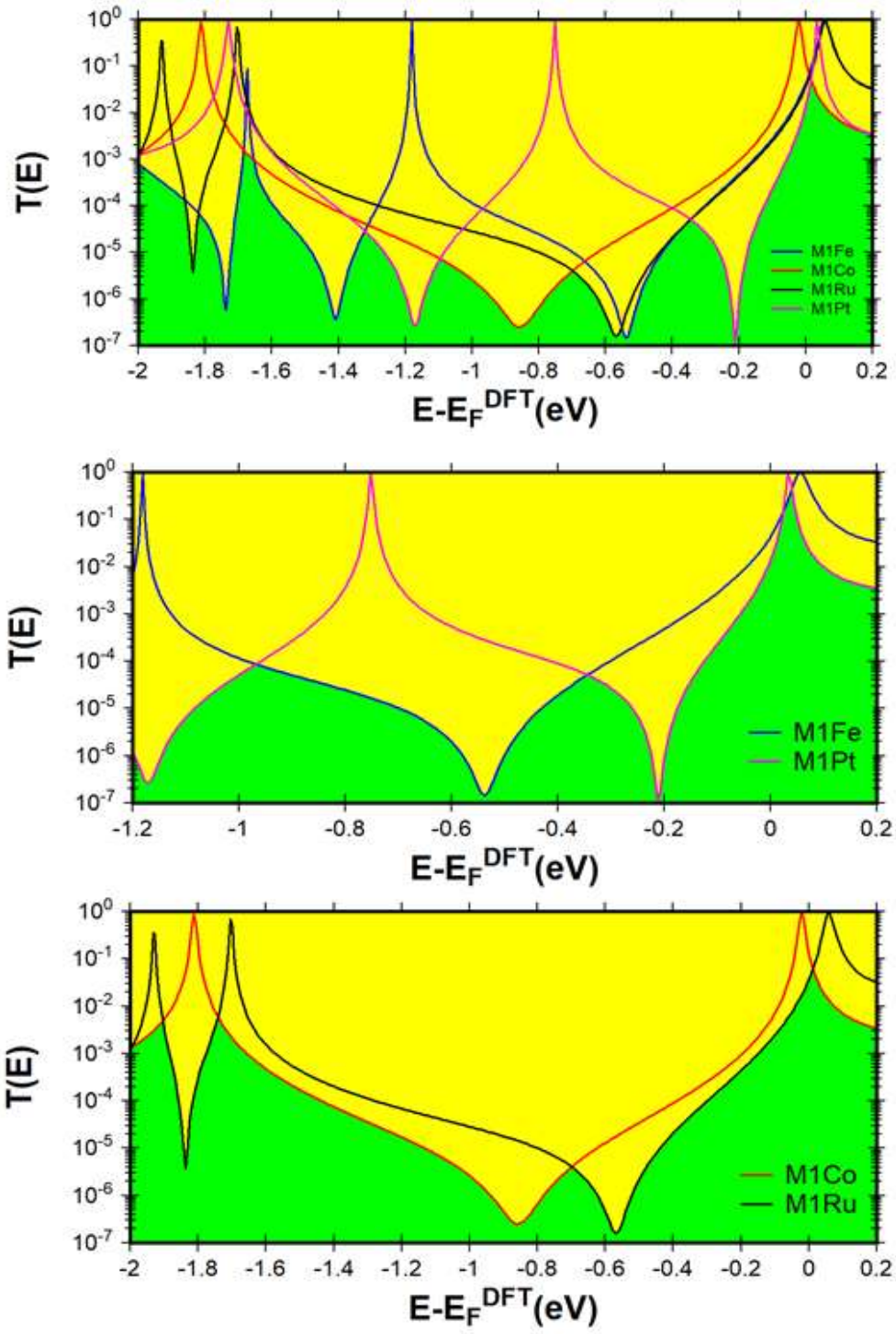

Figure (4-6): Transmission coefficient T(E) and electrical conductance as a function of the Fermi energy for BCP-Metal molecules.

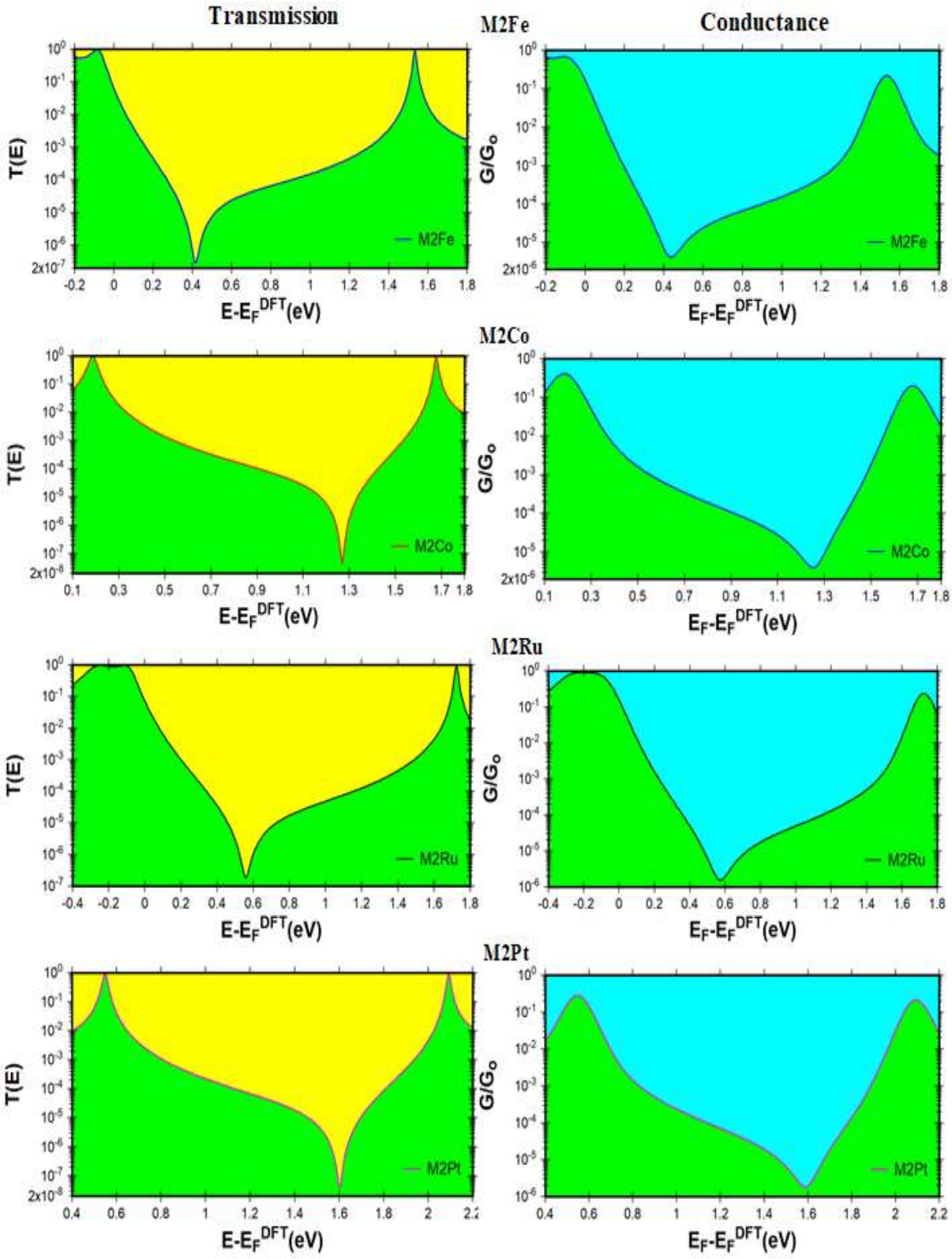
Transmission
Conductance
M2Fe
T(E)
G/G$_o$
E-E$_F^{DFT}$(eV)
E$_F$-E$_F^{DFT}$(eV)
M2Fe
M2Co
M2Ru
M2Pt

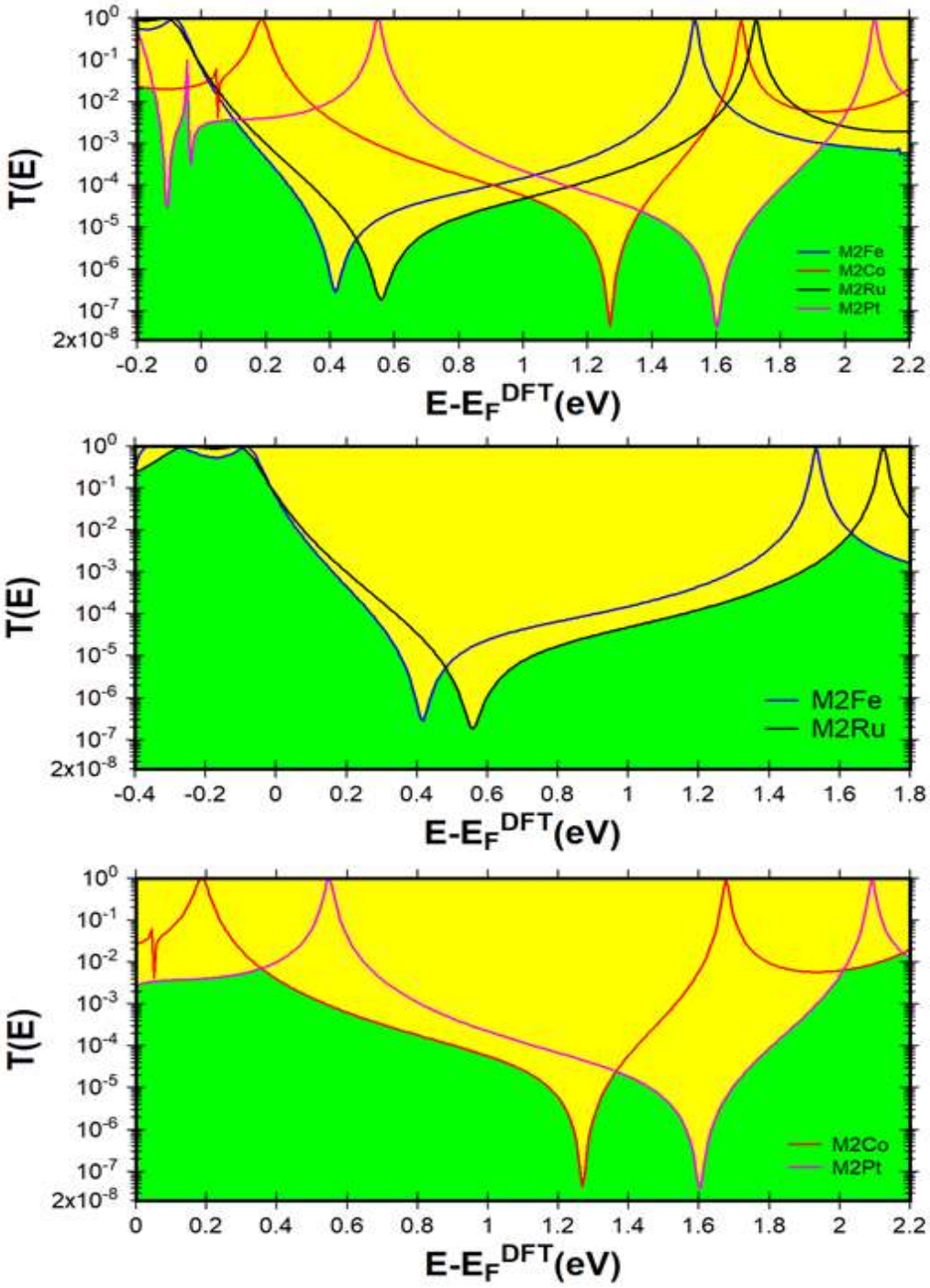

Figure (4-7): Transmission coefficient T(E) and electrical conductance as a function of the Fermi energy for BCPT-Metal molecules.

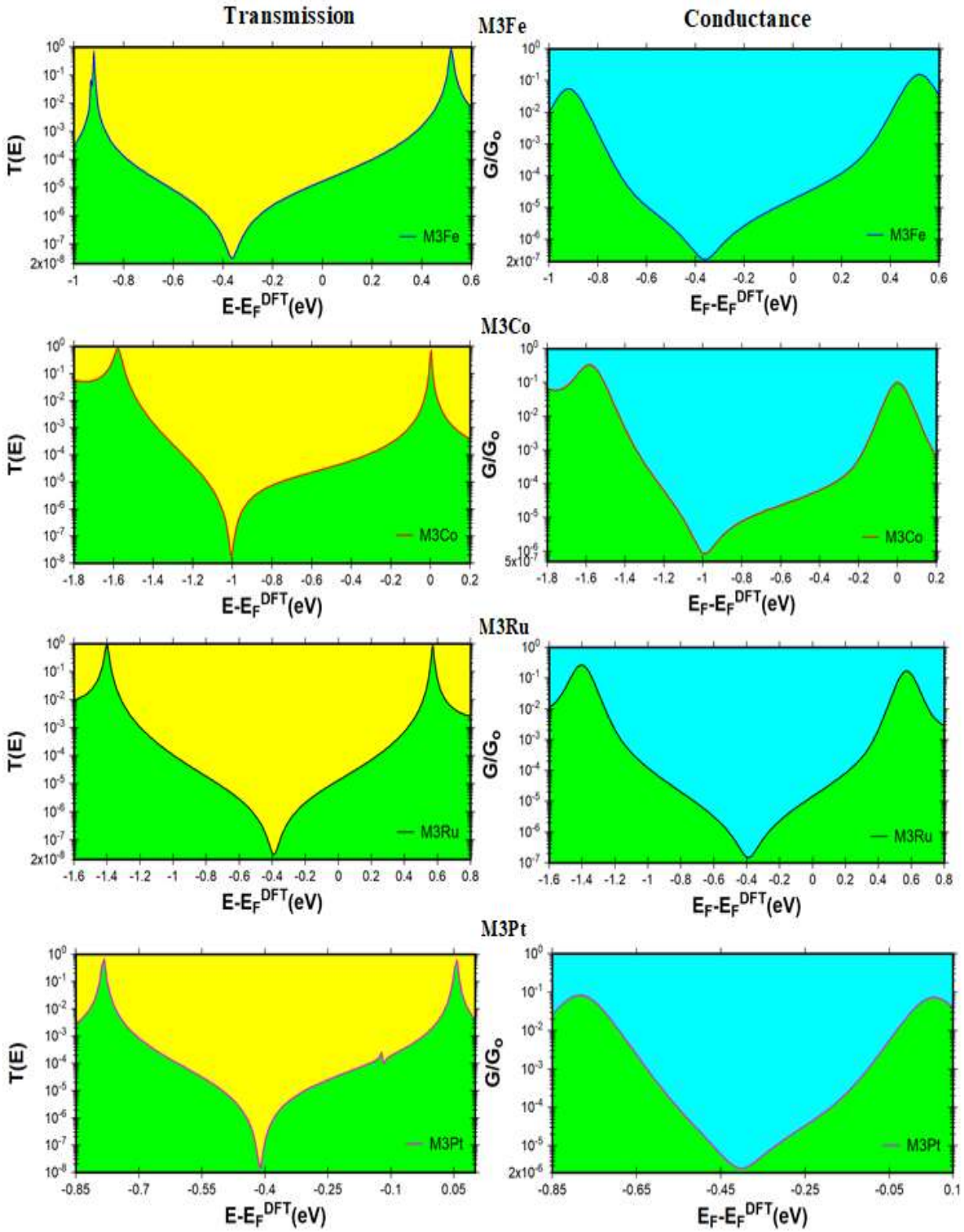
Transmission
Conductance
M3Fe
T(E)
G/G$_o$
E-E$_F^{DFT}$(eV)
E$_F$-E$_F^{DFT}$(eV)
M3Fe
M3Co
M3Ru
M3Pt

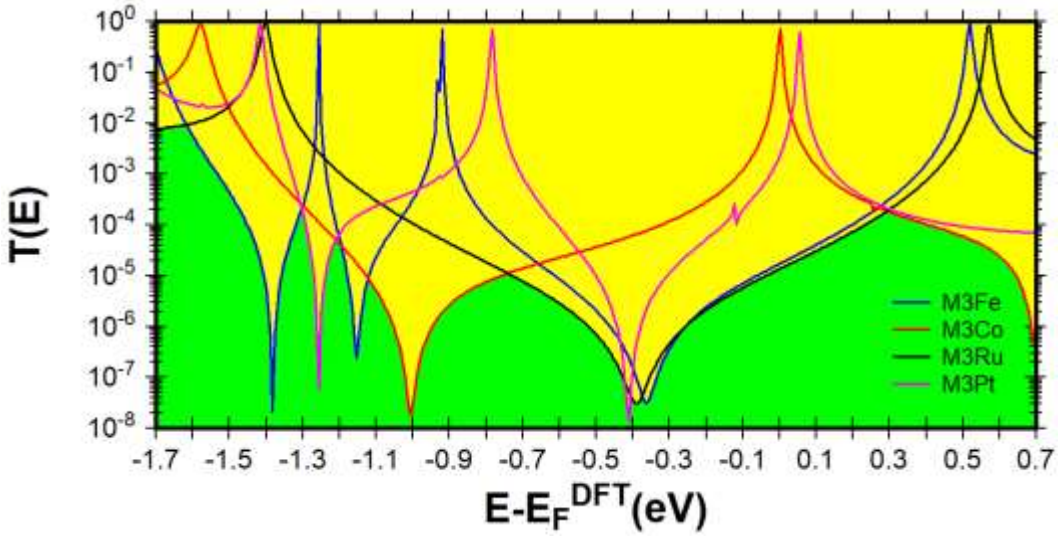

Figure (4-8): Transmission coefficient T(E) and electrical conductance as a function of the Fermi energy for BCPTM-Metal molecules.

Specifically, there are anti-resonance peaks in the transport spectrum for the structure with all metal centers under investigation, which is caused by destructive quantum interference between discrete and continuous states. Additionally, the location of the anti-resonance peak enables us to calculate the theoretical Fermi energy, it is found that the *T(E)* values of group1 (BCP) in the LUMO-dominated regime -0.14 eV < *E* < 0 are quite similar., while Fig. (4-7), it is found that the *T(E)* values of group2 (BCPT) in the HOMO-dominated 0.142 eV > *E* > 0 system are quite similar. group3 (BCPTM) in the LUMO-dominated regime -0.29 eV < *E* < 0 are quite similar. It is obvious that this phenomenon results in a increases in the transmission coefficient for the all anchor groups over a wide range of electron energies (-3 - 3 eV), as illustrated in Figures (4-6), (4-7), and (4-8). A significant finding of these figures is that changing the metals in the middle of the molecules and the anchor group at the ends of the molecules affects not only the transmission coefficient and electrical conductance, but also causes the quantum size effect.

Table 4.3: The Transmission and Electrical Conductance of all molecules.

Compounds	T(E)	G/G_o	H-L gap Isolated	H-L gap Junction
Group 1				
BCP-Fe	0.126×10^{-2}	0.284×10^{-2}	3.251	1.238
BCP-Co	0.263×10^{-2}	0.364×10^{-2}	2.556	1.792
BCP-Ru	0.315×10^{-2}	0.408×10^{-2}	3.235	1.762
BCP-Pt	0.1006	0.534×10^{-2}	2.259	0.785
Group2				
BCPT-Fe	0.127×10^{-2}	0.593×10^{-2}	3.273	1.618
BCPT-Co	0.164×10^{-2}	0.621×10^{-2}	1.817	1.487
BCPT-Ru	0.402×10^{-2}	0.782×10^{-2}	3.244	1.833
BCPT-Pt	0.490×10^{-2}	0.974×10^{-2}	1.872	1.546
Group3				
BCPTM-Fe	0.171×10^{-3}	0.113×10^{-3}	3.254	1.438
BCPTM-Co	0.174×10^{-3}	0.169×10^{-3}	1.951	1.582
BCPTM-Ru	0.198×10^{-3}	0.698×10^{-3}	3.228	1.977
BCPTM-Pt	0.275×10^{-3}	0.916×10^{-3}	1.851	0.839

We see from the results in Fig. (4-7) that altering the metal used in the core of the organometallic molecule has an effect on both the transmission coefficient and electrical conductivity. We obtained it during the transition process as a result of the peak anti- resonance's and it reaches its maximum value at BCP-Pt (0.1006).

The data indicate that there is no statistically significant differential in conductance between the compounds in group 1 and the bridging metal (Fe, Co, Ru and Pt). It is instructive to compare our results to Chen et alwork's on a series of compounds with comparable structures to Fe, Ru, and Pt, except that they were connected to gold electrodes using thiol anchors rather than pyridyl anchors as examined here. Pyridyl, ThioMethyl, and thiol anchors produce conductance's that are dominated by LUMO and HOMO, respectively. BCPT-Pt > BCPT-Ru > BCPT-Co > BCPT-Fe was the clear conductance trend for the Pyridyl anchors. This resulted in the conclusion that aromaticity improves the conductance of single-molecule junctions[171]. Additionally, due to the various anchoring groups, the conductance of the Thiol compounds is consistently greater than that of the Pyridyl and thiomethyl anchored analogs [172-173].

Figures (4-6), (4-7) and (4-8) reflects an important fact that the metal in centre molecular or the different anchor groups unites not only affected the transmission coefficient value but also it influenced the width HOMO-LUMO gap. These results can be explained in terms of combining the path of electrons and the effects of quantum size. In general, we find that the H-Lgap of the studied molecules, which is isolated, differs greatly from the H-L gap, which is connected to the electrodes, where we find that the H-Lgap is reduced by half or more when connecting the gold electrodes, and this is due

to the high conductivity of the gold metal compared to other metals. These results as I mentioned could be interpreted in terms of tunneling distance, since the short molecular length means short tunneling distance and this means the highest conductance and vice versa. The variation in the value of HOMO-LUMO gaps could be attributed to the quantum size effects.

4.8 The Thermoelectric Properties

Organometallic-based molecular junctions are finding importance in applications such as solar cells, field effect transistors (FETs), touch screens, light emitting diodes (LEDs), electrochemical sensors, super capacitors and batteries [44-47].

From the thermal and electrical properties of nanowires [38], this type of material has the ability to generate electricity by heating via the Seebeck effect [172]. The Seebeck effect is defined as the generation of potential when there is a temperature difference between the two sides of the material.

In contrast, the Peltier effect describes the observed heating or cooling effect if an electric current is cross through a junction [167]. There has been a lot of effort and many studies to investigate the types of materials that aim to increase the efficiency of these effects and to identify the parameters that control the performance of such devices [168]. It is hoped that these efforts will lead to a wide application of thermoelectric devices from refrigerators to power generators [169].

4.8.1 Thermopower and Figure of Merit

There are four thermal parameters that are used to describe the thermal and electrical properties of a molecular device. It is defined as electrical conductivity G, which is the ability to pass an electric current through a material, thermopower *S* refers to the electrothermal potential produced in response to a temperature gradient across the material that is measured in units of Volts/Kelvin.

Thermal conductance *k* is the heat current due to a temperature gradient in units of W/K and the figure of merit *ZT* is a measure of the efficiency of a device [166,167]. The most important parameters are the thermopower *S* and the Figure of merit *ZT*. Therefore, I have calculated these parameters as shown in the results below Fig. (4-9).

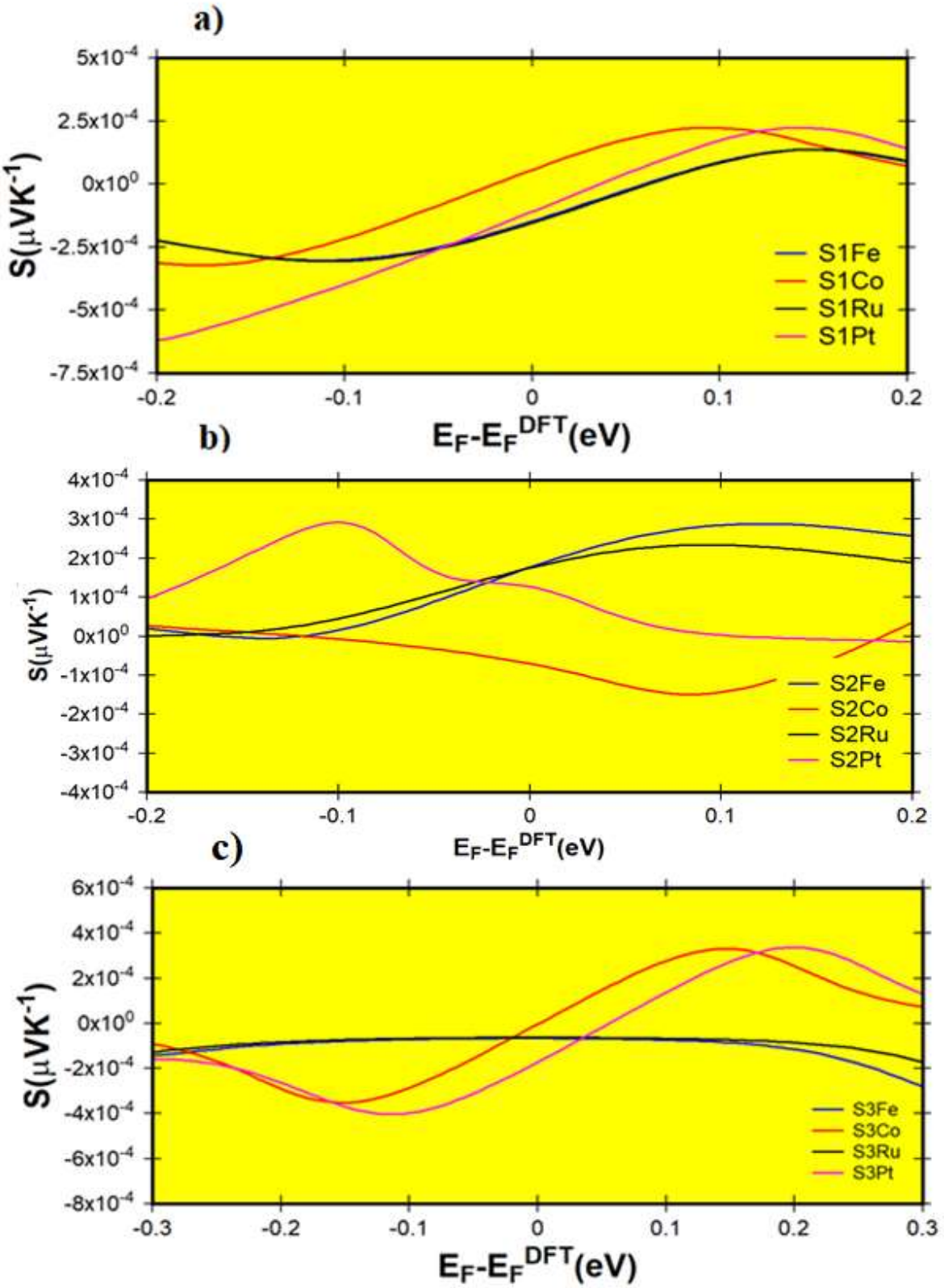

Figure (4-9). Thermopower as a function of the Fermi energy of all molecular junctions.

Figure (4-9) shows the calculated thermopower coefficient of all three groups molecular junctions. The calculated thermopower (*S*) of compounds were obtained using the Gollum code. Provided $T(E)$ Figures (4-6), (4-7) and (4-8) can be approximated by a straight line on the scale of $k_B T$, the Seebeck coefficient is given by $\boldsymbol{S \approx -L|e|T\left(\frac{d\, lnT(E)}{dE}\right)_{E=E_F}}$,where *L* is the Lorenz number $\boldsymbol{L = \left(\frac{k_B}{e}\right)^2 \frac{\pi^2}{3}}$ = **2.44.10^{-8} WΩK^{-2}**. In other words, *S* is proportional to the negative of the slope of $\ln T(E)$, evaluated at the Fermi energy. As noted above, the DFT calculation places the Fermi energy near the middle of the HOMO-LUMO gap where its value for group1(-0.14eV), for group2 (0.142eV) and for group3 at (-0.29 eV) , but slightly closer to the HOMO-dominated for group2 and LUMO-dominated for groups (1,3), consistent with the measured positive and negative sign of the Seebeck coefficient.

These results provided an excellent idea for the design of thermo-molecular devices. Since then, we found in group1 the structure (BCP-Fe) giving the highest thermopower (-0.288 x 10^{-3} VK^{-1}). While the structure (BCP-Pt) shows the lowest thermopower (-0.499 x 10^{-3} VK^{-1}), while we found in group2 the structure (BCPT-Fe) gives the highest thermopower (0.288 x10^{-3} VK^{-1}). While the structure (BCPT-Pt) shows the lowest thermopower (0.073 x 10^{-3} VK^{-1}) and in group3 we found that the structure (BCP-Fe) gives the highest thermopower (-0.113 x $10^{-3}VK^{-1}$). While the structure (BCP-Pt) shows the lowest thermopower (-0.401 x 10^{-3} VK^{-1}), as shown in Table (4.4).

Table 4.4. The thermopower (S), and Figure of Merit (ZT) of all molecules.

Compounds	S(VK^{-1})	ZT_e	H-L gap Junction
Group1			
BCP-Fe	-0.286×10^{-3}	1.18	1.238
BCP-Co	-0.321×10^{-3}	2.01	1.792
BCP-Ru	-0.391×10^{-3}	1.23	1.762
BCP-Pt	-0.499×10^{-3}	9.75	0.785
Group2			
BCPT-Fe	0.288×10^{-3}	1.44	1.618
BCPT-Co	0.196×10^{-3}	0.88	1.487
BCPT-Ru	0.129×10^{-3}	0.96	1.833
BCPT-Pt	0.073×10^{-3}	0.151	1.546
Group3			
BCPTM-Fe	-0.113×10^{-3}	0.502	1.438
BCPTM-Co	-0.179×10^{-3}	0.334	1.582
BCPTM-Ru	-0.221×10^{-3}	0.567	1.977
BCPTM-Pt	-0.401×10^{-3}	3.76	0.839

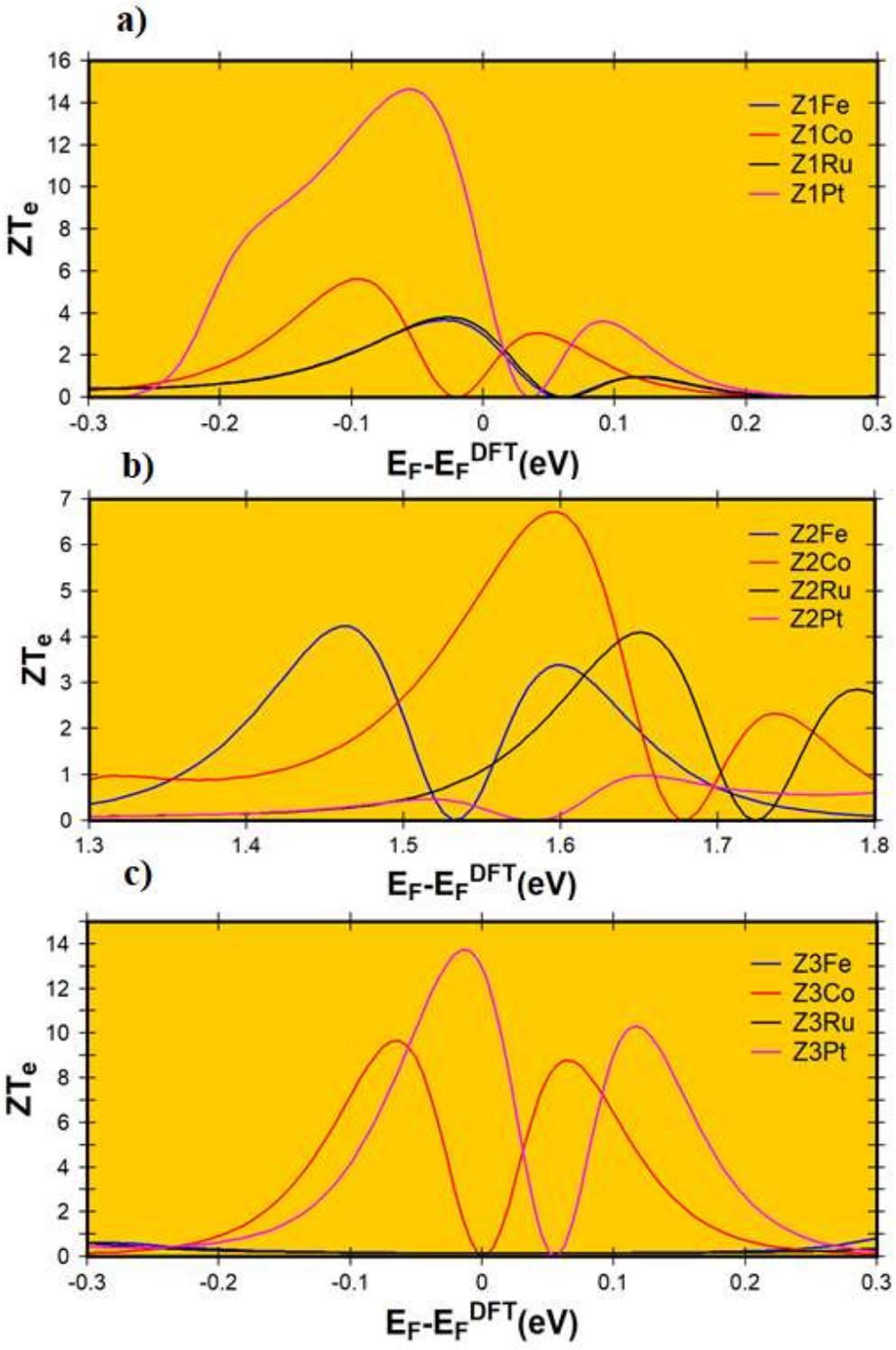

Figure (4-10): Figure of merit ZT_e as a function of the Fermi energy of all molecular junctions.

The explanation of our results in Figures (4-9) and (4-10) is the thermopower *S* and Figure of merit *ZT* being sensitive to the Fermi-energy value. If the Fermi-energy sits within the HOMO-LUMO gap where the transport curve is rather flat this will cause the thermopower value to be high but when the Fermi-energy sits at or near to an anti-resonance position, the transport curve will show low values [75].

However, these results provided an interesting strategy to enhance the merit number (*ZT*) by way of the molecule in which the Pt-metal from group1 is present in the LUMO as much (9.75). While the molecules in the HOMO-domain which is the group2 group at the ends of the thiol anchor group is the best form of merit for Fe-metal molecule as shown in Table (4.4).

In terms of low electrical conductance yields high thermopower, our results presented in Table (4.3) and (4.4) show that the lowest conductance is introduced by Fe-metal, which leads to a significant raising of Seebeck coefficient. On the other hand, it is obvious that there is a strong link between the HOMO-LUMO gap and electronic and thermoelectric properties of these structures, which definitely needs more investigation.

Part III

4.9 Transmission Coefficient and Electrical Conductance for different Groups

Here in this part, every metal of one type will be studied in all the groups used in which a specific anchor group is used. The intention is that Fe-metal will be studied in three groups, and so on for the rest of the metals used in our study. Understanding molecular conduction behavior is an important starting point for calculating the electronic structures and electrical behavior of electron transitions based on the DFT theory. The transmission properties *T(E)* were calculated using Gollum code, in addition, according to the results we obtained from the HOMO and LUMO molecular orbitals, they have an similar sign, that is, there is no constructive interference, which means we get destructive interference inside the gap.

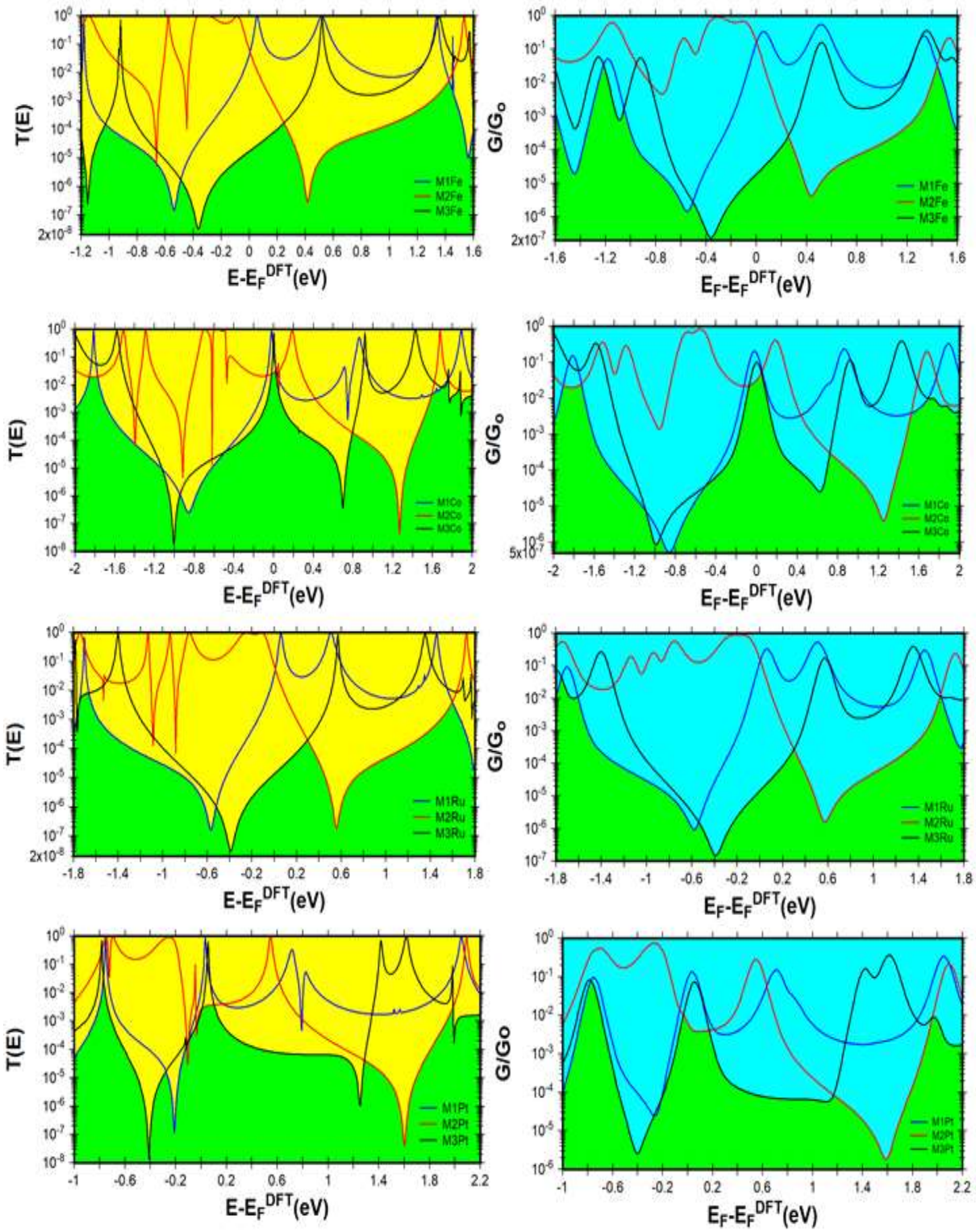

Figure (4-11): Transmission coefficient T(E) and electrical conductance as a function of the Fermi energy for every metal in three anchor group molecules.

Table 4.5: The Transmission, Electrical Conductance and Thermoelectric properties (Seebeck coefficient and Figure of merit) of all molecules at E_F=-0.14, 0.142 and -0.29 eV for metallic (Fe, Co, Ru, Pt) respectively, and the HOMO-LUMO gaps Junctions.

Compounds	T(E)	G/G_o	$S(VK^{-1})$	ZT_e	H-L gap Junction
Fe					
BCP-Fe	0.126×10^{-2}	0.284×10^{-2}	-0.286×10^{-3}	1.18	1.238
BCPT-Fe	0.127×10^{-2}	0.593×10^{-2}	0.288×10^{-3}	1.44	1.618
BCPTM-Fe	0.171×10^{-2}	0.113×10^{-3}	-0.113×10^{-3}	0.502	1.438
Co					
BCP-Co	0.263×10^{-2}	0.364×10^{-2}	-0.321×10^{-3}	2.01	1.792
BCPT-Co	0.164×10^{-2}	0.621×10^{-2}	0.196×10^{-3}	0.88	1.487
BCPTM-Co	0.174×10^{-3}	0.169×10^{-3}	-0.179×10^{-3}	0.334	1.582
Ru					
BCP-Ru	0.315×10^{-2}	0.408×10^{-2}	-0.391×10^{-3}	1.230	1.762
BCPT-Ru	0.402×10^{-2}	0.782×10^{-3}	0.129×10^{-3}	0.96	1.833
BCPTM-Ru	0.198×10^{-3}	0.698×10^{-3}	-0.221×10^{-3}	0.576	1.977
Pt					
BCP-Pt	0.1006	0.534×10^{-2}	-0.499×10^{-3}	9.75	0.785
BCPT-Pt	0.49×10^{-2}	0.974×10^{-2}	0.073×10^{-3}	0.151	1.546
BCPTM-Pt	0.275×10^{-3}	0.916×10^{-3}	-0.401×10^{-3}	3.76	0.839

The transmission coefficient usually describes the diffusion of electrons from the left gold electrode through the molecule and then to the right gold electrode. Therefore, the transmission coefficient and electrical conductance were calculated by obtaining the matrix Hamiltonian using SIESTA and then using the GOLLUM code. In this part, we note the effect of changing the metal core of the molecule and anchor group on the results we obtained as shown in Fig. (4-11).

Where we find from the results obtained as shown in Table (4.5) the beginning of the Fe-metal transmission coefficient in the ThioMethyl group is the highest value than the rest of the groups (*T(E)* BCPTM-Fe > *T(E)* BCPT-Fe > *T(E)* BCP-Fe). So, From this, we find that the transmission coefficient for all the metals used in the study is that the pyridine anchor group has the highest electron transfer as shown in Table (4.5) and the results obtained, and this is due to the fact that the N-atom is the best bond with gold, which leads to an easy transition for electrons.

4.10 Thermopower and Figure of Merit for different Groups

Each molecular device can be accurately described based on the electrical and thermal parameters of the device. One of the most important thermodynamic parameters that has been used to describe the thermal properties of a molecular system. We will test the thermal properties of organometallic molecule from different metals (Fe, Co, Ru, Pt). Therefore, I have calculated these parameters as shown in the results below Figure(4-12). Through the results we obtained, it gave us a new idea about the fabrication of molecular devices, using different metals in the synthesis of the molecules of the three groups (BCP-Metal, BCPT-Metal, BCPTM-Metal). Fig. (4.12) for

three groups containing Fe-metal shows that the highest thermopower obtained for (BCPT-Fe) molecule was (0.288 x 10^{-3} VK^{-1}), while the lowest thermopower obtained for this metal with another group molecule (BCP-Fe)) amounted to (-0.286 x 10^{-3} VK^{-1}).

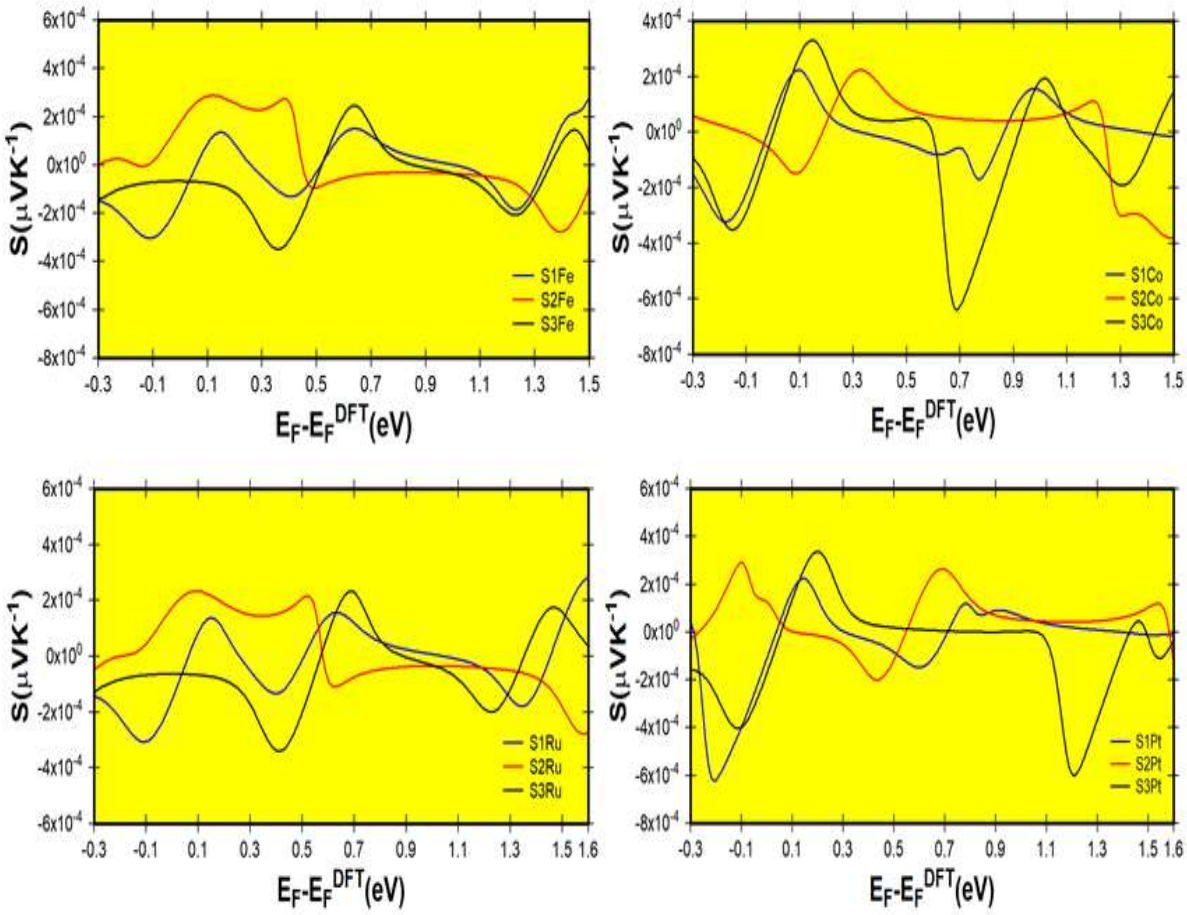

Figure (4-12): Thermopower as a function of the Fermi energy for each metal in three anchor groups molecular junctions.

Of these three anchor groups used in the study with the studied metals, we find the best electrical conductance was for Fe-metal in the second anchor group(BCPT) and its value is (0.593 x 10^{-2}), Also, the highest thermopower was for Fe-metal in the second anchor group (BCPT) with a value of (0.288 x 10^{-3} VK^{-1}). We can explain the wonderful results that we have reached in

Figures (4-12 and 4-13). It is known that both the Thermopower and the figure of merit are directly affected by the Fermi energy site. Since the Fermi energy is located in LUMO and HOMO due to anti-resonance shown in Figures (4-7), (4-8) and (4-9), this leads to an increase in Thermopower with lowest electrical conductance [172].

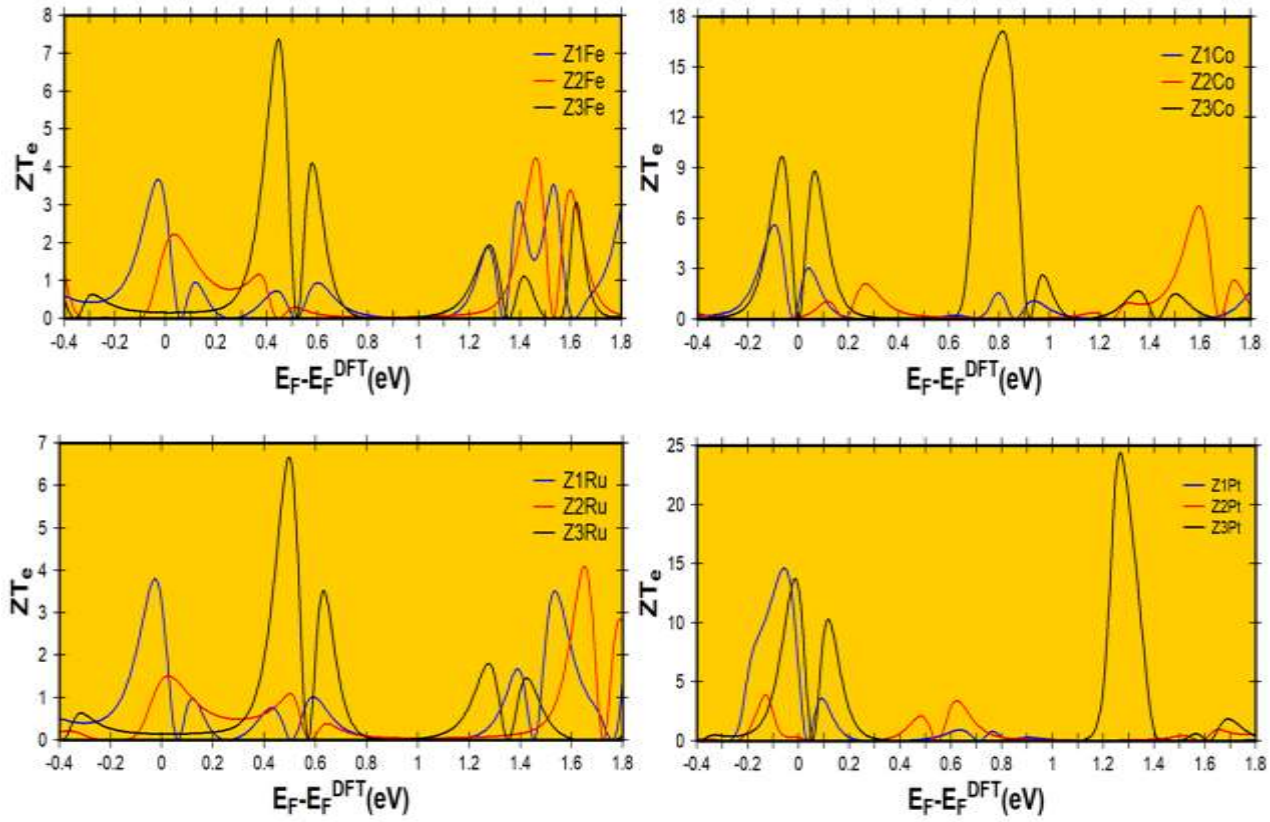

Figure (4-13): Figure of merit ZT as a function of the Fermi energy for each metal in three anchor groups molecular junctions.

Normally, lower Thermopower leads to a higher ZT_e value of (0.502) for BCPTM-Fe molecule as shown in Fig. (4-12), and thus will make the BCPTM-Fe molecule attractive in thermoelectric devices. The reason for the high value of ZT_e is the appearance of anti-resonance in the LUMO and HOMO curve, and this is all due to the binding of the anchor group with the

gold electrodes be meta-linked, which causes destructive quantum interference.

Similarly, for the metals (Co, Ru, and Pt), the highest figure of merit is found in the Pyridyl group, which also has a high thermopower value of (2.01, 1.23, and 9.75). As a result of this, we determine that the highest figure of merit value in the three anchor groups used in the study is at the Pt-metal in the first group (Pyridyl group), and this value is calculated based on the efficiency of the devices during manufacturing or measurement, with a higher figure of merit value indicating greater device efficiency.

4.11 Conclusions

I have investigated the electronic and thermoelectric properties of three different groups for organometallic molecules using density functional theory DFT and the Green's function formalism, as described in Chapters 2 and 3. My thesis focused on the properties of single molecule transfer to electrodes utilizing a variety of metals and anchors, including the building blocks of the molecules, which are organometallic compounds such as BiCyclobentedine connected to the anchor groups at the ends of the molecules.

The dream of manipulating quantum interference in single molecules has been discussed for many years, and molecular Mach-Zehnder interferometers have been the topic of much theoretical work. Therefore, the results of this thesis may aid to develop this kind of scientific research by introduce reasonable and reliable predications and conclusions, which could be summarized as follows:

- In conclusion, the results that have been presented in section 4.1 (Part I) of chapter 4 exhibit a theoretical study using the density function theory methods to investigate the optoelectronic properties of organometallic molecules. It has been proved that the organometallic structures based on (BiCyclobentedine-metal- anchor groups) molecules can be a powerful devices for the optoelectronics applications, particularly for the laser active mediums, since these structures introduced a high value of the emission oscillator strength (f_{em}). In addition, has been suggested a useful strategy to enhance the thermoelectric properties of these devices by changing an anchor group with metal, which makes these structures promising as well for the thermoelectric applications.

- The results of section 4.2 (Part II) of chapter 4 provided a considerable body of information about the design of thermoelectric materials and control the thermoelectric properties of single molecule devices. By using the density functional theory and a non-equilibrium Green's function, the researcher has investigated the thermoelectric properties of BiCyclobentedine-based molecular junctions with different metals (Fe, Co, Ru and Pt). Although the existence of destructive quantum interference as an anti-resonance decreases the thermopower and figure of merit sharply, but it is a powerful strategy to enhance the electrical conductance. The position of the anti-resonance is not only an important factor to determine the sign of Seebeck coefficient, but also it is a useful technique to predicate the value of Fermi energy. Further, the electrons transfer ratio from molecule to the electrodes can be a support factor to promotes or increase the electrical conductance and decrease thermopower respectively.
- In terms of novelty, it can be concluded from the results in section 4.3(Part III) of chapter 4, that this work defined the state-of-the-art in single molecule quantum interference devices by bringing together for the first time, pioneering work on molecular wires. In addition, exhibits a novel strategy to control the quantum mechanical interference and enhance the electronic and thermoelectric properties of the molecular based devices, and its applications.

4.12 Future Works

Molecular Nanotechnology is a field that can be considered as source of scientific and cognitive inspiration and innovation, so the researcher suggests some of ideas for the future work as follows:

1- Studying the electronic and optical properties of porphyrin nanotubes.
2- Investigation the thermoelectric properties of porphyrin molecular junctions under magnetic field effects.
3- Studying the optoelectronics properties of porphyrin nanorings with shapes of square, rectangle and conical.

References

[1] M. Di Ventra, S. Evoy and J. R. Heflin, "Introduction to Nanoscale Science and Technology", Series: Nanostructure Science and Technology, Springer, p. 611, (2004).

[2] U. M. Ravaioli, "Computational Nanotechnology: Simulation of Nanoscale Electronic Systems", Department of Electrical and Computer Engineering University of Illinois at Urbana-Champaign Urbana, IL 61801 USA (2007).

[3] J. C. Cuevas and E. Scheer, "Molecular Electronics An Introduction to Theory and Experiment", Series: World Scientific Series in Nanoscience and Nanotechnology, Vol. 1, p.724 (2010).

[4] G. E. Moore, "Cramming more components onto integrated circuits", Electronics Magazine, IEEE, Vol. 38(8): pp. 114–117, (1965).

[5] A. Nitzan, "Chemical Dynamics in the Condensed Phases: Relaxation, Transfer, and Reactions in Condensed Molecular Systems", (Oxford Graduate Texts) Book, 1st Edition, 744 pages, (2014).

[6] A. Nitzan, "Electron transmission through molecules and molecular interfaces", Annual Review Physical Chemistry, Vol. 52, pp. 681–750, (2001).

[7] R.A. Mark, "Brief history of molecular electronics", Journal Nature Nanotechnology. Vol. 8(6), pp. 378–381, (2013).

[8] R. A. Marcus, "Electron transfer reactions in chemistry Theory and experiment", Rev. Mod. Phy. Vol.(65), pp. 599–610, (1993).

[9] C. Robert, D. Brian, D. Suman, K. Jack and Z. Kevin, "Integrated nanoelectronics for the future", Journal Nature Materials, Vol. 6(11), pp. 810–812, (2007).

[10] R. H. James and A. R. Mark, "Molecular electronics", Journal Physics Today, Vol. 56(5), pp. 43–49, (2003).

[11] E. Scheer, M. Ruben and R. Naaman, "Visions for a molecular future", Journal Nature nanotechnology Vol.(6), pp. 385-389,(2013).

[12] G. Pascal, M. Jos Thijssen and S. J. van der Zan Herre, "Single-molecule quantum-transport phenomena in junctions", Journal Nature Reviews Physics, Vol. (1), pp. 381–396, (2019).

[13] M. Sarhan Musa, "Computational Nanotechnology: Modeling and Applications with MATLAB". (Nano and Energy) Book,1st Edition, CRC Press, Taylor & Francis group, (2011).

[14] K. Yuki, F. Shintaro, I. Madoka and K. Manabu, "Single-molecule junctions for molecular electronics", Journal of Materials Chemistry C, Vol. 4(38), pp. 8842-8858, (2016).

[15] M. Rosa Axet and P. Karine, "Catalysis with Colloidal Ruthenium Nanoparticles", Journal American Chemical Society, Chemical Review, Vol. 120(2), pp. 1085–1145, (2020).

[16] B. I. Kharisov, O. V. Kharissova, V. J. Jacobo Ruíz and V. M. Pérez, "Coordination and Organometallic Nanomaterials: A Microreview", Synthesis and Reactivity in Inorganic, Metal-Organic, and Nano-Metal Chemistry, Metal-Organic and Nano-Metal Chemistry, Vol. 40(9), pp. 640 - 650, (2010).

[17] L. Keller and M. Huth, " Pattern generation for direct-write three-dimensional nanoscale structures via focused electron beam induced deposition", Beilstein Journal of Nanotechnology, Vol. 9(1),: pp. 2581-2598, (2018).

[18] R. A. Webb, S. Washburn, C.P. Umbach and R.B. Laibowitz, "Observation of h/e Aharonov–Bohm oscillations in normal-metal rings", Physical Review Letters, Vol. 54(25), p. 2696, (1985).

[19] M. Mayor, H. B. Weber, J. Reichert, M. Elbing, C.V. Hänisch, D. Beckmann and M. Fischer, "Electric current through a molecular rod-

relevance of the position of the anchor groups", National Library Medicine, National Center for Biotechnology Information, Vol. 42(47), pp. 5834–5838, (2003).

[20] Z. Wen Hong, M. Ali Ben Aissa, L. Peng, Hujun Xie, D. Chen, J. Zheng, Y. Shao and X. Shun Zhou, "Quantum interference effect of single-molecule conductance influenced by insertion of different alkyl length", Electrochemistry Communications, Vol. 68, pp. 86-89, (2016).

[21] R. Baer and D. Neuhauser, "Phase coherent electronics:A molecular switch based on quantum interference", Journal American Chemical Society, Vol. 124(16), p. 4200–4201, (2002).

[22] H. Szatylowicz, M. A. Domanski, and T. M. Krygowski, "Classical and Reverse Substituent Effects in Substituted Anthrol Derivatives", Chemistry Open, Vol. 8(1), pp. 64–73, (2019).

[23] L. J. O'Driscoll and M. R. Bryce, "Extended curly arrow rules to rationalise and predict structural effects on quantum interference in molecular junctions", Journal Nanoscale, Vol. 13(2), pp. 1103-1123, (2021).

[24] C. M Guédon, H. Valkenier, T. Markussen and K. S. Thygesen, "Observation of quantum interference in molecular charge transport", National Library Medicine, National Center for Biotechnology Information, Nature Nanotechnology, Vol. 7(5), pp. 305-309, (2012).

[25] C. J. Lambert, "Basic concepts of quantum interference and electron transport in single-molecule electronics", Chemical Society Reviews, Vol. 44 (4), pp. 875-888, (2015).

[26] M. H. Garner, H. Li, Y. Chen, A. Timothy Su, Z. Shangguan, D. W. Paley, T. Liu, Fay Ng, S. Xiao, C. Nuckolls, L. Venkataraman and G. C. Solomon "Comprehensive suppression of single-molecule conductance using destructive σ-interference", National Library Medicine, National

Center for Biotechnology Information, Nature, Vol. 558(7710), pp. 415-419, (2018).

[27] R. Frisenda, V. A. E. C. Janssen, F. C. Grozema, H. S. J. van der Zant and N. Renaud, "Mechanically controlled quantum interference in individual π-stacked dimers", Journal Nature Chemistry, Vol. 8(12): pp. 1099-1104, (2016).

[28] H. Liang Yan and H. Rabitz, "Single-molecule phenyl-acetylene-macrocycle-based optoelectronic switch functioning as a quantum-interference-effect transistor", Physical Review Letters. Vol. 109(18), (2012).

[29] J. P. Bergfield, G. C. Solomon, C. A. Stafford and M. A. Ratner, " Novel quantum interference effects in transport through molecular radicals" Journal American Chemical Society, Nano Letters, Vol. 11(7), pp. 2759-2764, (2011).

[30] D. Z. Manrique, C. Huang, M. Baghernejad, X. Zhao, A. A. Oday Al-Owaedi, H. Sadeghi, V. Kaliginedi, W. Hong, M. Gulcur, T. Wandlowski, M. R. Bryce and C. J. Lambert "A quantum circuit rule for interference effects in single-molecule electrical junctions", Nature Communications, Vol. 6, pp.6389-6397, (2015).

[31] S. Sangtarash, C. Huang, H. Sadeghi, G. Sorohhov, J. Hauser, T. Wandlowski, W. Hong, S. Decurtins, S. X. Liu and C. J. Lambert, "Searching the hearts of graphene-like molecules for simplicity, sensitivity, and logic", Journal American Chemical Society, Vol. 137(35), pp. 11425-11431, (2015).

[32] X. Liu, S. Sangtarash, D. Reber,D. Zhang, H. Sadeghi, J. Shi,Z-Y Xiao, W. Hong, C. J. Lambert and S. X. Liu " Gating of quantum interference

in molecular junctions by heteroatom substitution", Journal Angewandte Chemistry International Edition, Vol. 56(1), pp. 173-176, (2017).

[33] C. Huang, M. Jevric, A. Borges, S. T. Olsen, J. M. Hamill, J. Ting Zheng, Y. Yang, A. Rudnev, M. Baghernejad, P. Broekmann, A. U. Petersen, T. Wandlowski, K. V. Mikkelsen, G. C. Solomon, M. B. Nielsen and Wenjing Hong, "Single-molecule detection of dihydroazulene photo-thermal reaction using break junction technique", Journal Nature Communications, Vol. 8, p. 15436, (2017).

[34] N.A. Melosh, A. Boukai, F. Diana, B. Gerardot, A. Badolato, P. M. Petroff and J. R. Heath , " Ultrahigh-Density Nanowire Lattices and Circuits", National Library Medicine, National Center for Biotechnology Information, Science, Vol. 300(5616), pp. 112-117, (2003).

[35] S. Das, A. J. Gates, H. A. Abdu and G. S. Rose, "Designs for Ultra-Tiny, Special-Purpose Nanoelectronic Circuits", IEEE Xplore, Vol. 54(11), pp. 2528-2540, (2007).

[36] W. Lu, L. Wang, Z. Lie and D. Xiang, "Advance of Mechanically Controllable Break Junction for Molecular Electronics", Springer, Book Series, Chapter First, Part of the Topics in Current Chemistry Collections (TCCC), Molecular-Scale Electronics, pp. 45-86, (2017).

[37] A. Vilan, D. Aswal and D. Cahen, "Large-Area, Ensemble Molecular Electronics: Motivation and Challenges", Chemistry Reviewer, Journal American Chemical Society, Vol. 117(5), pp. 4248-4286, (2017).

[38] Y. Komoto, S. Fujii, M. Iwane and M. Kiguchi, "Single-molecule junctions for molecular electronics", Journal Materials Chemistry C, Vol. 4(38), pp.8842-8858, (2016).

[39] M. Kiguchi and S. Kaneko, "Single molecule bridging between metal electrodes", Physical Chemistry Chemical Physics, Vol. 15(7), pp. 2253-2267, (2013).

[40] R. J. Nichols and S. J. Higgins, "Single-Molecule Electronics: Chemical and Analytical Perspectives", National Library Medicine, National Center for Biotechnology, Annu. Reviewer Anal Chemistry, Vol. 8, pp. 389-417, (2015).

[41] R. J. Nichols, W. Haiss, S. J. Higgins, E. Leary, S. Martin and D. Bethell, "The experimental determination of the conductance of single molecules", Journal Physical Chemistry Chemical Physics, Vol. 12(12), pp. 2801-2815, (2010).

[42] X. P. Chen, M. Roemer, L. Yuan, W. Du, D. Thompson, E. del Barco and C. A. Nijhuis, "Molecular diodes with rectification ratios exceeding 10^5 driven by electrostatic interactions", National Nanotechnology, Vol. 12 (8), pp. 797-803, (2017).

[43] H. Song, "Electrostatic Gate Control in Molecular Transistors", Journal Topics in Current Chemistry, Vol. 376(5), (2018).

[44] S. Richter, E. Mentovich and R. Elnathan, "Realization of Molecular-Based Transistors", Article Advanced Materials, Literature Review, Vol. 30(41), (2018).

[45] S. Y. Guo, M. J. Artes and I. Diez-Perez, "Electrochemically-gated single-molecule electrical devices", Electrochimical, Contribution to Journal, Article, peer-review, Vol. 110, pp. 741-753, (2013).

[46] N. J. Kay, S. J. Higgins, J. O. Jeppesen, E. Leary, J. Lycoops, J. Ulstrup and R. J. Nichols, "Single-Molecule Electrochemical Gating in Ionic Liquids", Journal of the American Chemical Society, Vol. 134 (40), pp. 16817-16826, (2012).

[47] H. M. Osorio, S. Catarelli, P. Cea, J. B. Gluyas, F. Hartl, S. J. Higgins, E. Leary, P. Low, S. Martin, R. J. Nichols, J. Tory, J. Ulstrup, A. Vezzoli, D. C. Milan and Q. Zeng, "Electrochemical Single-Molecule Transistors with Optimized Gate Coupling", Journal American Chemical Society, Vol. 137(45), pp. 14319-14328, (2015).

[48] S. Plimpton, "Fast Parallel Algorithms for Short-Range Molecular Dynamics", Journal of Computational Physics, Vol. 117(1), pp. 1-19, (1995).

[49] W. Smith and T.R. Forester, "DL-POLY-2.0: A general-purpose parallel molecular dynamics simulation package", Journal of Molecular Graphics, Vol. 14(3), pp. 136-141, (1996).

[50] A. Aviram and M.A. Ratner, " Molecular rectifiers", Chemical Physics Letters, Vol. 29(2), pp. 277-283, (1974).

[51] D. Xiang, X. Wang, C. Jia, T. Lee and X. Guo, "Molecular-Scale Electronics: From Concept to Function", Chemical Reviews, Journal American Chemical Society, Vol. 116(7), pp. 4318-4440, (2016).

[52] S. Y. Sayed, J. A. Fereiro, H. Yan, R. L. Mccreery and A. J. Bergren, "Charge transport in molecular electronic junctions: Compression of the molecular tunnel barrier in the strong coupling regime", Proceedings of the National Academy of Sciences, Vol. 109(29),pp.11498-11503,(2012).

[53] C. J. Lambert and S. X. Liu, "A Magic Ratio Rule for Beginners: A Chemist's Guide to Quantum Interference in Molecules", Chemistry A European Journal, Vol. 24(17), pp. 4193- 4201, (2018).

[54] G. C. Solomon, J. P. Bergfield, C. A. Stafford and M. A. Ratner, "When "small" terms matter: Coupled interference features in the transport properties of cross-conjugated molecules", Beilstein Journal Nanotechnology, Vol. 2, pp. 862-871, (2011).

[55] D. Q. Andrews, G. C. Solomon, R. P. Van Duyne and M. A. Ratner, "Single Molecule Electronics: Increasing Dynamic Range and Switching Speed Using Cross-Conjugated Species", Journal American Chemical Society, Vol. 130(51), pp. 17309-17319, (2008).

[56] M. Famili, I. M. Grace, Q. Al-Galiby, H. Sadeghi and C. J. Lambert, "Toward High Thermoelectric Performance of Thiophene and Ethylenedioxythiophene (EDOT) Molecular Wires", Advanced Functional Material, Vol. 28(15), (2018).

[57] Q. H. Al-Galiby, H. Sadeghi, D. Z. Manrique and C. J. Lambert, "Tuning the Seebeck coefficient of naphthalenediimide by electrochemical gating and doping", Nanoscale Journal, Vol. 9(14), pp. 4819-4825, (2017).

[58] C. J. Lambert, H. Sadeghi and Q. H. Al-Galiby, "Quantum-interference-enhanced thermoelectricity in single molecules and molecular films", Académie des sciences. Published by Elsevier Masson SAS, Comptes Rendus Physique, Vol. 17(10), pp 1084-1095, (2016).

[59] H. Sadeghi, S. Sangtarash and C. J. Lambert, "Oligoyne Molecular Junctions for Efficient Room Temperature Thermoelectric Power Generation", Journal American chemical Society, Nano Lett. , Vol. 15(11), pp. 7467-7472, (2015).

[60] V.M. Garcia-Suarez, C.J. Lambert, D.Z. Manrique, and T. Wandlowski, "Redox control of thermopower and figure of merit in phase-coherent molecular wires", IOP Science, Nanotechnology, Vol. 25(20), (2014).

[61] I. Díez-Pérez, J. Hihath, Y. Lee, L. Yu, L. Adamska, M. A. Kozhushner, I. I. Oleynik and N. Tao, "Rectification and stability of a single molecular diode with controlled orientation", Journal Nature Chemistry, Vol. 1, pp. 635-641, (2009).

[62] L. Yuan, R. Breuer, L. Jiang, M. Schmittel and C. A. Nijhuis, "A Molecular Diode with a Statistically Robust Rectification Ratio of Three Orders of Magnitude", Journal American Chemical Society, Nano Lett., Vol. 15(8), pp. 5506-5512, (2015).

[63] A. Batra, P. Darancet, Q. Chen, J. S. Meisner, J. R. Widawsky, J. B. Neaton, C. Nuckolls and L. Venkataraman, "Tuning rectification in single-molecular diodes", Journal American Chemical Society, Nano Lett. Vol. 13(12), pp. 6233-6237, (2013).

[64] B. Xu, X. Xiao, X. Yang, L. Zang and N. Tao, "Large Gate Modulation in the Current of a Room Temperature Single Molecule Transistor", Journal American Chemical Society, Vol. 127(8), pp. 2386-2387, (2005).

[65] H. Song, Y. Kim, Y. H. Jang, H. Jeong, M. A. Reed and T. Lee, "Observation of molecular orbital gating", Journal Nature Materials, Vol. 462(7276), pp. 1039-1043, (2009).

[66] A. S. Blum, J. G. Kushmerick, D. P. Long, C. H. Patterson, J. C. Yang, J. C. Henderson, Y. Yao, J. M. Tour, R. Shashidhar and B. R. Ratna, "Molecularly inherent voltage-controlled conductance switching", Journal Nature Materials, Vol. 4, pp. 167-172, (2005).

[67] S. J. van der Molen, J. Liao, T. Kudernac, J. S. Agustsson, L. Bernard, M. Calame, B. J. Van Wees, B. L. Feringa and C. S. Schönenberger, "Light-controlled conductance switching of ordered metal-molecule-metal devices", Journal American Chemical Society, Nano Lett. Vol. 9(1), pp. 76-80, (2009).

[68] C. C. Jia, A. Migliore, N. Xin, S. Y. Huang, J. Y. Wang, Q. Yang, S. P. Wang, H. L. Chen, D. M. Wang, B. Y. Feng, Z. R. Liu, G. Y. Zhang, D. H. Qu, H. Tian, M. A. Ratner, H. Q. Xu, A. Nitzan and X. F. Guo, "Covalently bonded single-molecule junctions with stable and reversible

photo-switched conductivity", Science, Vol. 352(6292), pp. 1443-1445, (2016).

[69] R. Frisenda, G. D. Harzmann, J. A. Celis Gil, J. M. Thijssen, M. Mayor and H. S. J. Van der Zant, "Stretching-Induced Conductance Increase in a Spin-Crossover Molecule", Journal American Chemical Society, Nano Lett., Vol. 16(8), pp. 4733-4737, (2016).

[70] G. Yzambart, L. Rincón-Garcí, A. Alaa Al-Jobory, A. K. Ismael, G. Rubio-Bollinger, C. J. Lambert, N. Agraït and M. R. Bryce, "Thermoelectric Properties of 2,7-Dipyridylfluorene Derivatives in Single-Molecule Junctions", Journal American Chemical Society, Vol. 122(48), pp. 27198-27204, (2018).

[71] Y. Kim, W. Jeong, K. Kim, W. Lee and P. Reddy, "Electrostatic control of thermoelectricity in molecular junctions", Journal Nature Nanotechnology, Vol. 9, pp. 881-885, (2014).

[72] H. Yan, A. J. Bergren and R. L. McCreery. "All-carbon molecular tunnel junctions", Journal American Chemical Society, Vol. 133(47), pp.19168-19177, (2011).

[73] J. Zhu, J. McMorrow, R. Crespo-Otero, A. Geyou, M. Zheng , W. P. Gillin and M. Palma, "Solution-processable carbon nanoelectrodes for single-molecule investigations", Journal of the American Chemical Society, Vol. 138(9), pp. 2905-2908, (2016).

[74] C. Jia, and G. Xuefeng, "Molecule–electrode interfaces in molecular electronic devices", Journal Chemical Society Reviews, Vol. 42(13), pp. 5642-5660, (2013).

[75] J. M. Soler, E. Artacho, J. D. Gale, A. Garcia, J. Junquera, P. Ordejon and D. Sanchez-Portal, "The SIESTA method for ab initio order-N materials

simulation", IOP Science, Journal of Physics: Condensed Matter, Vol. 14(11), pp. 2745–2779, (2002).

[76] A. Emilio, E. Anglada, O. Dieguez, J. D. Gale, J. Junquera, R. M. Martin, P. Ordejon, J. M. Pruneda and D. Sanchez-Portal, "The SIESTA method; developments and applicability", IOP Science, Journal of Physics: Condensed Matter, Vol. 20(6), 64208, (2008).

[77] J. Ferrer, C. J. Lambert, V. M. Garcia-Suarez, D. Zs. Manrique, D. Visontai, L. Oroszlany, R. Rodriguez-Ferradas, I. Grace, S. W. D. Bailey, K. Gillemot, H. Sadeghi and L. A. Algharagholy, "GOLLUM: a next-generation simulation tool for electron, thermal and spin transport", New Journal of Physics, Vol. 16(9), 093029, (2014).

[78] M. Kiguchi, H. Nakamura, Y. Takahashi, T. Takahashi and T. Ohto, "Effect of anchoring group position on formation and conductance of a single disubstituted benzene molecule bridging Au electrodes: change of conductive molecular orbital and electron pathway", Journal Physics Chemistry C, Vol. 114(50): pp. 22254–22261, (2010).

[79] L. Luo, A. Benameur, P. Brignou, S. H. Choi, S. Rigaut and C. D. Frisbie, "Length and Temperature Dependent Conduction of Ruthenium-Containing Redox-Active Molecular Wires", Journal Physics Chemistry C. Vol. 115(40): pp. 19955–19961, (2011).

[80] H. M. Wen, Y. Yang, X. S. Zhou, J. Y. Liu, D. B. Zhang, Z. B. Chen, J. Y. Wang, Z. N. Chen and Z. Q. Tian, "Electrical conductance study on 1,3-butadiyne-linked dinuclear ruthenium(ii) complexes within single molecule break junctions", Journal Chemical Science, Vol. 4(6), pp. 2471–2477, (2013).

[81] J. Ponce, C. R. Arroyo, S. Tatay, R. Frisenda, P. Gavina, D. Aravena, E. Ruiz, H. S. J. Van der Zant and E. Coronado, "Effect of metal

complexation on the conductance of single-molecular wires measured at room temperature", Journal American Chemistry Society, Vol. 136(23), pp. 8314–8322, (2014).

[82] A. C. Aragonès, D. J. Aravena, Z. Acís-Castillo, H. Li, J. A. Real, F. Sanz, J. Hihath, E. Ruiz and I. Díez-Pérez, "Large Conductance Switching in a Single-Molecule Device through Room Temperature Spin-Dependent Transport", Nano Lett. Vol. 16(1), pp. 218–226, (2016).

[83] L. A. Zotti, E. Leary, M. Soriano, J. C. Cuevas and J. J. Palacios, "A Molecular Platinum Cluster Junction: A Single-Molecule Switch", Journal American Chemistry Society, Vol. 135(6), pp. 2052–2059, (2013).

[84] A. Oday Al-Owaedi, C. D. Milan, O. Marie-Christine, B. Sören, S. Y. Dmitry, A. K. Judith Howard, S. J. Higgins, R. J. Nichols, C. J. Lambert, M. R. Bryce and P. J. Low. "Experimental and Computational Studies of the Single-Molecule Conductance of Ru(II) and Pt(II) trans-Bis (acetylide) Complexes", Journal American Chemistry Society, Organometallics, Vol. 35(17), pp. 2944−2954, (2016).

[85] A. Oday Al-Owaedi, S. Bock, D. C. Milan, O. Marie-Christine, S. I. Michael, S. Y. Dmitry, N. S. Alexandre, J. L. Nicholas , T. Albrecht, J. H. Simon, R. B. Martin, J. N. Richard, C. J. Lambert and Paul J. Low. "Insulated molecular wires: inhibiting orthogonal contacts in metal complex based molecular junctions", Journal Nanoscale, Vol. 9(28), pp. 9902–9912, (2017).

[86] P. Sam-ang and G. R. Matthew, "Characterizing destructive quantum interference in electron transport", IOP Science, New Journal of Physics, Vol. 19, (2017).

[87] R. J. Davidson, D. C. Milan, O. A. Al-Owaedi, A. K. Ismael, R. J. Nichols, S. J. Higgins, C. J. Lambert, D. S. Yufita and Andrew Beeby, "Conductance of 'bare-bones' tripodal molecular wires", Journal RSC Advanced, Vol. 8(42), pp. 23585–23590, (2018).

[88] Z. Guang-Ping, M. Yan-Qi, Z. Jin-Ming, H. Huangb, H. Gui-Chao, L. Zong-Liang and W. Chuan-Kui, "Optimizing the conductance switching performance in photos witch able dimethyldihydropyrene/cyclophanediene single-molecule junctions", Elsevier, Physica E: Low-dimensional Systems and Nanostructures, Vol. 109, pp. 1-5, (2019).

[89] A. A. Baraa Al-Mammory, A. Oday Al-Owaedi and M. Enas Al-Robayi, "Thermoelectric Properties of Oligoyne-Molecular Wires", IOP Science, Journal of Physics: Conference Series, Vol. 1818(1), (2021).

[90] M. Rasool Al-Utayjawee and A. Oday Al-Owaedi, "Enhancement of Thermoelectric Properties of Porphyrin based Molecular Junctions by Fano Resonances", IOP Science Journal of Physics: Conference Series, Vol. 1818(1), (2021).

[91] F. Schedin, A. K. Geim, S.V. Morozov, E. W. Hill, P. Blake, M. I.Katsnelson and K. S. Novoselov, "Detection of individual gas molecules adsorbed on grapheme", Nature materials ,Vol. 6, pp. 652-655, (2007).

[92] P. Richard Wallace, "The band theory of graphite", Physical Review Journal Archive, Vol. 71(9), pp. 622, (1947).

[93] W. Yang-Yang , Z. Feng-Qi and J. Xue-Hai, "A Comparison of the Accuracy of Semi-empirical PM3, PDDG and PM6 methods in Predicting Heats of Formation for Organic Compounds", Journal of the Mexican Chemical Society, Vol. 58(2), 223-229, (2014).

[94] D. Young, "Computational Chemistry: A Practical Guide for Applying Techniques to Real World Problems", Hand Book, 3rd Edition, Wiley & Sons, Inc., New York, p. 408, (2001).

[95] M. Mueller, "Fundamentals of Quantum Chemistry: Molecular Spectroscopy and Modern Electronic Structure Computations", Book, Springer, 1st Edition, Kluwer Academic/Plenum Publishers, New York, p. 278, (2001).

[96] C. J. Cramer, " Essentials of Computational Chemistry: Theories and Models", Book, 2nd Edition, John Wiley & Sons Ltd., The Atrium, Southern Gate, Chichester, England, p. 624, (2004).

[97] C. L. Tang, "Fundamentals of Quantum Mechanics for Solid State Electronics and Optics", Book, 1st Edition, Cambridge University Press, NY publishes, Ithaca, p. 224, (2009).

[98] H. F. Hameka, "Quantum Mechanics: A Conceptual Approach", Wiley-Interscience, Leiden University, John Wiley & Sons, Inc., p. 204, (2004).

[99] P. A. Cox., "Introduction to Quantum Theory and Atomic Structure", Book, 1st Edition, Oxford University Press, Lecture in Organic Chemistry, p. 96, (1996).

[100] D.D. Fitts, "Principles of Quantum Mechanics: As Applied to Chemistry and Chemical Physics", Book, 1st Edition, Cambridge University Press, New York, p. 364, (1999).

[101] P. A. Cox, "introduction to Quantum Theory and Atomic Structure", Book, 1st Edition, Oxford University Press , New York, p. 96 (1996).

[102] D.W. Rogers, "Computational Chemistry Using the PC", Book, 3rd Edition., John Wiley & Sins, Inc., Hoboken, New Jersey, p.349 (2003).

[103] V. Sahni, "Quantal Density Functional Theory II: Approximation Methods and Applications", Springer Verlag, Berlin Heidelberg, p. 426, (2009).

[104] N. Ira Levin, "Quantum Chemistry", Book, 7th Edition, Pearson Education, Inc., New Jersey, USA, p. 720, (2013).

[105] C. David Sherrill, "Introduction to Electronic structure Theory", Lecture Notes, School of Chemistry and Biochemistry Georgia Institute of Technology, p. 10, (2002).

[106] M. L. Chabinyc, X. Chen, R. E. Holmlin, H. Jacobs, H. Skulason, C. D. Frisbie, V. Mujica, M. A. Ratner, M. A. Rampi and G. M. Whitesides, "Molecular rectification in a metal-insulator-metal junction based on self-assembled monolayers", Journal American Chemistry Society, Vol. 124(39), pp. 11730-11736, (2002).

[107] I. Gablech, J. Pekárek, J. Klempa, V. Svatoš, A. S. Moghaddam, P. Neužil and M. Pumera, "Monoelemental 2D materials-based field effect transistors for sensing and biosensing: Phosphorene, antimonene, arsenene, Silicene, and Germanene go beyond grapheme", TrAC Trends in Analytical Chemistry, V. 105, pp.251-262, (2018).

[108] S.Mehdi Aghaei, M.M.Monshi, I.Torres, M.Banakermani and I.Calizo, "Lithium-functionalized Germanene: A promising media for CO2 capture", Physics Letters A, Vol. 382(5), pp. 334-338, (2018).

[109] A. Hazim, H. Mohammed and A. Hashim, "First Principles Calculations of Electronic, Structural and Optical Properties of (PMMA–ZrO2–Au) and (PMMA–Al2O3–Au) Nanocomposites for Optoelectronics Applications", Springer Science, Transactions on Electrical and Electronic Materials, Vol. 22(2), pp. 185-203, (2020).

[110] F. Jensen, "Introduction to Computational Chemistry", Book, 3rd Edition, John Wiley and Sons, p. 664, (2017).

[111] E.d. Jeffrey and R. Reimers, "Computational Methods for Large systems: Electronic Structure Approaches for Biotechnology and Nanotechnology", Book, Computational Chemistry and Molecular Modeling, Wiley, The University of Sydney, Australia, p. 688, (2011).

[112] V. Nagarajan and R. Chandiramouli, "NO_2 adsorption behaviour on Germanene nanosheet – A first-principles investigation", Elsevier, Superlattices and Microstructures, Vol. 101, pp. 160-171, (2017).

[113] J. Chen, M. A. Reed, A. M. Rawlett and Tour, "Large on-off ratios and negative differential resistance in a molecular electronic device", Science, Vol. 286(5444): pp. 1550−1552, (1999).

[114] M. A. Reed, C. Zhou, C. J. Muller, T. P. Burgin and J. M. Tour, "Conductance of a molecular junction", Science, Washington, Vol. 278(5336), pp.252–254, (1997).

[115] R. H. M. Smit, Y. Noat, C. Untiedt, N. D. Lang, M. C. Van Hermert and J. M. Ruitenbeek, "Measurement of the conductance of a hydrogen molecule", Nature Letters article, Vol. 419(6910), pp. 906–909, (2002).

[116] B. Q. Xu and N. J. Tao, "Measurement of single-molecule resistance by repeated formation of molecular junctions", Science, 301(5637): pp. 1221–1223, (2003).

[117] S. M. Woodley and C. Richard A. Catlow, "High Performance Computing in Chemistry and physics of materials", Proceedings of the Royal Society, John von Neumann Institute for Computing, NIC Series, Vol. 467(2131),pp. 1880-1884, (2011).

[118] J. Runmble, "Handbook of Chemistry and Physics", Handbook, 1st Edition, CRC Press LLC, USA, p. 2556, (2000).

[119] W. Demtroder, "Molecular Physics – Theoretical Principles and Experiment Methods", Book, 1st Edition, Wiley, p.484, (2005).

[120] R. R. Gotwals and C. Send linger Shawn, "A Chemistry Educator's Guide to Molecular Modelling", 1st Edition, North Carolina School of Science and Mathematics Center, USA, (2008).

[121] O. Kwon, V. Coropceanu, N. E. Gruhn, J. C. Durivage, J. G., Katz H. E. Laquindanum, J. Cornil and J. L. Bredas, "Characterization of the Molecular Parameters Determining Charge Transport in Anthradithiophene", AIP, Journal Chemistry Physics, Vol. 120(17), pp. 8186-8194, (2004).

[122] A. Hazim, H. Mohammed and A. Hashim, "Analysis of Structural and Electronic Properties of Novel (PMMA/Al2O3, PMMA/Al2O3-Ag, PMMA/ZrO2, PMMA/ZrO2-Ag, PMMA-Ag) Nanocomposites for Low Cost Electronics and Optics Applications", Springer Science, Transactions on Electrical and Electronic Materials, Vol. 21(1), pp. 48-67, (2019).

[123] Ś. S. miga and L. A. Constantin, "Unveiling the Physics Behind Hybrid Functionals", The Journal of Physical Chemistry, 124 (27), 5606-5614, (2020).

[124] W. Kohn and L. J. Sham. "Self-Consistent Equations Including Exchange and Correlation Effects", Journal American Physical Society, Physical Review, Vol. 140, (1965).

[125] Richard M. Martin. "Electronic Structure: Basic Methods and Practical Methods", Cambridge University Press, Cambridge, (2004).

[126] R. G. Parr, Y. Weitao, "Density-Functional Theory of Atoms and Molecules", Oxford University Press Scholarship, (1995).

[127] R. M. Dreizler and E. K. U. Gross, "Density Functional Theory", eBook Packages, 1st Edition, Springer-Verlag Berlin Heidelberg, p. 304, (1990).

[128] G. J. David, "Introduction to Quantum Mechanics", Pearson Prentice Hall, 2nd Edition, Pearson Education International, America, p. 480, (1995).

[129] M. Levy and J. P. Perdew, "Density Functional Methods in Physics", eBook Packages, 1st Edition, Springer, Boston, MA, p. 533, (1985).

[130] P. Hohenberg and W. Kohn, "Inhomogeneous Electron Gas", Physical Review Journals Archive, Journal American Physical Society, Vol. 136, pp. 864-878, (1964).

[131] J. C. Santos, J. Andres, A. Aizman and P. Chem Fuentealba, "An Aromaticity Scale Based on the Topological Analysis of the Electron Localization Function Including σ and π Contributions", Journal Chemistry Theory Compute, Vol. 1(1), pp.83-86, (2005).

[132] W. Theil, "Semiempirical quantum–chemical methods", WIREs Computational Molecular Science, Wiley Interdisciplinary Reviews, Vol. 4(2), pp. 145-157, (2014).

[133] R.O. Jones, "Introduction to Density Functional Theory and Exchange-Correlation Energy Functional", Journal Computational nanoscience , series , John Von Neumann institute for Computing , Julich ,Vol. 31, pp. 45-70, (2016).

[134] B. Kenny Lipkowitz, R. Larter, R. Thomas Cundari and D. B. Boyd, "Reviews in Computational Chemistry", Computational Chemistry & Molecular Modeling, John Wiley & Sons, Inc., Hoboken, New Jersey, Vol. 20, p. 488, (2004).

[135] S. Giarrusso and P. Gori-Giorgi, “Exchange-Correlation Energy Densities and Response Potentials: Connection between Two Definitions and Analytical Model for the Strong-Coupling Limit of a Stretched Bond”, Journal Physics Chemistry A, Vol. 124(12), 2473-2482, (2020).

[136] J. P. Perdew, K. Burke and Matthias Ernzerhof. “Generalized Gradient Approximation Made Simple”, Physical Review Letters, Vol. 77(18), pp. 3865-3873, (2006).

[137] M. Dion, H. Rydberg, E. Schroder, D. C. Langreth, and B. I. Lundqvist, “Van der Waals Density Functional for General Geometries”, Physical Review Letters, 92(24), pp. 22- 25, (2014).

[138] B. Hammer, L. B. Hansen and J. K. Norskov. “Improved adsorption energetics within density-functional theory using revised perdew-burke-ernzerhof functional”, Physical Review, Vol. 59, pp. 7413-7421, (1999).

[139] D. R. Hamann, M. Schluter, and C. Chiang, “Norm-Conserving Pseudopotentials”, Physical Review Letters, Vol. 43(20), pp. 1494-1503, (1979)

[140] T. Pope. “Quantum and Classical Dynamics of Molecular-Scale Junctions”, PhD thesis, Lancaster University, (2013).

[141] S. Botti, “Applications of Time-Dependent Density Functional Theory”, IOP Science, Physica Scripta, Vol. 2004(109), pp. 54-60, (2004).

[142] M. Petersilka, U. J. Gossmann and E. K. U. Gross, "Excitation Energies from Time-Dependent Density-Functional Theory", Physical Review Letters, Vol. 76(8), pp. 1212-1215, (1996).

[143] A. Szabo and N. S. Ostlund, "Modem quantum chemistry: Introduction to advanced electronic structure theory", Dover Publication, Inc. Mineola, New York, p. 484, (2012).

[144] R.Chandiramouli," Structural and electronic properties of germanane nano-sheet upon molecular adsorption of alcohol and aldehyde molecules: DFT comparative analysis", Elsevier, Journal of Molecular Liquids, Vol. 242, pp. 571-579, (2017).

[145] W. J. Hehre, "A Guide to Molecular Mechanics and Quantum Chemical Calculations", Wave function, Inc., Printed in the USA, p. 796, (2013).

[146] C. A. Tsipis, "DFT flavor of coordination chemistry", Elsevier, Coordination Chemistry Reviews, Vol. 272, pp. 1-29, (2014).

[147] N. E. Economou, "Green's functions in quantum physics", Book, 3rd Edition, Springer Series in Solid-State, p. 474, (2006).

[148] A. M. Pier and N. Kumar. "Quantum transport in mesoscopic systems: complexity and statistical fluctuations", A Maximum Entropy Viewpoint (Mesoscopic Physics and Nanotechnology) Reissue Edition, Oxford University Press on Demand, p. 416, (2010).

[149] D. S. Fisher and A. L. Patrick, "Relation between conductivity and transmission matrix", Physical Review B, Vol. 23(12), (1981).

[150] R. Landauer, "Spatial variation of currents and fields due to localized scatterers in metallic conduction", IBM Journal of Research and Development, Vol.1(3), pp. 223-231, (1957).

[151] M. Buttiker, Y. Imry, R. Landauer, and S. Pinhas. "Generalized many channel conductance formula with application to small rings", Physical Review B, Vol. 31(10), pp. 6207-6215, (1985).

[152] M. D. Hanwell, D. E. Curtis, D. C. Lonie, T. Vandermeersch, E. Zurek and G. R. Hutchison, "Avogadro: an advanced semantic chemical editor, visualization, and analysis platform", Journal of Cheminformatics Vol. 4(17), (2012).

[153] R. Mera-Adasme , F. Mendizabal, C. Olea-Azar, S. Miranda-Rojas and P. Fuentealba, "A Computationally Efficient and Reliable Bond Order Measure", Journal American Chemica Society, Vol. 115(17), 4397–4405, (2011).

[154] E. Artacho, J. Gale, A. Garc, J. Junquera, P. Ordej, D. anchez-Portal and J. Soler, "SIESTA-trunk-462", Book, User's Guide, CIC-Nanogune and University of Cambridge, Fundaci on General Universidad Autonoma de Madrid, p. 141, (2014).

[155] E. Artacho, E. Anglada, O. Dieguez, J. D. Gale, A. Garcia, J. Junquera, R. M. Martin, P. Ordejon, J. M. Pruneda, D. Sanchez-Portal and J. M. Soler, "The SIESTA Method; Developments and Applicability", IOP Science, Journal of Physics, Condensed Matter, Vol. 20(6), pp. 1−6, (2008).

[156] M. D. Hanwell, D. E. Curtis, D. C. Lonie, T. Vandermeersch, E. Zurek and G. Hutchison , "Avogadro: an advanced semantic chemical editor, visualization, and analysis platform", BMC Part of Springer Nature, Journal of Cheminformatcs, Vol. 4(17), (2012).

[157] N. M. O'Boyle, M. Banck, C. A. James, C. Morley, T. Vandermeersch, G. R. Hutchison, "Open Babel: an open chemical toolbox", BMC Part of Springer Nature, Journal of Cheminformatics, Vol. 3(33), (2011).

[158] L. G. Zhuo, W. Liao and Z. X. Yu, "A Frontier Molecular Orbital Theory Approach to Understanding the Mayr Equation and to Quantifying Nucleophilicity and Electrophilicity by Using HOMO and LUMO Energies", Asian Journal of Organic Chemistry, Vol. 1(4), pp. 336-345, (2012).

[159] R. D. Bach, G. J. Wolber and H. B. Schlege, "The Origin of the Barriers to Thermally Allowed, Six-Electron, Pericyclic Reactions: The Effect of

HOMO-HOMO Interactions on the Trimerization of Acetylene", Journal American Chemical Society, Vol. 107(10), pp. 2838-2841, (1985).

[160] N. Egbedi, I. Obot, M. Khaiary, S. Umoren and E. Ebenso, "Computational Simulation and Statistical Analysis on the Relationship Between Corrosion Inhibition Efficiency and Molecular Structure of Some Phenanthroline Derivatives on Mild Steel Surface", International Journal of Electrochemical Science, Vol. 6, pp. 5649-5675, (2011).

[161] H. P. William, "Numerical recipes 3rd edition: The art of scientific computing", Book, 3rd Edition, Cambridge university press, p. 1256, (2007).

[162] W. C. James and W. T. John, "An algorithm for the machine calculation of complex fourier series", American Mathematical Society,Mathematics of computation, Vol. 19(90), pp. 297–301, (1965).

[163] A. D. Polyanin and V. F. Zaitsev, "Exact Solutions for Ordinary Differential Equations", Handbook, 2nd Edition, Chapman Hall/CRC Press, Boca Raton, p. 816, (2002).

[164] A. D. Polyanin and V. E. Nazaikinskii, "Linear Partial Differential Equations for Engineers and Scientists", Handbook, 2nd Edition, Chapman and Hall/CRC Press, Boca Raton, p. 1643, (2016).

[165] U. Sivan and Y. Imry, "Multichannel Landauer formula for thermoelectric transport with application to thermopower near the mobility edge", Journal Physical Review B, Vol. 33(1), pp. 551-563, (1986).

[166] C. M. Finch, V. M. Garcia Suarez and C. J. Lambert, "Giant thermopower and figure of merit in single-molecule devices", Journal American Physical Society, Physical Review B, Vol. 79(3), (2009).

[167] N. Mohammed, H. Sadeghi and C. J. Lambert, "High-performance thermoelectricity in edge-over-edge zinc-porphyrin molecular wires", Journal of Nanoscale, Vol. 9(16), pp. 5299-5304, (2017).

[168] V. M. García-Suárez, C. J. Lambert, D. Z. Manrique and W. Thomas, "Redox control of thermopower and figure of merit in phase-coherent molecular wires", IOP Science, Journal of Nanotechnology, Vol. 25(20), (2014).

[169] Q. H. Al-Galiby, H. Sadeghi, L. A. Algharagholy, I. Grace and C. J. Lambert, "Tuning the thermoelectric properties of metallo-porphyrins", Journal of Nanoscale, Vol. 8(4), pp. 2428-2433, (2016).

[170] M. J. Frisch, G. W. Trucks, H. B. Schlegel, G. E. Scuseria, M. A. Robb, J. R. Cheeseman, G. Scalmani, V. Barone, B. Mennucci, G. A. petersson, H. Nakatsuji, M. Caricato, X. Li, H. P. Hratchian, A. F. Izmaylov, J. Bloino, G. Zheng, J. L. Sonnenberg, M. Hada, M.Ehara, K. Toyota, R. Fukuda, J. Hasegawa, M. Ishid, T. Nakajima, Y. Honda, O. Kitao, H. Nakai, T. Vreven, J. A. Montgomery, Jr., J. E. Peralta, F. Ogliaro, M. Bearpark, J. J. Heyd, E. Brothers, K. N. Kudin, V. N. Staroverov, R. Kobayashi, J. Normand, K. Raghavacharii, A. Rendell, J. C. Burant, S. S. Iyengar, J. Tomasi, M. Cossi, N. Rega, J. M. Millam, M. Klene, J. E. Knox, J. B. Cross, V. Bakken, C. Adamo, J. Jaramillo, R. Gomperts, R.E Stratmann, O. Yazyev, A. J. Austin, R. Cammi, C. Pomelli, J. W. Ochterski, R. L. Martin, K. Morokuma, V. G. Zakrzewski, G. A. Voth, P. Salvador, J. J. Dannenberg, S. Dapprich, A. D. Daniels, O. Farkas, J. B. Foresman, J. V. Ortiz, J. Cioslowski and D. J. Fox, "Gaussian 09, revision A. 02 Gaussian, Inc", Wallingford CT., (2009).

[171] W. Chen, H. Li, R. Jonathan Widawsky, C. Appayee, L. Venkataraman and Ronald Breslow, "Aromaticity Decreases Single-Molecule Junction

Conductance", Journal of the American Chemical Society, Vol. 136(3): pp. 918-920, (2014).

[172] S. Sangtarash, H. Sadeghi, and C. J. Lambert, "Exploring quantum interference in heteroatom-substituted graphene-like molecules", Journal of Nanoscale, Vol. 8(27): pp. 13199-13205, (2016).

[173] C. R Arroyo, R. Frisenda, K. Moth-Poulsen, J. S Seldenthuis, T. Bjørnholm and H. S. J. Van der Zant, "Quantum interference effects at room temperature in OPV-based single-molecule junctions", Springer, Nanoscale Research Letters, Vol. 8(234), pp. 1-6, (2013).

جمهورية العراق
وزارة التعليم العالي والبحث العلمي
جامعة بابل
كلية العلوم / قسم الفيزياء

خصائص النقل الكمي لمفارق العضوية المعدنية الجزيئية وتطبيقاتها كوسط ليزري فعال

أطروحة مقدمة إلى

مجلس كلية العلوم في جامعة بابل كجزء من متطلبات
نيل درجة فلسفه دكتوراه في العلوم/ الفيزياء

من قبل

عباس ابراهيم عبيس محيسن الزهيري

بكالوريوس علوم فيزياء ٢٠٠٢

ماجستير علوم فيزياء ٢٠١٠

إشراف

الأستاذ الدكتورة

أيناس محمد سلمان الربيعي

١٤٤٣ هـ ٢٠٢٢م

الخلاصة

تتضمن هذه الأطروحة ثلاثة أعمال علمية جديدة ، يمكن تلخيصها على النحو التالي: العمل الأول يؤكد ويثبت أن الجزيء الأحادي BiCyclobentedine مع تطبيقات مجموعة الربط يلفت الانتباه باستخدام الجزيئات ككتل أولية من المكونات الإلكترونية التي تشتمل على ذرات معدنية. من الناحية النظرية ، يتم استخدام نوع واحد من أجهزة مجموعات المرساة المعدنية ثنائية السايكلوبينتيداين ذات المقياس النانوي في هذه الأطروحة ، وتتألف من جزيئات عضوية مفردة مع معادن مختلفة (Fe ، Co، Ru و Pt) ، محصورة بين أقطاب كهربائية ذهبية مرتبطة بمجموعات المرساة البيريدين و الثايول والثايومثيل.

تمت دراسة الخصائص الإلكترونية والكهروحرارية للوصلات الجزيئية المكونة من جزيئات فلزية عضوية مفردة في هذه الأطروحة. يعد استكشاف وفهم الخصائص الإلكترونية للجزيئات المقترنة بالخيوط المعدنية أمرًا بالغ الأهمية لمستقبل الإلكترونيات الجزيئية. تم استخدام برنامج Gaussian وبرنامج SIESTA للتحقيق في مجموعة متنوعة من هذه الجزيئات باستخدام مزيج من نظرية دالة الكثافة (DFT) ونظرية النقل صيغة دالة Green (كود Gollum). فيما يلي أهم نتائج الأطروحة:

يوضح العمل الأول أن الوصلات الجزيئية BiCyclobentine–metal–anchor ذات أهمية خاصة بسبب ميزاتها الإلكترونية والتركيبية ، والتي تقدمها كمرشح مناسب للتطبيقات الضوئية والكهروحرارية. باستخدام طرائق نظرية دالة الكثافة (DFT) ، وصياغة دالة Green ، يتضمن هذا العمل تحقيقًا نظريًا في الخصائص البصرية والتركيبية والإلكترونية والكهروحرارية لجزيئة BiCyclobentedine مع مجموعة مرساة مختلفة. يشير هذا العمل إلى نتيجة مهمة ، وهي استبدال المعدن بمعدن آخر ومجموعة مرساة جديدة، مما يؤدي إلى زيادة ملحوظة في قوة مذبذب الانبعاث ($0.0008 - 0.5014\ mol.cm^2.L^{-1}$) ($f_{em}$). في المقابل ، يتم تقديم أقل توصيل كهربائي (0.113×10^{-3} Siemens), في المجموعة الثالثة عند الجزيئة التي تحتوي الفلز Fe ، بينما يُظهر أعلى قوة حرارية (معامل سيباك) ($0.113 \times 10^{-3}\ \mu VK^{-1}$). قد يساعد ذلك في ابتكار

جزيئات مرشحه جديده واعده لتصميم الأجهزة الكهروضوئية والحرارية ، فضلاً عن الوسط الفعال لأجهزة أشعة الليزر.

الجزء الثاني تم حساب معامل النقل ومعامل سيبيك لمركبات Au | جزيء | Au باستخدام (DFT). تظهر النتائج أن هناك مقاومة قوية للرنين في سلوك النقل حول طاقة فيرمي ، فقط للجهاز القائم على BiCyclobentedine مع جميع المعادن. تُعزى هذه النتيجة إلى التداخل الكمي المدمر بين الحالات المستمرة والمنفصلة. لا يشير هذا العمل فقط إلى وجود علاقة بين التوصيل الكهربائي والطاقة الحرارية ، ولكنه يقدم أيضًا استراتيجية واعدة للتأثير على هذه الخصائص والتحكم فيها من خلال إنشاء ظاهرة مضادة للرنين.

يحدد العمل الثالث أحدث أجهزة التداخل الكمي للجزيء الفردي من خلال الجمع معًا، والعمل الرائد على الأسلاك الجزيئية. بالإضافة إلى ذلك ، فإنه يعرض استراتيجية جديدة للتحكم في التداخل الميكانيكي الكمي وتعزيز الخصائص الإلكترونية والحرارية للأجهزة الجزيئية وتطبيقاتها. تظهر نتائج هذا العمل أن أفضل قيمة لمعامل النقل للمعدن العضوي (BCP–Pt) هي أكثر بكثير من باقي الجزيئات بعشرات المرات. بل إنه يمثل آلية للتحكم في التداخل الميكانيكي الكمي وتعزيز خصائصه.